GLYCOSYLATION DIVERSITY IN *CAMPYLOBACTER FETUS*

by

JUSTIN M. DUMA

(Under the Direction of Robert J. Maier)

ABSTRACT

Campylobacter fetus is an emerging pathogen and causative agent in veterinary disease. N-linked protein glycosylation by the Pgl system in *Campylobacter jejuni* is important for host colonization and adherence to intestinal cells. Interestingly, the Pgl system in *C. fetus* produces two distinct N-glycans in a ratio of 4:1. Production of multiple N-glycans is consistent in all non-thermotolerant *Campylobacters*, but the mechanism facilitating this differentiation is unknown. Annotation of the *C. fetus pgl* locus indicated the presence of two unannotated *pgl* glycosyltransferases and a putative bacteriophage three-component glucosylation system. Here, we characterized these genes and their physiological functions.

Mutations in *C. fetus pglJ* and *pglX* glycosyltransferases provided insight into the biosynthesis of N-acetyl glucosamine (GlcNAc) termini, versus the N-acetyl galactosamine terminus of *C. jejuni*. Functional transfer of these genes into *Escherichia coli* produced only the minor N-glycan, indicating a need for further studies into this biochemical pathway. Proteomic analysis of the *pgl* mutants indicated effects consistent with *C. jejuni*, including decreased motility and increased antibiotic sensitivity. In addition, we discovered a novel connection

between protein N-glycosylation, H_2-uptake hydrogenase complex HynABC, and metal homeostasis.

The three-component glucosylation system showed similarity with the putative bacteriophage *gtr* glucosylation system, canonically involved in adding glucose to the O-antigen of host lipopolysaccharide (LPS). N-glycan analysis of a *gtr*-negative strain indicated that it plays no role in N-glycosylation. *In vitro* analysis of *C. fetus* GtrB indicated that it solely transfers glucose (Glc); however, mutagenesis of the *gtr* operon resulted in the loss of a -GlcNAc-3--GlcNAc- cap. It is currently unclear how Glc is modified into a GlcNAc residue. Moreover, the mutant had no detectable S-layer and decreased serum resistance. Binding between S-layer protein (*sap*) and LPS occurs via the N-terminus and is dependent on *sap*-type and LPS serotype. Strikingly, the *gtr* operon correlates exclusively with all sequenced type A *sap*-/sero-type strains. Further work will assess whether Sap-LPS binding occurs through the *gtr*-dependent -GlcNAc-3--GlcNAc-LPS cap.

This body of work connects glycosylation to important mechanisms of pathogenesis and host survival in a non-model *Campylobacter* species. Additionally, it provides novel insights into a system for studying N-glycan diversity.

INDEX WORDS: *Campylobacter fetus*, N-glycosylation, protein glycosylation, proteomics, lipopolysaccharide, S-layer, glycosyltransferase

GLYCOSYLATION DIVERSITY IN *CAMPYLOBACTER FETUS*

by

JUSTIN M. DUMA

BS, The University of Alberta, Canada, 2013

A Dissertation Submitted to the Graduate Faculty of The University of Georgia in Partial Fulfillment of the Requirements for the Degree

DOCTOR OF PHILOSOPHY

ATHENS, GEORGIA

2020

GLYCOSYLATION DIVERSITY IN *CAMPYLOBACTER FETUS*

by

JUSTIN DUMA

Major Professor:	Robert Maier
Committee:	Vincent Starai
	Fikri Avci
	Lance Wells
	Fred Quinn

Electronic Version Approved:

Ron Walcott
Interim Dean of the Graduate School
The University of Georgia
August, 2020

DEDICATION

I would like to dedicate this doctoral work to all the important people in my life who supported me through my PhD. Foremost, I would like to dedicate this dissertation to my wife and partner in science Jennifer E. Kurasz. She has been a constant source of support and inspiration throughout my PhD and I would not have been able to do this without her. I would also like to dedicate this work to current and past Szymanski and Maier lab members who have become close friends and like family in my academic voyage. In addition, I would like to include my non-academic friends, which provide me the greatest creative outlets giving me much needed balance in my life. Thanks to all of you, for supporting and caring for me through the good and bad times.

ACKNOWLEDGEMENTS

First, I would like to thank Dr. Christine Szymanski for giving me the opportunity to work in her lab at the University of Alberta and allowing me to transfer with her to the University of Georgia. She has pushed me to be a better version of myself that I never thought possible and for that I am grateful. I would also like to thank all lab members who have become like family at times and together, we made a pretty kick-butt laboratory. Especially Cory Wenzel and Bernadette Beadle for being great friends and teachers and cheering me up when times are rough. Extra-special acknowledgements to my mentors Dr. Harald Nothaft and Dr. Stéphane Benoit who have been essential in teaching me what it takes to be a good research scientist. Their passion and patience gave me the room to grow as an individual and instill me with love for science. Additionally, I would like to thank Dr. Robert Maier, who has been an incredible collaborator, avid supporter, and supervisor. Your enthusiasm of science is absolutely contagious and inspiring, thank you for those moments Dr. Maier.

I would like to thank all the individuals that make the CCRC possible and the Microbiology department. I would like to thank my committee who have provided me feedback and support through a rough time in my life. This work would not be possible without the support great collaborators, especially Dr. Nichollas Scott who has spent countless hours working with me on my research. To all mentioned deep and personal thank you for taking me into your lab, providing me guidance, and being patience and understanding.

TABLE OF CONTENTS

Page

LIST OF TABLES

Page

LIST OF FIGURES

Page

CHAPTER 1

INTRODUCTION AND LITERATURE REVIEW

Bacterial glycosylation

Carbohydrates are a highly abundant molecule and are found in all domains of life. They are oftentimes linked to other types of macromolecules through the process of glycosylation. Microbial glycobiology was once an understudied field with research focus on only a few model organisms. Focus has historically involved the structures associated with the glycan rich surface of bacteria such as lipopolysaccharide (LPS), lipooligosaccharides (LOS), capsular polysaccharide (CPS), peptidoglycan (PG), glycosylated teichoic acids (TAs), exopolysaccharides (EPS), glycoproteins, and other surface associated glycoconjugates (Figure 1.1). These glycan structures have revealed a vast amount of diversity and heterogeneity. The surface carbohydrate macromolecules vary in glycan composition, stereochemistry, and linkage (Gagneux et al. 2015). Studying these systems can be difficult due to the inability to accurately determine glycan composition by genetic analysis. However, recent improvements in mass spectrometry, lectin arrays, and bioinformatics have led to further advancements in microbial glycobiology (Wuhrer 2013).

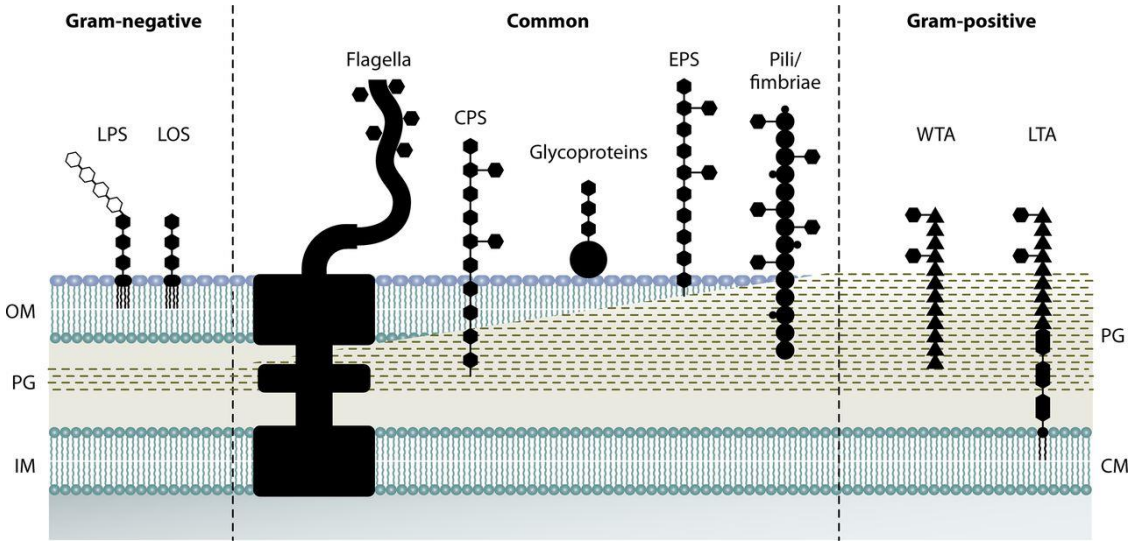

Figure 1.1. Bacterial surface glycans (Tytgat and Lebeer 2014). Lipopolysaccharide (LPS) and lipooligosaccharide (LOS) are glycans characteristic of gram-negative bacteria. While teichoic acids such as lipoteichoic acid (LTA) and wall teichoic acid (WTA) have only been found in gram-positive bacteria. While glycoproteins such as glycosylated flagella, S-layer, pili, fimbriae, and other surface glycoproteins have been found in various bacterial species. In addition, peptidoglycan, capsular polysaccharide (CPS), and exopolysaccharide (EPS) can be found in both Gram-negative and -positive bacteria. Circles represent proteins, sugars are denoted by a hexagon, and triangles are ribitol/glycerol phosphate groups.

These glycans are synthesized through a non-template dependent process that requires multiple enzymes, called glycosyltransferases (GTs) that, sequentially assemble the glycans like an assembly line. The mechanism involves the transfer of a glycosyl donor to an acceptor resulting the formation of a glycosidic bond (Rini and Esko 2015). Leloir GTs can use sugar nucleotide donors and non-Leloir GTs use non-sugar nucleotide donor, like isoprenoid-phosphate lipid-linked sugars, (Luis F. Leloir Biosynth. Saccharides 2005). This donor specificity can be derived from three main GT folds, GT-A, GT-B, and GT-C (Figure 1.2 Top). Currently, all Leloir or nucleotide-dependent GTs contain either a GT-A or GT-B catalytic fold. While both folds use sugar nucleotides, unlike GT-A, the GT-B fold consists of two Rossmann binding folds and is metal-independent (Liu and Mushegian 2003; Rosén et al. 2004). The non-

Leloir GTs primarily contain the GT-C fold, which consist of hydrophobic integral membrane loops (Oriol et al. 2002).

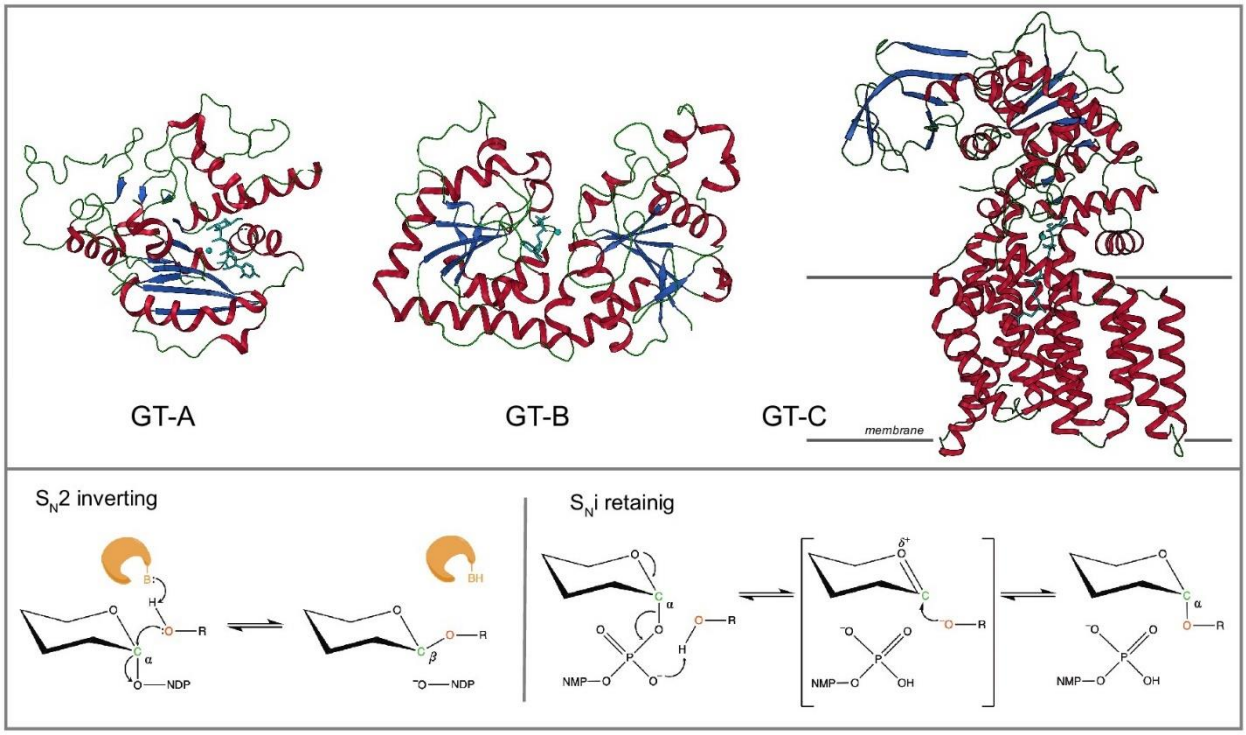

Figure 1.2. Glycosyltransferase (GT) folds and linkage stereochemistry mechanisms (Taujale et al. 2020). Top: The GT-A and GT-B folds both contain nucleotide-binding Rossmann folds, which consist of a α-helix (red), β-sheet (blue), and another α-helix. Unlike GT-A fold enzymes, GT-B enzymes contain two Rossmann folds in addition to being metal-independent. GT-C fold enzymes consist of multiple hydrophobic transmembrane helices and generally use lipid-donors. Bottom: Inverting and retaining mechanisms of GTs. Inverting enzymes use an S_N-2-like mechanism resulting in an inversion in stereochemistry at the anomeric carbon. While retaining mechanism is still unknow, it is believed that a S_Ni-like reaction occurs. The donor phosphate oxygen acts as a base catalyzing the removal of a proton from the acceptor's hydroxyl. Orange oxygen atoms represent the catalytic base in each reaction.

A wide array of GT acceptors have been identified such as carbohydrates, proteins, lipids, DNA, and small molecules (Rini and Esko 2015). A monosaccharide has multiple hydroxyls, sites at which a glycosidic bond can form. The formation of glycosidic bonds can occur through inverting (α→β) or retaining (α→α) mechanisms, which can alter the stereochemistry at the anomeric center of the glycosyl donor (Figure 1.2 Bottom). To date, very few GTs have been found to use more than one substrate or form multiple linkages (Kukowska-Latallo et al. 1990;

Kitagawa et al. 1999; Senay et al. 2000; Schmid et al. 2016). In addition to variations in stereochemistry and composition, glycans can be post-glycosylationally modified by acetylation, sulfation, methylation, phosphorylation, and lactylation, which further increases glycan diversity (Yu and Chen 2007). Together these mechanisms lead to remarkable glycan diversity compared to other macromolecules like proteins, nucleic acids, and lipids. Notably, bacterial glycans have a ten-fold greater diversity at a monosaccharide level compared to eukaryotic glycans (Herget et al. 2008). This is important in bacterial physiology; for example these glycans are typically displayed at the surface where they can play important roles in specific recognition events dictating host-microbe interactions (Schäffer and Messner 2017).

Discovery of bacterial N-linked protein glycosylation

Bacteria were once thought to be unable to glycosylate proteins. However, in 1999, *Campylobacter jejuni* was shown to possess a N-linked protein glycosylation system, located on the 17-Kb protein glycosylation locus, or *pgl* locus (Szymanski et al. 1999). Since then, four types of protein glycosylation systems have now been identified, O, N, C, and S-linked, all four having been identified in bacteria. To date most studies have focused on N- and O-linked glycosylation which are ubiquitous in prokaryotes and eukaryotes.

N-linked protein glycosylation has been found in all domains of life and consists of largely conserved biosynthesis mechanisms and biological roles. This process involves the covalent attachment of an oligosaccharide or glycan to the asparagine residue of a protein. It was discovered by Szymanski et al. in 1999, where the authors demonstrated that *C. jejuni* may produce glycoproteins with associated potential functions (Szymanski et al. 1999). Subsequent studies provided deeper insight into the mechanisms and functions of the *pgl* loci in *C. jejuni*.

Additional orthologous *pgl* systems have been found in all *Campylobacter* species in addition to other ε- and δ-*Proteobacteria* such as select *Helicobacter* spp., *Desulfovibrio desulfuricans*, *Wolinella succinogenes*, *Deferribacter desulfuricans*, *Sulfurovum* sp., *Nitratiruptor* sp., (Figure 1.3) (Nakagawa et al. 2007; Jervis et al. 2010; Ielmini and Feldman 2011; Nothaft et al. 2012; Mills et al. 2016). It is worth noting that two alternative N-glycosylation systems have now been discovered in bacteria, which perform all glycosylation and conjugations in the cytoplasm (Gross et al. 2008; Naegeli et al. 2014). The *pgl* gene nomenclature also applies to the O-linked protein glycosylation system in *Neisseria meningitidis* (Faridmoayer et al. 2007; Schulz et al. 2013; Harding et al. 2015). For the purposes of this work, N-glycosylation and *pgl* are represent the N-glycosylation system in *Campylobacter* and other select species in δ- and ε- *Proteobacteria* family.

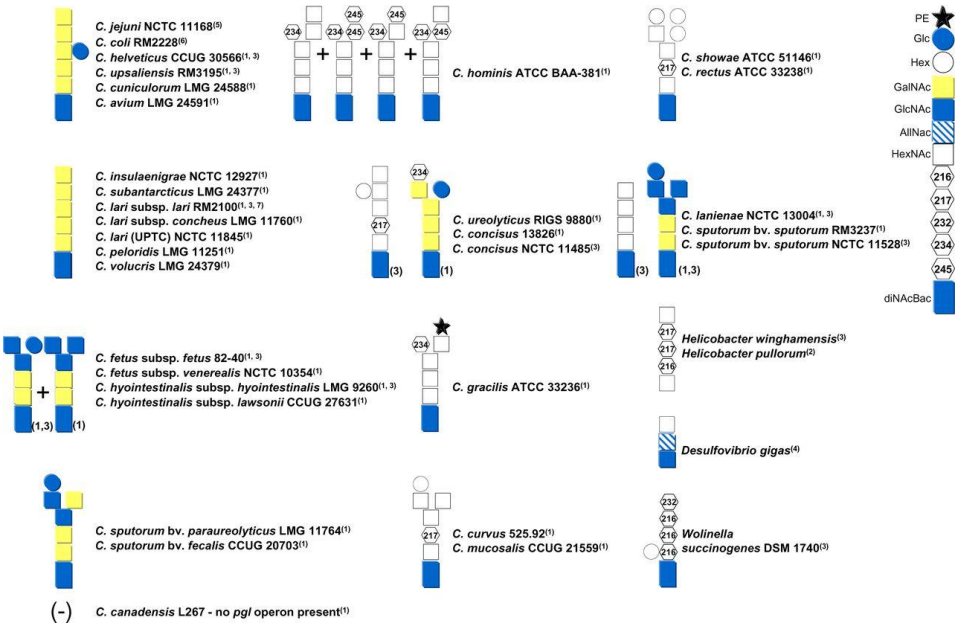

Figure 1.3. Orthologous *pgl* N-glycan structures (Nothaft and Szymanski 2013). The numbers in parentheses next to strain designation represent the works associated with the structure. Additionally, number in parentheses appearing next to the N-glycan represent differences in reported structures. 1, (Nothaft et al. 2012); 2 (Jervis et al. 2010); 3, (Jervis et al. 2012); 4, (Santos-Silva et al. 2007); 5, (Young et al. 2002); 6, (Szymanski et al. 2003); 7, (Ielmini and Feldman 2011).

Initially the *pgl* locus, specifically *pglA* to *pglG*, was believed to be involved in LPS biosynthesis due to high gene homology with LPS machinery and that expression of the *pgl* locus in *E. coli* resulted in modifications in the LPS structure (Korolik et al. 1997; Fry et al. 1998). However, mutagenesis of *pgl* genes in *C. jejuni* did not yield LPS or LOS alterations (Szymanski et al. 1999). Instead, disruption of these genes resulted in a significant decrease in the immunoreactivity of several *C. jejuni* proteins (Szymanski et al. 1999). This observation led to the conclusion that this locus is involved in protein glycosylation and not in the LPS biosynthesis pathway. This discovery led to advances in both basic and applied glycobiology, the latter being in bioengineered vaccines and glycoconjugates (Lizak et al. 2011; Nothaft and Szymanski 2013; Perez et al. 2017).

N-glycosylation biosynthesis

The *C. jejuni pgl*, N-glycosylation system, is the best characterized and the modern model for studying N-linked protein glycosylation in bacteria. In general, cytoplasmic nucleotide-linked sugars are assembled on the lipid carrier, undecaprenyl-phosphate (Und-P), via *pgl* GTs. The result is a conserved heptasaccharide structure, which is translocated into the periplasm and transferred to Asn of a protein or released as free oligosaccharide (fOS) by the oligosaccharyl transferase PglB (Figure 1.4) (Szymanski et al. 2003; Kelly et al. 2006). This process is initiated by the transfer of 2,4-diamino-2,4,6-trideoxy-D-glucose (diNAcBac) to Und-P via PglC. Prior to this, diNAcBac is synthesized by the sequential action of three Pgl enzymes, PglF (dehydratase), PglE (amino transferase) and PglD (acetyltransferase) on the uridine di-phosphate (UDP)-HexNAc (Glover et al. 2005; Linton et al. 2005; Morrison and Imperiali 2013). Subsequently, α1→3-linked GalNAc is added to Und-P-diNAcBac by PglA. After PglJ adds the required α1→4-linked GalNAc residue PglH is able extend the glycan by three GalNAc residues

forming a hexasaccharide (Glover et al. 2005; Glover et al. 2006). Interestingly, PglH controls glycan additions through a ruler helix, which limits the addition to three GalNAc residues (Ramírez et al. 2018). Addition of the final branching β1→3-glucose residue is carried out by the PglI enzyme, which completes the heptasaccharide lipid-linked oligosaccharide (LLO) (Glover et al. 2005; Troutman and Imperiali 2009). After the heptasaccharide is assembled the LLO is translocated into the periplasm via the ATP-driven flippase, PglK (Kelly et al. 2006; Alaimo et al. 2006; Perez et al. 2017). Through a high-resolution structure and simulations, PglK has been shown to accumulate a higher concentration of LLO, likely to facilitate translocation across the inner membrane into the periplasm (Perez et al. 2017; Perez et al. 2019).

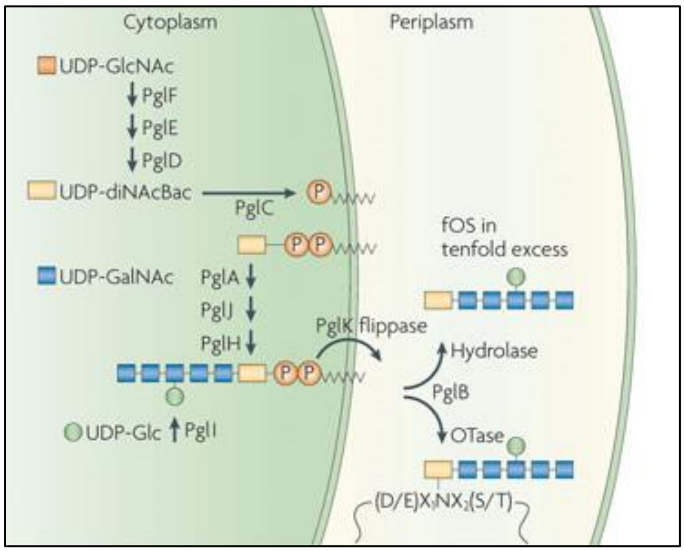

Figure 1.4. The *pgl* biosynthesis pathway in *C. jejuni* (Modified without permission (Nothaft and Szymanski 2010). Various *pgl* glycosyltransferases utilize nucleotide-linked sugars to synthesize the N-glycan, prior to the transfer of the initiating sugar diNAcBac to the lipid-carrier. The completed glycan is then flipped into the periplasm by PglK where it can be released as free oligosaccharide (fOS) or transferred to the Asn by the OST, PglB.

The key enzyme involved in the transfer of the N-glycan from the LLO onto a protein's Asn in a consensus sequence is the oligosaccharyltransferase (OST) PglB (Wacker et al. 2002; Nothaft and Szymanski 2010). It was further demonstrated that PglB has promiscuous substrate

specificity with the exception that the reducing end monosaccharide contains an acetamido group (Wacker et al. 2006; Jervis et al. 2012; Nothaft et al. 2012). In *E. coli*, PglB's has been shown to transfer various LPS structures, eukaryotic glycans, and monosaccharides to various protein acceptors (Wacker et al. 2002; Feldman et al. 2005; Kowarik et al. 2006; Wacker et al. 2006; Valderrama-Rincon et al. 2012; Wetter et al. 2012). However the acceptor protein requires an extended consensus sequon, (D/E)-X-N-X-(S/T), where X is any amino acid except proline and N is the site of glycosylation (Kowarik et al. 2006; Nothaft and Szymanski 2010; Yates et al. 2018). Only sequons found on exposed flexible loops are accessible for glycosylation (Rangarajan et al. 2007). This system only glycosylates folded proteins in *C. jejuni*; however it has been shown that PglB is also capable of glycosylating unfolded proteins (Wacker et al. 2006).

In addition to transferring the N-glycan to proteins, PglB can also release the N-glycan into the periplasm, through hydrolytic activity, as free oligosaccharides (fOS) (Nothaft et al. 2009; Nothaft and Szymanski 2010; Dwivedi et al. 2013). It is believed that fOS is important for osmoregulation in *C. jejuni* (Nothaft et al. 2009; Dwivedi et al. 2013). Interestingly, PglB shares similar mechanisms and structural homology to the eukaryotic STT3 N-glycosylation oligosaccharyltransferase (Maita et al. 2010; Lizak et al. 2011). In addition to being able to use PglB for glycoengineering, the *C. jejuni* N-glycosylation system represents a well-studied model for prokaryotic protein glycosylation.

Biological function of N-glycosylation in *C. jejuni*

All studies on the biological function of N-glycosylation in bacteria were only performed in *C. jejuni* (Figure 1.5). The first assessment of the N-glycosylation system indicated that N-glycosylated proteins were immunoreactive (Szymanski et al. 1999). This was further confirmed

through *pgl* mutants and N-glycan based vaccine studies indicating that the N-glycan is recognized by immune sera in mice, chickens, rabbits, and humans (Szymanski et al. 2002; Ketley and Konkel 2005; Nothaft et al. 2012; Nothaft et al. 2016; Nothaft et al. 2017). Furthermore the *C. jejuni* N-glycan was also recognized by the innate immune system through a C-type lectin, MGL (macrophage galactose lectin), which recognizes N-acetylgalactosamine (van Sorge et al. 2009). This indicated that the *C. jejuni* N-glycan is recognized by the innate and adaptive immune system.

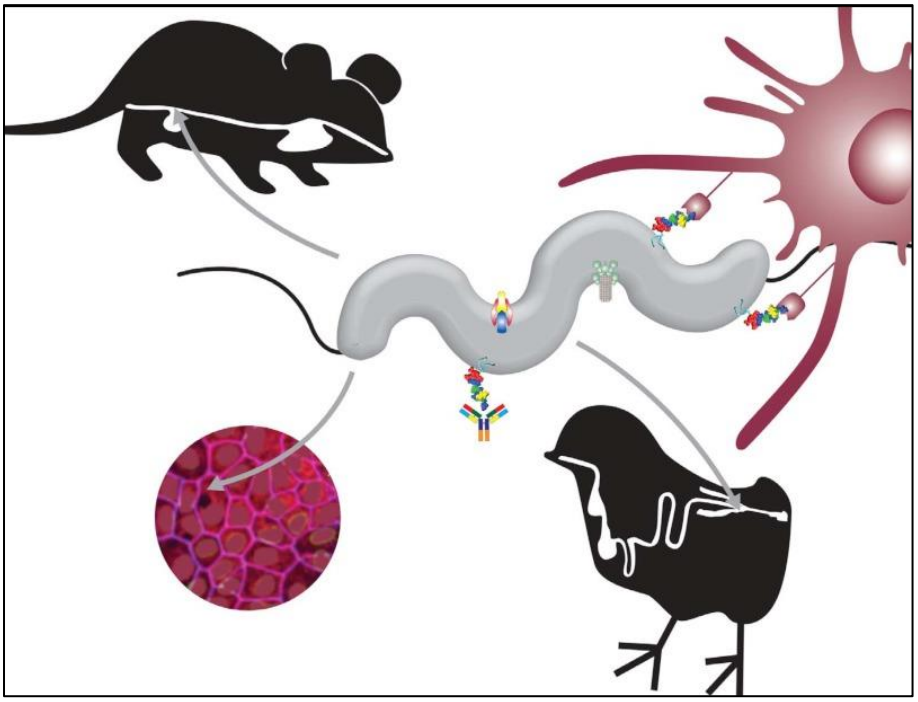

Figure 1.5**.** Function of *C. jejuni* N-glycosylation (Nothaft and Szymanski 2013). Studies in *C. jejuni* N-glycosylation indicate that it is important in intestinal cell adhesion, host colonization, recognition of the immune system, and is essential in protein complexes, such as the CmeABC multidrug efflux pump and the type IV secretion system.

C. jejuni is a major foodborne pathogen, and is predominantly found in chickens as commensal (Humphrey et al. 2014). Multiple studies have connected N-glycosylation-deficient strains to decreased colonization in mice and chickens (Szymanski et al. 2002; Hendrixson and DiRita 2004; Szymanski and Wren 2005; Abouelhadid et al. 2019). This decreased colonization

may be due to the N-glycan protecting exposed loop regions of glycoproteins from self and endogenous proteases (Alemka et al. 2013; Cain et al. 2019). N-glycosylation was also found to influence bacterial invasion and adherence to cultured intestinal cells (Szymanski et al. 2002; Hendrixson and DiRita 2004; Szymanski and Wren 2005). Together these studies indicate that N-glycosylation plays a role in *C. jejuni* colonization. These findings were essential in developing a *C. jejuni* vaccine targeting the N-glycan; these trials showed a significant reduction in *C. jejuni* colonization of chickens (Nothaft et al. 2016; Nothaft et al. 2017).

Prior proteomics studies have indicated that the *pgl* system can N-glycosylate ~80 proteins in *C. jejuni*, most of which have no known function (Young et al. 2002; Kowarik et al. 2006; Houliston et al. 2011; Scott et al. 2011; Nothaft et al. 2012; Scott et al. 2012; Scott et al. 2014; Cain et al. 2019). These proteins can be found in the periplasm, associated with the inner or outer membrane, or are surface-exposed lipoproteins. The considerable number of N-glycosylated proteins among the *C. jejuni* glycoprotein pool reflects the importance of this pathway, but also presents difficulty in uncovering the biological role of N-glycosylation due to multiple and pleiotropic effects.

Glycoproteins mutated so as to be unglycosylated resulted in no cell impairment or altered protein function (Larsen et al. 2004; Kakuda and DiRita 2006; Davis et al. 2009; Flanagan et al. 2009; Scott et al. 2009; Kakuda et al. 2012). However in 2004, Larsen et al. showed that the N-glycans added to the VirB10 periplasmic protein of the type IV secretion system resulted in decreases in DNA uptake and natural transformation (Larsen et al. 2004). Another study found that the removal of two N-glycosylation sites in CmeA resulted in a phenotype similar to a *cmeA* mutant (Dubb et al. 2019). This protein is part of the CmeABC multidrug efflux pump, which consists of three N-glycosylated proteins, which are essential to

the removal of antibiotics and bile salts in *C. jejuni* (Nita-Lazar et al. 2005; Kowarik et al. 2006; Scott et al. 2011; Dubb et al. 2019). Molecular dynamic stimulations and *in vitro* models of CmeA indicate that glycosylation plays no role in complex formation or association with peptidoglycan (Dubb et al. 2019). Efflux assays of cells expressing non-glycosylated forms of CmeA and CmeB had the lowest efflux activity compared to wild-type and *cmeA* or *cmeB* mutants (Abouelhadid et al. 2019). This would suggest that N-glycosylation has a larger role in maintaining molecule trafficking. *E. coli* expressing glycosylated CmeABC showed enhanced efflux and increased antibiotic sensitivity compared to unglycosylated CmeABC (Dubb et al. 2019). Numerous studies have noted decreases in antibiotic resistance in N-glycosylation-deficient strains, which may be due to deficiencies in the CmeABC complex (Abouelhadid et al. 2019; Cain et al. 2019; Dubb et al. 2019).

Mutations in *pglB*, N-glycosylation-deficient, resulted in considerably changes cell physiology (Abouelhadid et al. 2019; Cain et al. 2019). Proteomics studies found decreased activity in the NapAB, a nitrate reductase system (Abouelhadid et al. 2019; Cain et al. 2019). This decrease in activity is likely due to NapB being N-glycosylated at ^{50}N (Pittman et al. 2007; Scott et al. 2011). In general, *pglB* mutants had decreases in enzymes involved in the synthesis of the lipid carrier Und-P (Abouelhadid et al. 2019). These cells lacked the traditional helical shape associated with pathogenicity and instead were rod shaped with sporadic cell lengths (Abouelhadid et al. 2019). Although the *C. jejuni* flagella is O-glycosylated and not N-, *pglB* mutants have decreased motility, which could be attributed to decreased proton motive force through pleiotropic effects (Scott et al. 2012; Cain et al. 2019). Furthermore these mutants did not chemotactically respond to α-ketoglutarate or Glu, and they had reduced chemotaxis to Asp and succinate (Cain et al. 2019). This correlated with alterations in Tlp chemoreceptor-like

protein levels, which is necessary for chemoattractant sensing (Cain et al. 2019). All *pglB* mutants had altered cell stress factor proteins leading to reduced survival due to temperature changes (4°C and 46°C), or to osmotic shock, and they show enhanced biofilm formation (Cain et al. 2019). In conjunction, these mutants also had increases in predominantly periplasmically-localized chaperones and proteases, suggesting that there may be increased misfolding and aggregation of proteins (Abouelhadid et al. 2019; Cain et al. 2019). Together these studies indicate that N-linked protein glycosylation plays an important role in *C. jejuni* physiology and pathogenesis.

Campylobacter fetus pathogenesis

Campylobacter fetus is a microaerophilic, gram-negative, spiral-shaped, non-thermotolerant *Campylobacter* that can grow between 25°C and 37°C. Thermotolerant *Campylobacters* like *C. jejuni* and *C. lari* are able to grow at a higher temperature (42 °C) which is consistent with their host body temperature (Nothaft and Szymanski 2010; Nothaft et al. 2012). *Campylobacter fetus* is an emerging pathogen that is generally associated with venereal disease, infertility or abortions in cattle and sheep, or systemic infections in humans (Thompson 2005; Wagenaar et al. 2014). This species consists of three subspecies, *C. fetus* subsp. *fetus* (*Cff*), *C. fetus* subsp. *venerealis* (*Cfv*) and *C. fetus* subsp. *testudinum* (*Cft*), which have been assigned due to their niche. *Cfv* is almost exclusively found in bovine genital tracts where it can cause BGC (Bovine genital *Campylobacter*iosis) or BVC (bovine venereal *Campylobacter*iosis) leading to venereal disease and abortions in cattle (Mshelia et al. 2010). In contrast, *C. fetus* subsp. *fetus* can colonize a broader host range including sheep, humans, cattle and birds (Gilbert et al. 2016; Van Der Graaf-Van Bloois et al. 2016). *C. fetus* subsp. *testudinum* is a newly

sequenced isolate found in reptiles, predominantly turtles, and has also been found to colonize humans (Fitzgerald et al. 2014; Wang et al. 2015).

In 1947 and 1957, cases of *C. fetus* (previously called *Vibrio fetus*) causing systemic infections and an abortion in humans was documented (Spink 1957; Franklin and Ulmer 1974). The majority of human *C. fetus* infections occur in men indicating either increased exposure or a predisposition to *C. fetus* colonization (Tremblay et al. 2003; Patrick et al. 2013). Most patients are older than 60, immunocompromised, or have some other underlying condition (Patrick et al. 2013; Wagenaar et al. 2014). Until the discovery of *Cft*, *Cff* has been the reported cause of nearly all *C. fetus* infections (Wagenaar et al. 2014). Although human *C. fetus* infections are rare there have been documented outbreaks in small communities (1981; Morooka et al. 1992; Wagenaar et al. 2014). The majority of human cases may be lower due to inadequate culturing methods and diagnostic limitations (Wagenaar et al. 2014).

The majority of *C. fetus* infections result in septicemia, which represent the majority of *Campylobacter*-mediated septicemia (Maertzdorf and Mouton 1974; Guerrant et al. 1978; Pacanowski et al. 2008; Fernández-Cruz et al. 2010; Marchand-Senécal et al. 2017). Most septicemia cases involve fever with no signs of localized infection (Gazaigne et al. 2008; Pacanowski et al. 2008). In addition to septicemia, *C. fetus* has caused neurological infections, bone and genital infections, arthritis, and lung abscesses (Man 2011; Wagenaar et al. 2014). Approximately 30% of all cases develop acute diarrhea similar to *C. jejuni* infections (Blaser 1988; Skirrow et al. 1993; Gazaigne et al. 2008). In some rare circumstances, *C. fetus* has caused spontaneous abortions or fetal sepsis in humans, similar to infection outcomes in cattle and sheep (Fujihara et al. 2006). In infants, subsequent infections usually result in meningitis

(Fujihara et al. 2006). Although limited on data, one study determined that *C. fetus* has a fatality rate of 14% of in humans (Gazaigne et al. 2008).

The route of *C. fetus* transmission into humans remains unclear, but is likely due to exposure from host animals or consuming uncooked meat (Patrick et al. 2013; Wagenaar et al. 2014). In China, the majority of cases *Cft* infections are likely due to consumption of dishes consisting of turtles or reptiles (Patrick et al. 2013). In contrast, a new study proposed that *C. fetus* is a human pathobiont with it being found in 8% of healthy human stool metagenomes (Iraola et al. 2017). Furthermore, using sequence comparisons they proposed that all cattle-based *C. fetus*, *Cfv*, was acquired from humans during cattle domestication (Iraola et al. 2017). This is supported by the absence of *Cfv* in humans; conversely human-associated strains have caused infections in cattle (Marcel A.P. Van Bergen et al. 2005; M. A.P. Van Bergen et al. 2005; Iraola et al. 2017).

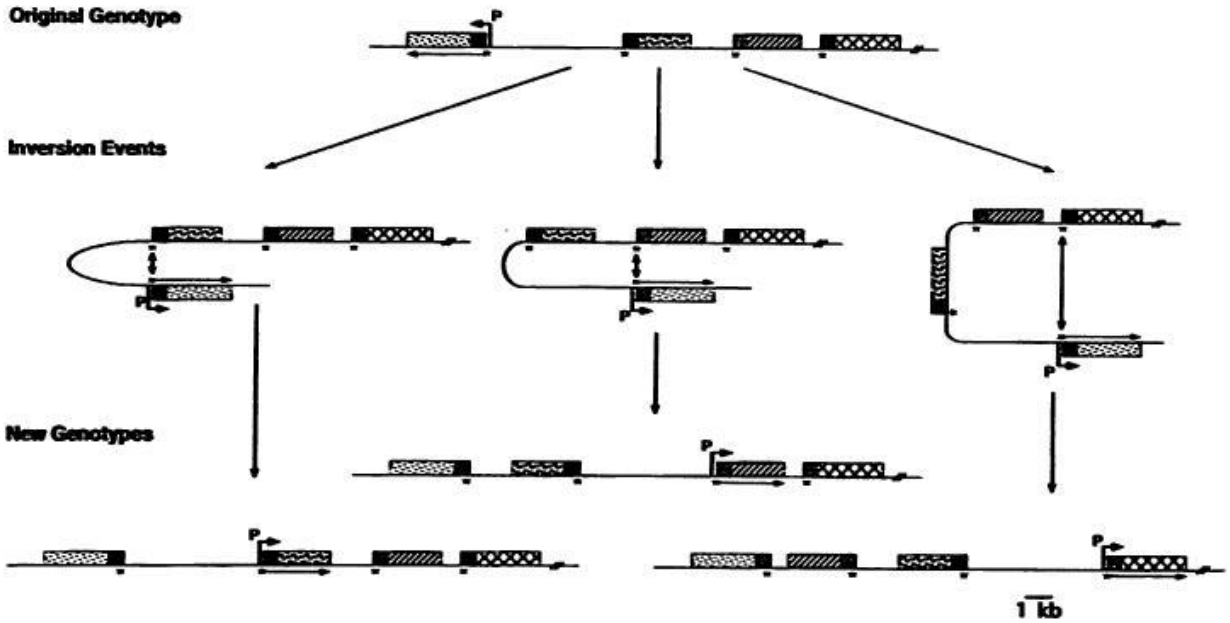

Figure 1.6. Mechanism of surface array protein (*sapA/B*) genetic inversion (Thompson 2002). The black square represents the 5' conserved region in the *sapA/B* genes. The shaded boxes represent genetic variability in the *sapA/B* genes. These *sapA/B* copies can be expressed once inverted into the promoter region, bent arrow, leading to the expression of antigenically different SapA/B proteins.

C. fetus infections can persist for as long as 7 years through multiple relapses (Neuzil et al. 1994; Ganeshram et al. 2000; Tu et al. 2005). This persistence is likely due to its surface layer (S-layer) proteins, which provide evasion from the immune system. This S-layer coating is a paracrystalline capsule-like protein coat that covers the exterior of the bacteria. The S-layer in *C. fetus* can confer serum and phagocytosis resistance through prevention of complement and antibody binding to the bacteria (Blaser et al. 1988). S-layer also obscures LPS from the LPS recognizing epitopes of the immune system (McCoy et al. 1975; Fogg et al. 1990).

The *C. fetus* S-layer can also alter the bacterium's surface antigen repertoire by switching its surface array protein (sapA/B) with up to 8 different protein variants (Dworkin and Blaser 1997; Thompson 2002). This likely occurs through genetic inversion of a *sapA/B* variant into the *sap* promoter through recombination of the conserved 5' region of the *sap* genes (Figure 1.6)(Tummuru and Blaser 1993; Thompson 2002). S-layer protein and LPS can consist of two associating sap-/sero-types (type), called type A and B (Yang et al. 1992; Dworkin et al. 1995b; Casadémont et al. 1998; Thompson 2002). Interestingly, type A is most commonly associated with pathogenesis suggesting a potential mechanism of pathogenesis (Kienesberger et al. 2014).

In addition to S-layer, *C. fetus* can contain up to 4 different type IV secretion systems, which are essential for adapting to host environments (Gorkiewicz et al. 2010; Kienesberger et al. 2014; Van Der Graaf-Van Bloois et al. 2016). It is currently believed that the type IV secretion system is used for intraspecies horizontal gene transfer. These type IV encoding regions correlate with subspecies and not strain type (Van Der Graaf-Van Bloois et al. 2016). In some of these encoding regions are fic (filamentation induced by cAMP) genes, which can alter host cell processes for survival (Van Der Graaf-Van Bloois et al. 2016). Together these mechanisms may explain the broad host range and increased septicemia of *C. fetus*.

C. fetus N-glycosylation

A glycomics analysis of all *Campylobacter* N-glycans revealed that non-thermophilic *Campylobacter* species were able to produce more than one N-glycan structure (Nothaft et al. 2012). In contrast, *C. jejuni* consistently produce the same heptasaccharide N-glycan (Scott et al. 2011). Analysis of *C. fetus* fOS and N-glycans showed that it was able to produce two hexasaccharide structures (Nothaft et al. 2012; Dwivedi et al. 2013). These structures were found in a ratio of 4:1, where the major N-glycan consists of a terminal branching N-acetylglucosamine and the minor hexasaccharide substituted with a glucose (Figure 1.7) (Nothaft et al. 2012). Both major and minor N-glycans share the same branching linkage of α1→6 to the backbone of the N-glycan.

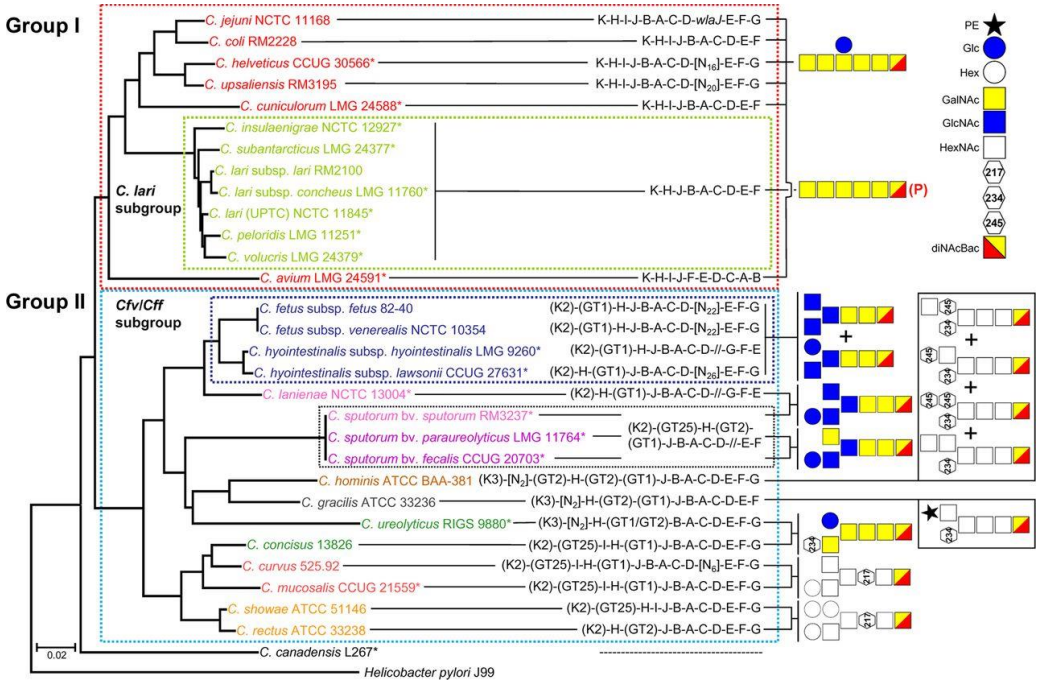

Figure 1.7. *Campylobacter pgl* loci and subsequent N-glycan and fOS structure (Nothaft et al. 2012). *Campylobacter* species were arranged in a dendrogram based on their AtpA protein. Within this tree two groups were defined group I, the thermotolerant *Campylobacters*, and group II, the non-thermotolerant species. N-glycan diversity appears to only be a feature found in group II *Campylobacter* species, which correlates with changes in *pgl* genes. GT, represents undefined *pgl* genes and their associated CAZy family number. Single letters represent the previously defined *pgl* locus genes.

Changes in the N-glycan terminus is likely attributed to unannotated GTs in the *C. fetus* locus (Figure 1.8). Previously this locus was annotated as having a PglH GT and two PglK flippases (Nothaft and Szymanski 2010; Jervis et al. 2012; Nothaft et al. 2012). However, *C. fetus* lacks the three terminal GalNAc residues indicative of PglH activity and recent improvements in bioinformatics indicates that there is only one PglK (Ramírez et al. 2018). Interestingly, when the *C. fetus pgl* GTs were expressed in a *E. coli/C. jejuni* hybrid expression system only fragments of the minor N-glycan was observed (Jervis et al. 2012). In between *gne* (encoding UDP-glucose 4-epimerase) and *ugd* (encoding UDP-glucose 6-dehydrogenase), there is an additional three gene hypothetical glucosylation operon. This operon is similar to three-component systems, that can transfer a monosaccharide to a carbohydrate structure in the periplasm (Mann and Whitfield 2016). The *C. fetus* locus also shares homologs with other unannotated *pgl* GT in other non-thermotolerant *Campylobacter* species.

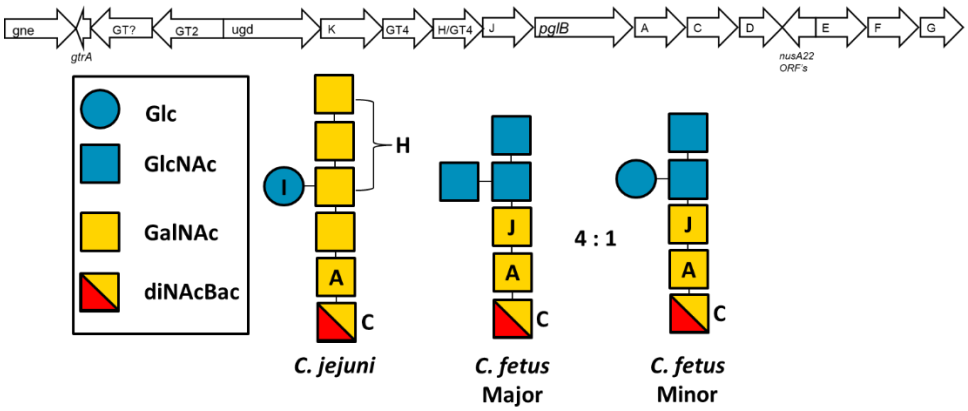

Figure 1.8. *Campylobacter fetus* N-glycosylation locus and N-glycan compared to *C. jejuni*. Annotated *pgl* locus from *C. fetus* subsp. *fetus* strain 82-40. Individual letters represent the annotated *pgl* genes in *C. jejuni*. The *C. fetus* N-glycan consists of predicted *pgl* enzyme function based on the *C. jejuni pgl* enzymes and homology. GT, represents predicted CAZy glycosylation families. The region *nusA22* represents 22 ORF's between *pglD* and *pglEFG*.

Changes in the terminal monosaccharide in *Campylobacter* N-glycans may be due to recognition by the immune system. In the case of *C. jejuni*, only the chicken C-type lectin has been shown to bind GlcNAc, while human C-type lectin binds the GalNAc residues on the *C.*

jejuni heptasaccharide (Burrows et al. 1997; van Sorge et al. 2009). Bovine lectins preferentially bind β-linked GlcNAc over α-linked GlcNAc, which is found on the *C. fetus* N-glycan (Nothaft et al. 2012; Jégouzo et al. 2020). Suggesting that N-glycan termini may play a role in host recognition.

The benefit of using *C. fetus* as a model for studying N-glycan diversity in prokaryotes is that it has the potential to be genetically manipulated (Kienesberger et al. 2007). *C. fetus* also represents a known veterinary and human pathogen. Therefore, understanding the *C. fetus* N-glycan biosynthesis in molecular detail could be a useful for bioengineering a N-glycan conjugate, such as a vaccine or diagnostic tool (Nothaft et al. 2012; Nothaft et al. 2016; Nothaft et al. 2017).

CHAPTER 2

INFLUENCE OF PROTEIN GLYCOSYLATION ON *CAMPYLOBACTER FETUS* PHYSIOLOGY[1]

[1]**Duma, J.**, Nothaft, H., Weaver, D., Fodor, C., Beadle, B., Linton, D., Benoit, S., Scott, N. E., Maier, R., Szymanski, C.M., June 7, 2020. *Frontiers of Microbiology.* (Special Issue). Reprinted here with permission.

Abstract

Campylobacter fetus is commonly associated with venereal disease and abortions in cattle and sheep and can also cause intestinal or systemic infections in humans that are immunocompromised, elderly, or exposed to infected livestock. It is also believed that *C. fetus* infection can result from the consumption or handling of contaminated food products, but *C. fetus* is rarely detected in food since isolation methods are not suited for its detection and the physiology of the organism makes culturing difficult. In the related species, *Campylobacter jejuni*, the ability to colonize the host has been linked to N-linked protein glycosylation and a label-free quantitative (LFQ) proteomics approach demonstrated that N-glycosylation is interconnected with cell physiology. Using LFQ, we found more than 100 proteins significantly altered in expression in two *C. fetus* subsp. *fetus* protein glycosylation (*pgl*) mutants (*pglX* and *pglJ*) compared to the wildtype. Significant increases in the expression of the [NiFe]-hydrogenase HynABC, catalyzing H_2-oxidation for energy harvesting, correlated with significantly increased levels of cellular nickel, improved growth in H_2, and increased hydrogenase activity, suggesting that N-glycosylation in *C. fetus* is involved in regulating the HynABC hydrogenase and nickel homeostasis. To further elucidate the function of the *C. fetus pgl* pathway and its enzymes, heterologous expression in *E. coli* followed by mutational and functional analyses revealed that PglX and PglY are novel glycosyltransferases involved in extending the *C. fetus* hexasaccharide beyond the conserved core, while PglJ and PglA have similar activities to their homologues in *C. jejuni*. In addition, the *pgl* mutants displayed a decreased motility and ability to efflux ethidium bromide and showed an increased sensitivity to antibiotics. This work not only provides insight into the unique protein N-glycosylation pathway

of *C. fetus*, it also expands our knowledge on the influence of protein N-glycosylation on *Campylobacter* cell physiology.

Introduction

Asparagine-linked protein glycosylation is a post-translational modification present in species from all three domains of life. The prototypical bacterial protein N-glycosylation system (referred to as *pgl*) was first identified in *Campylobacter jejuni* over two decades ago (Szymanski et al. 1999). This system utilizes five glycosyltransferases (*pglA, pglC, pglH, pglI, pglJ*) to produce the heptasaccharide GalNAc-α1,4-GalNAc-α1,4-[Glc-β1,3-]GalNAc-α1,4-GalNAc-α1,4-GalNAc-α1,3-diNAcBac-β1,N-Asn (diNAcBac is 2,4-diacetamido-2,4,6-trideoxyglucopyranose) which is attached to protein (Figure 2.1) (Glover et al. 2005; Linton et al. 2005; Glover et al. 2006). The assembly of the full-length glycan occurs on the cytoplasmic side of the inner membrane through the sequential transfer of nucleotide-activated sugars onto the lipid carrier undecaprenyl-phosphate. The lipid-linked heptasaccharide is then flipped into the periplasm by the flippase PglK (Kelly et al. 2006; Alaimo et al. 2006) and transferred to the asparagine residue within the consensus sequon D/E-X_1-N-X_2-S/T (where X_1, X_2 can be any amino acid except proline) by the oligosaccharyltransferase PglB (Kowarik et al. 2006; Chen et al. 2007; Scott et al. 2011), or is released as free oligosaccharide (Nothaft et al. 2009), a process that is conserved among *Campylobacter* species (Nothaft et al. 2012). In *C. jejuni*, the conserved heptasaccharide has been found on more than 80 periplasmic and membrane-bound proteins (Scott et al. 2011; Cain et al. 2019). Mutagenesis of the *pgl* genes indicates that this glycosylation system impacts multiple cell functions including: (i) colonization of chickens and mice; (ii) adherence and invasion of epithelial cells; (iii) functionality of the multidrug efflux complex CmeABC; (iv) stability of the type IV secretion system; and (v) interactions with the

immune system (Nothaft and Szymanski 2013; Dubb et al. 2019). More specifically, two recent proteomics studies of *C. jejuni pglB* mutants have revealed multiple physiological functions associated with N-glycosylation (Abouelhadid et al. 2019; Cain et al. 2019). These include increased expression of stress response proteins, decreased survival in high temperature and osmolarity, altered metabolic activities, decreased chemotaxis, impaired efflux, and decreased nitrate reductase activity (Abouelhadid et al. 2019; Cain et al. 2019).

Orthologues of the *pgl* pathway have been found in all *Campylobacter* spp., select *Helicobacter* spp. *Desulfovibrio desulfuricans*, *Wolinella succinogenes*, *Deferribacter desulfuricans*, *Sulfurovum* sp., *Nitratiruptor* sp., and some less characterized δ- and ε-Proteobacteria (Nakagawa et al. 2007; Jervis et al. 2010; Ielmini and Feldman 2011; Nothaft et al. 2012; Mills et al. 2016). Despite the conservation of the *pgl* pathway per se, different *Campylobacter* species produce N-glycans that vary in structure and composition (Jervis et al. 2012; Nothaft et al. 2012). This is particularly evident among the non-thermotolerant *Campylobacter* species which produce multiple N-linked glycoforms (Jervis et al. 2012; Nothaft et al. 2012). For instance, *Campylobacter fetus* synthesizes two distinct N-linked hexasaccharides: the major GlcNAc-α1-6-[GlcNAc-β1-3]-GlcNAc-α1-4-GalNAc-α1-4-GalNAc-α1-3-diNAcBac-β1,N-Asn and the minor GlcNAc-α1-6-[Glc-β1-3] -GlcNAc-α1-4-GalNAc-α1-4- GalNAc-α1-3-diNAcBac-β1,N-Asn at a 4:1 ratio, respectively (Nothaft et al. 2012).

C. fetus grows best between 25ºC and 37ºC and consists of three subspecies: *C. fetus* subsp. *fetus* (*Cff*), *C. fetus* subsp. *venerealis* (*Cfv*), and the more recently described subspecies *C. fetus* subsp. *testudinum* (*Cft*) thought to originate from reptiles, but also has been associated with human infections (Patrick et al. 2013; Fitzgerald et al. 2014). *Cff* has the broadest host range and

is found in cattle, sheep, reptiles, and humans (Tu et al. 2004; Wagenaar et al. 2014). In livestock, both *Cfv* and *Cff* are known to cause reproductive failure and infertility (Duncan et al. 2014), and although *Cfv* has been isolated from humans, it only causes disease in cattle (Holst et al. 1987). The majorities of human *C. fetus* infections are attributed to *Cff* and are associated with meningitis, acute diarrhea and most commonly bacteremia (Wagenaar et al. 2014). Human infections are generally sporadic, with only a few reported outbreaks (Klein et al. 1986; Marchand-Senécal et al. 2017). Recent metagenomic analysis found *C. fetus* in 8% of feces from healthy humans, suggesting it is a possible pathobiont (Iraola et al. 2017).

In this study, we examined the role of several *C. fetus pgl*-encoded glycosyltransferases through mutagenesis and functional transfer into *Escherichia coli*. We demonstrate that the *Cff*-PglA and *Cff*-PglJ homologues have the same function as their counterparts in *C. jejuni* building the conserved GalNAc-α1,4-GalNAc-α1,3-diNAcBac reducing-end core. PglX (previously annotated as PglH1) and PglY (previously annotated as PglH2) are associated with the biosynthesis of the structurally variable region at the non-reducing end of the *Cff*-hexasaccharides. To assess the potential impact of the N-glycan truncations on other cellular functions, a label-free quantitative proteomics approach was used to examine the *Cff-pglJ* and *pglX* mutants. Proteomics demonstrated widespread changes in protein abundance with a notable impact on metal transport proteins, several [NiFe] hydrogenase subunits, and oxidative response proteins compared to the wildtype. The results presented in this study provide new insights into the assembly and roles of N-linked glycoproteins in *C. fetus*.

Results

Characterization of *Cff pgl* cluster

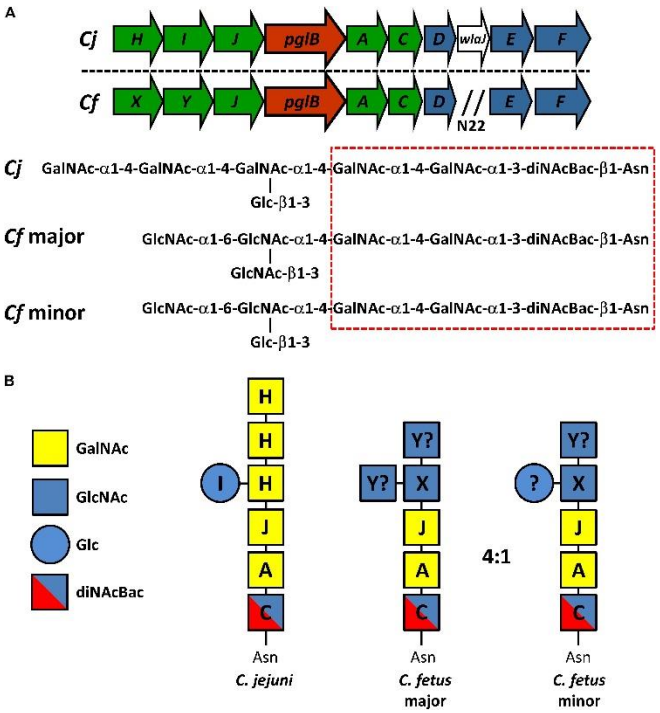

Figure 2.1. Model for the function of the components of the N-linked protein glycosylation (*pgl*) pathway in *C. fetus* (*Cf*) in comparison to *C. jejuni* (*Cj*). Similar to *Cj*, we propose that in *Cf* PglC transfers diNAcBAc which is synthesized by PglDEF (not shown) to undecaprenyl-phosphate (Nothaft and Szymanski 2010). Subsequently, PglA transfers the first GalNAc followed by a second GalNAc residue added by PglJ. To this trisaccharide, PglH transfers three GalNAc residues and PglI subsequently transfers the Glc branch (Kelly et al. 2006).

The *C. fetus* (*Cf*) *pgl* cluster is syntenic with the *C. jejuni* (*Cj*) *pgl* gene cluster (Jervis et al. 2012; Nothaft et al. 2012) apart from lacking *pglI* and possessing two homologues of *pglH* (Figure 2.1). The similarities between the two loci are reflected in their N-glycan structures, with both sharing the same three reducing end sugars. In *C. jejuni*, *pglC*, *pglA* and *pglJ* are responsible for the formation of this initial DiNAcBac-GalNAc2 trisaccharide that is conserved across nearly all *Campylobacter* species (Jervis et al. 2012; Nothaft et al. 2012). Previously, *Cf* was annotated to possess two *pglH* homologues; however, compositional and structural analyses of the *Cf-pgl* pathway products showed that it does not contain the three GalNAc residues added

by the *Cj-pglH* gene product (Nothaft et al. 2012). Since it is the non-reducing end of the *C. jejuni* and *C. fetus* N-glycans that varies in structure, the *pgl* genes in the "variable" glycosyltransferase (GTase) region upstream of *pglB* most likely differ in function. We therefore named the two *pglH* homologues, *pglX* and *pglY* (Figure 2.1). Interestingly, both proteins contain the catalytic EX_7E motif previously annotated in PglH (Cid et al. 2000; Troutman and Imperiali 2009) (Figure 2.2). In addition to this catalytic EX_7E, PglY and PglX contain one and two additional EX_7E motifs, respectively. K68 of *Cj*-PglH, which is believed to be involved in lipid-linked oligosaccharide (LLO) association, is altered to N67 and T70 in PglX and PglY, respectively. In addition, the binding site of the *Cj*-PglH catalytic EX_7E motif that involves L269 and P270 was found to be altered in PglX and PglY. Both enzymes possess a G instead of a P at position P270; however, only PglY possesses an F at position 267 that corresponds to L269 in *C. jejuni*. These minor changes in the amino acid residues may explain the differences in enzyme specificity and the formation of the shorter glycans when compared to *C. jejuni.*

Figure 2.2. Sequence alignment of *C. fetus* (*Cf*) PglX, PglY and *C. jejuni* (*Cj*) PglH. Black boxes indicate specific amino acids associated with activity in PglH (Troutman and Imperiali 2009; Ramírez et al. 2018). Black and dark grey amino acids represent functional residues that show non-conserved substitutions in PglX and PglY. Light grey highlighted sequences indicate EX_7E motifs commonly found in glycosyltransferases (Cid et al. 2000; Coutinho et al. 2003; Troutman and Imperiali 2009). The catalytic EX_7E motif of *Cj* PglH is located at residues E266 to E274. *Cf* PglX CFF8240_1386, *Cf* PglY CFF8240_1385 and *Cj* DDV78_00080 sequences were analyzed by Jalview (Waterhouse et al. 2009).

N-glycan analysis of *Cff pgl* mutants

To assess the functions of the "variable" GTases, we constructed mutants by insertion of a kanamycin resistance cassette (referred to as "kan") into the respective gene loci. Both *pglX* (*pglX::kan*, further referred to as *pglX*-) and *pglJ (pglJ::kan*, further referred to as *pglJ*-) were constructed in the *Cff* strain ATCC 27374 (Figure S1), however multiple attempts at generating mutants in *pglY* were unsuccessful.

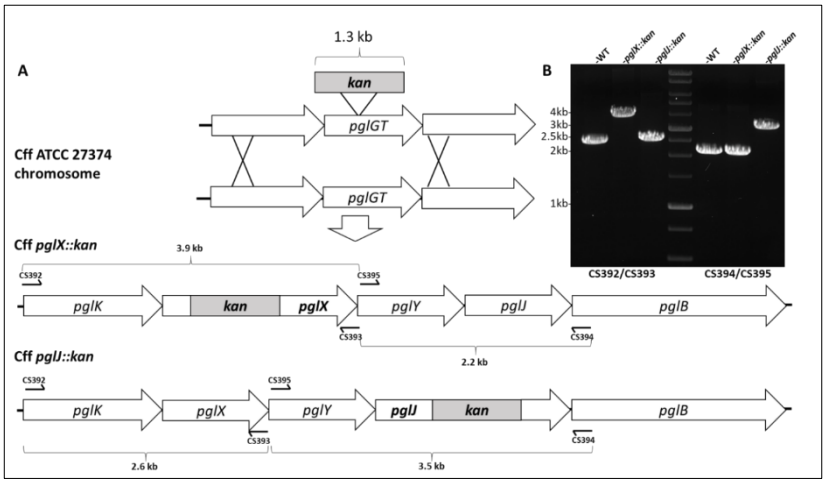

Figure 2.3. Insertional mutagenesis of *pglX* and *pglJ* in *C. fetus* subsp. *fetus* ATCC 27374. (A) The *pgl* genes were inactivated by insertion of the kanamycin resistance gene (*kan*) into the chromosome of *C. fetus* subsp. *fetus* ATCC 27374. PCR products were introduced by electroporation and double-crossover events resulted in the formation of *pglX*- and *pglJ*-. Primer sets CS392/CS393 and CS394/395, were used to confirm the correct insertion of the antibiotic cassette. (B) Agarose gel with PCR products amplified to verify the insertion of the cassette. Genomic DNA from WT or the respective *pgl* mutant strain that was used as template is indicated above each lane. The primer set used for each PCR reaction is indicated below the gel.

Insertion of the *kan* cassette in the *pglJ* and *pglX* genes was verified by PCR with oligonucleotides hybridizing outside of the recombination event (Figure 2.3). When compared to the PCR product size obtained with chromosomal DNA isolated from *Cff*-wildtype, an increase in size by approximately 1.8 kb was observed when the *kan* cassette was present on the respective PCR product, clearly indicating insertion at the correct position within the *Cff* chromosome. To further investigate the effect of the mutations on N-glycan biosynthesis,

western blot analysis of whole cell lysates probed with *Cff*-N-glycan specific serum was performed. Complete loss of serum reactivity in *pglX*- and *pglJ*- was observed when compared to the wildtype (Figure 2.4A). Lectin blotting with WGA confirmed those results, *i.e.* loss of reactivity in whole cell lysates of the *pglJ* mutant and strongly reduced reactivity (with only one signal present) in lysates of the *pglX* mutant (Figure 2.4B, Figure 2.5). Similarly, no free oligosaccharides (fOS) could be detected in the two *pgl* mutants when analyzed by thin layer chromatography (TLC) (Figure 2.4C). Here, two spots for the *Cff*-fOS variants could be seen when a fOS preparation of the wildtype was applied, confirming previous observations (Dwivedi et al. 2013) and these spots were absent in similar preparations from the *pglX*- and *pglJ*- strains.

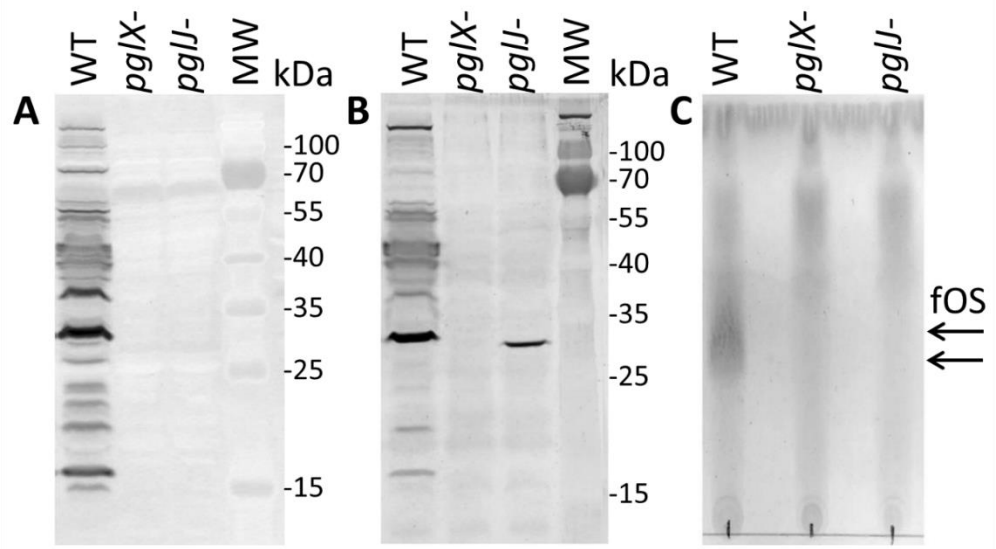

Figure 2.4. Pgl pathway product analysis of *Cf* WT and *pglX*- and *pglJ*- strains. (A) Western blot of whole-cell lysates with *Cff*-N-glycan-specific antiserum, and (B) Wheat germ agglutinin reactivity of whole cell lysates of the WT and the *pglX*- and *pglJ*- strains. (C) Thin-layer chromatography (TLC)-free oligosaccharide (fOS) analysis of WT, *pglX*- and *pglJ*- strains. Molecular weight (MW) markers for the western blots (in kDa) are indicated on the right; arrows indicate the migration of WT fOS on the TLC plate.

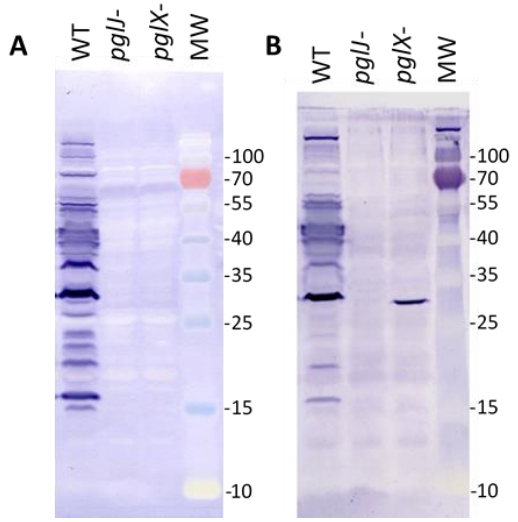

Figure 2.5. Pgl pathway product analysis of *Cf* WT and *pglX*- and *pglJ*- strains. Full scans (top to bottom) of the original western blots shown in Figure 3A and B are provided. (A) Western blot of whole-cell lysates with *Cff*-N-glycan-specific antiserum, and (B) wheat germ agglutinin reactivity of whole cell lysates of the WT and the *pglJ*- and *pglX*- strains are shown.

To investigate the N-glycan in the two *Cff-pgl* mutants in more detail, proteomics analysis of *Cff*-wildtype (WT) and the *pgl* mutants was performed. As the disruption of *Cff pgl* was predicted to truncate the N-linked glycan, we examined whole cell lysates to avoid potential biases in the detection of glycoforms which can result from glycopeptide enrichment (Alagesan et al. 2017). Consistent with our previous work (Nothaft et al. 2012), we observed both GlcNAc-α1-6-[GlcNAc-β1-3]-GlcNAc-α1-4-GalNAc-α1-4- GalNAc-α1-3-diNAcBac and GlcNAc-α1-6-[Glc-β1-3]-GlcNAc-α1-4-GalNAc-α1-4- GalNAc-α1-3-diNAcBac glycans on multiple protein substrates within the WT (Figure 2.6A and B) which were absent within *pglX- and pglJ-* (Supplementary MS data, not shown here). Consistent with our western and lectin blotting assays, multiple truncated N-linked glycans were observed within *pglX*- and *pglJ*- including diNAcBac-$HexNAc_2$ glycans, diNAcBac-HexNAc glycans (Figure 2.6C and D) as well as diNAcBac alone. Within *pglX*-, the diNAcBac-$HexNAc_2$ glycan was the predominant glycoform (not shown here) and is consistent with the *Cff* N-glycan core structure, diNAcBac-$GalNAc_2$ (Nothaft et al. 2012). In contrast, multiple glycoforms were identified in *pglJ*- including

diNAcBac-HexNAc$_2$-, diNAcBac-HexNAc, and diNAcBac glycans (not shown here). Taken together these results confirm the involvement of PglJ in the formation of the conserved reducing end trisaccharide and that PglX functions in extension of the non-conserved N-linked glycan structure.

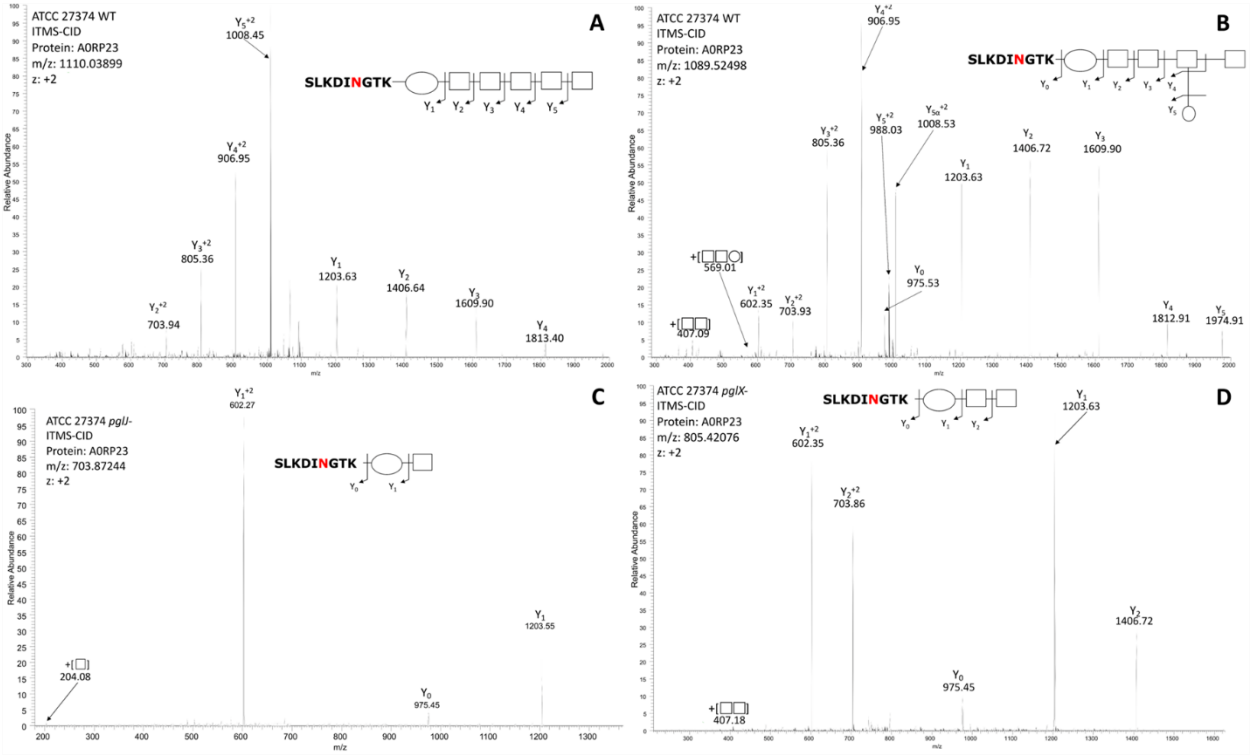

Figure 2.6. Mass-spectrometric analysis of *Cff* WT, *pglJ*- and *pglX*- glycopeptides. Fragmentation of characteristic ions obtained by precursor ion scanning of digested *Cff* lysate samples using liquid chromatography-mass spectrometry. Red lettering indicates possible glycosylation site. Spectra of WT *Cff* have two glycans: (A) HexNAc5-diNAcBac and (B) HexNAc-[Hex]-HexNAc$_3$-diNAcBac. (C) The peptide from the *pglJ*- mutant only shows the presence of a mass consistent with HexNAc-diNAcBac. (D) The peptide from the *pglX*- mutant indicates that it is modified with HexNAc-HexNac-diNAcBac.

Mutations in *pglX* and *pglJ* have no effect on growth and the expression of down-stream genes but reduces motility

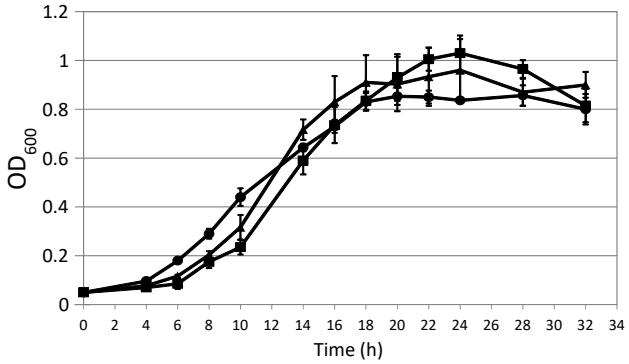

Figure 2.7. *In vitro* growth of *Cff*. *Cff* wildtype (circles), the *pglX* (squares) and the *pglJ* mutant (triangles) were grown in BHI broth under microaerobic conditions with shaking at 37°C. Growth curves were recorded at OD_{600} over a time frame of 32 h. Results shown represent the average values from three independent biological replicates. The standard deviation for each data point is indicated by an error bar.

Growth curves were performed to investigate influence the influence of *pgl* mutation. Although the *pgl* mutants reached a slightly higher optical density in the late logarithmic phase when compared to the WT, the final optical densities, as well as the growth rates in the early and mid-exponential phases, were similar among the three strains (Figure 2.7). In addition, we did not observe a significant difference in *pgl* gene transcript levels after the insertion of the *kan* cassette in either *pglX* or *pglJ* (Figure 2.8). This indicates that expression of the antibiotic cassette has no effect or that other transcriptional start sites in the *Cff-pgl* operon are compensating, as observed in the *C. jejuni pgl* operon (Dwivedi et al., personal communication, (Szymanski et al. 1999)). A downstream effect would influence expression of *pglB* but we see similar abundance of the PglB protein in WT when compared to either mutant (not shown here). In addition, we still observe different forms of glycans on each mutant whereas in the absence of PglB we would not expect any glycans at all. However, we observed a significantly reduced swimming behavior in *pglX*- and *pglJ*- when compared to *Cff*-wild-type (Figure 2.9) indicating that N-glycosylation either directly or indirectly affects motility.

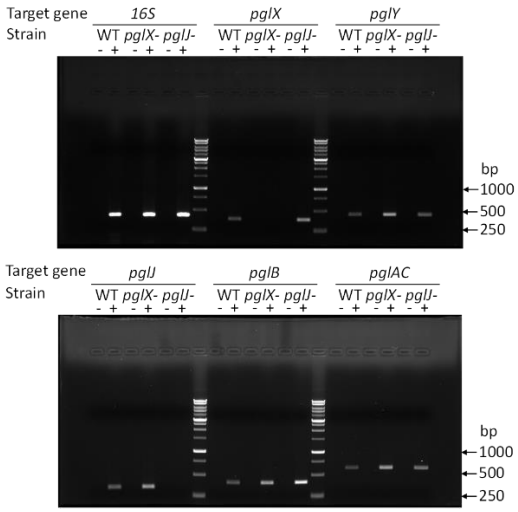

Figure 2.8. RT-PCR analyses of *pgl* genes. Pgl gene-specific PCR products obtained after reverse transcription of purified RNA of the *Cff* wild-type (WT), the *pglX* (*pglX-)* and the *pglJ* (*pglJ-)* mutant strains were analyzed by 0.8% agarose gel electrophoresis. (+) indicates RNA reverse transcribed with SuperScript (-) indicates the no-SuperScript RT control. No polar effects were observed on the transcription of the genes downstream (target, as indicated) after integration of the kan cassette in either *pglX*- or *pglJ*-. Significant bands of the DNA standard (in base pairs, bp) are indicated on the left. The obtained gene-specific PCR products were in agreement with the expected sizes for 16S (421 bp), *pglJ* (330 bp), *pglY* (443 bp), *pglX* (371 bp), *pglB* (399 bp) and *pglAC* (609 bp).

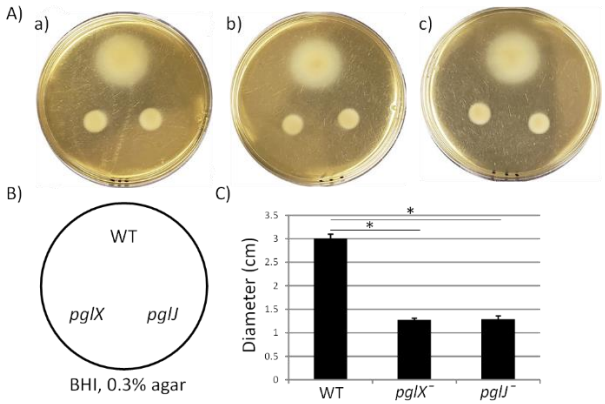

Figure 2.9. Mutation of *pglX* or *pglJ* resulted in reduced motility. (A) Triplicates of 0.3% BHI swarm agar plates (a, b, c) are shown at 60% of their original size. The low percentage of the agar allows the bacteria to swim and form a ring of growth around the point of inoculation. All three strains (*Cff*-wildtype (WT), the *pglX* (*pglX*-) and the *pglJ* (*pglJ*-) mutant) were analyzed in parallel (as depicted in (B)) on each plate to exclude plate-to-plate variations. (C) The average diameter (in cm) of the halo for each strain is depicted, standard deviations are indicated by error bars, statistically significant differences (p-value ≤ 0.001 analyzed by a two-tailed t- test) are indicated by an asterisk.

Characterization of PglJ and PglA in *E. coli*

Since the N-glycan phenotype observed in the *pglJ* mutant was somewhat unexpected, the function of *Cff*-PglJ and *Cff*-PglA was further investigated by using a modified heterologous *E. coli Cj*/*Cff* hybrid glycosylation system (Wacker et al. 2002). Within this system, *Cff*-Pgl proteins are expressed in the presence of a mutant *Cj-pgl* operon (lacking select *Cj-pgl* genes). The glycans produced are then transferred to *Cj*-CmeA-His_6 (N-glycosylation acceptor protein) via *Cj*-PglB. Western blotting of whole cell lysates of *E. coli* CLM24 prepared after co-expression of *Cj*-CmeA-His_6 and *Cj-pglA* or *Cj-pglJ* in the presence of p*pgl* operon derivatives lacking either *pglA* or *pglJ* were probed with anti-His_6 and anti-*Cj*-N-glycan antibodies (Figure 2.10). The three *Cj*-Cme-His_6-specific signals with anti-His (Figure 2.10) and two N-glycans specific signals with the *Cj*-N-glycan specific R1 antiserum (Figure 2.10A, lower panel) clearly identified the bands as non-(0N), mono-(1N), and di-(2N) glycosylated CmeA-His_6. A similar *Cj*-CmeA-His_6 pattern was produced in cells harboring the native *Cj-pgl* operon (from p*pgl*) and upon expression of *Cff-pglA* or *Cff-pglJ* (although with lower glycosylation efficiency) only when the *Cj*-homologous gene was knocked-out. In addition, no cross-complementation could be observed when *Cj* or *Cff pglA* or *pglJ* were expressed in the presence of the p*pgl* plasmid lacking *pglJ* or *pglA*, respectively. These results confirm that *Cff*-PglA and *Cff*-PglJ fulfill the same functions as the homologous *Cj*-Pgl proteins, *i.e.* the addition of the second and third monosaccharide building blocks, respectively, to Und-diNAcBac, to form the diNAcBac-$GalNAc_2$- trisaccharide. As expected, no *Cj*-CmeA-His_6 glycosylation was observed in the absence of p*pgl* resulting in only non-glycosylated (0N) acceptor protein represented by a single band in the anti-His_6 western blot and further confirmed by the absence of the N-glycan-specific signals in the anti-N-glycan (R1) blot (Figure 2.10A lower panel). Mass spectrometric analysis

of isolated *Cj*-CmeA confirmed the modification of CmeA glycopeptides with the expected glycoforms supporting these western blot results (Figure 2.10). Here, the full length *Cj*-heptasaccharide was produced only when the *Cj-pgl* operon plasmids with mutations in *pglA* or *pglJ* were co-expressed with plasmids containing the corresponding *pglA* or *pglJ* from *Cj* or *Cff*.

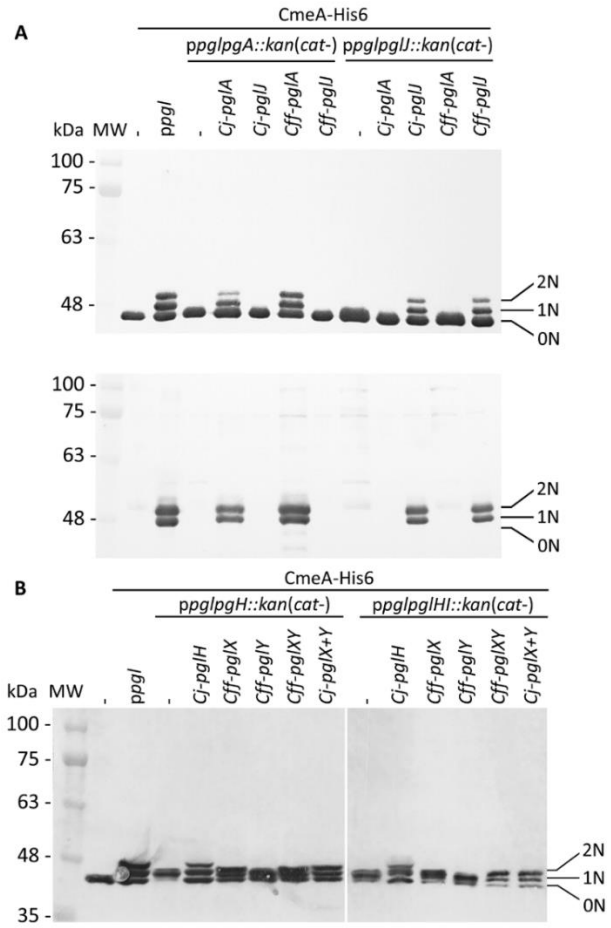

Figure 2.10. Functional analysis of *Cff*-Pgl pathway glycosyltransferases (GTases) in the heterologous *E. coli* glycosylation system. The GTase-activities of (A) PglA and PglJ were analyzed in western blots of CmeA-His6 with His6-tag (upper panel) and *Cj*-N-glycan specific (lower panel), R1) antibodies (B) PglX and PglY activities were analyzed with His6-tag specific antibodies in western blots of CmeA-His6 used as the glycan acceptor to determine N-glycosylation activities. Whole cell extracts (5 µg) of *E. coli* CLM24 expressing the indicated gene/plasmid combinations are indicated above each lane. None, mono, and di-glycosylated CmeA-His6 proteins are labelled as 0N, 1N and 2N, respectively. Molecular weight markers (MW) in kDa are indicated on the left.

Characterization of *Cff-pglX* and *pglY* using the *E. coli* heterologous glycosylation system

Since we could not obtain a mutant in *Cff-pglY* and therefore could not assign the functions of the two remaining GTases in the "variable" *pgl* region, we decided to analyze PglX and PglY using the heterologous *E. coli* glycosylation system (Wacker et al. 2002). In this case we employed the *Cj-pgl* operon lacking *pglH* that produces a trisaccharide (diNABacGalNAc$_2$) identical to that found in *Cff,* potentially providing a substrate for PglX or PglY activity. In addition, we constructed and analyzed the complementation of a p*pgl-pglHI*::*kan* mutant plasmid (lacking *Cj-pglH* and *Cj-pglI*) to rule out the possibility of the *Cj*-PglI GTase adding or competing with the potential addition of a glucose residue to the N-glycan chain by either *Cff*-PglX or *Cff*-PglY. To do so, plasmid pCE111/28 derivatives expressing *Cj-pglH* (positive control), *Cff-pglX*, *Cff-pglY* or *Cff-pglXY* served as complementation vectors. Western blots of whole cell lysates probed with anti-His$_6$ antibodies were performed to investigate the *Cj*-CmeA-His$_6$ glycosylation pattern in the underlying strains (Figure 2.10B). Expression of p*pgl* in combination with CmeA-His$_6$ and CmeA-His$_6$ alone served as positive and negative glycosylation controls, respectively. First, we demonstrated that expression of *Cj-pglH* in combination with the *pgl* operon lacking *pglH* resulted in a glycosylation pattern similar to the strain co-expressing CmeA-His$_6$ and the *Cj*-wildtype *pgl* operon (on p*pgl*) *i.e.* production of non-(0N), mono-(1N) and di-(2N) glycosylated CmeA-His$_6$, whereas in the absence the complementation plasmid, glycobands were migrating slightly faster due to the addition of only the trisaccharide N-glycan (missing the GalNAc$_3$-Hex that is added by PglH and PglI in the full length *Cj*-heptasaccharide). Expression of *Cff-pglY* with p*pgl-pglH*::*kan* did not alter the migration behaviour of the glycobands when compared to p*pgl-pglH*::*kan* alone, whereas transformation of *Cff-pglX* resulted in a slight mass increase compared to p*pgl-pglH*::*kan/Cff-*

pglY, indicating that PglX, but not PglY, might be responsible for the addition of a sugar residue to the p*pgl-pglH*::*kan* glycan (Figure 2.10B). A slight increase in mass of the *Cj*-CmeA-His_6 glycoprotein was also observed upon expression of the two *Cff-pglXY* constructs, however a difference in the running behavior compared to p*pgl-pglH*::*kan*/*Cff-pglY* could not be resolved by SDS-PAGE and western blotting analysis alone (Figure 2.10B).

Similar results were obtained upon introduction of *Cj-pglH* and *Cff pglX*, *Cff-pglY* and *Cff-pglXY* into CLM24 expressing p*pgl-pglHI::kan* and *Cj*-CmeA-His_6. Here, the glycobands in the *Cj-pglH* complements were expected to display a slightly faster running behavior when compared to the full length heptasaccharide due to the loss of the Glc residue, however, similar to the complementation analysis of the p*pglH::kan* strains, an obvious difference in the running behavior of the CmeA-His_6 glycobands upon introduction of *Cff-pglX*, and *Cff-pglXY* could not be resolved (Figure 2.10B).

To further investigate the N-glycans produced upon expression of the different *Cj-pgl* operon mutants in combination with the *Cff-pglX* and *pglY* complementation plasmids, mass-spectrometric analyses of trypsinized CmeA was undertaken. While N-glycan structures observed upon complementation with the *Cj*-control (p*pgl-pglH* mutant expressing *Cj-pglH*) resulted in the formation of the expected full length *Cj*-N-glycan, only one plasmid combination, the expression of *Cff-pglXY* in the p*pgl-pglH* mutant background resulted in the formation of a structure that was similar in composition and sequence to the minor form of the native *Cff*-N-glycan, diNAcBac-$HexNAc_4$-Hex (not shown here).

Mutations in *pglX* and *pglJ* have an impact on multiple cellular functions in *Cff*

To further understand the role of N-glycosylation in *Cff*, label-free quantitative (LFQ) proteomics analysis of whole cell lysates of *Cff*-wildtype (WT), and the *pglX*- and *pglJ*- was

done. Across five biological replicates of each sample type (Figure 2.11), 914 proteins were identified representing ~ 77% of the *Cff* ATCC 27374 predicted proteome of 1190 proteins (not shown here). Quantitative proteome analyses revealed more than 100 proteins with significantly different abundance across various biological groups as shown in heat maps of the most prominent differences in abundance comparing WT to *pglX*- and *pglJ*- strains (Figure 2.12A-B). These results indicate that mutating glycosyltransferases involved in assembly of the N-linked glycan has a significant effect on abundance of numerous cellular proteins.

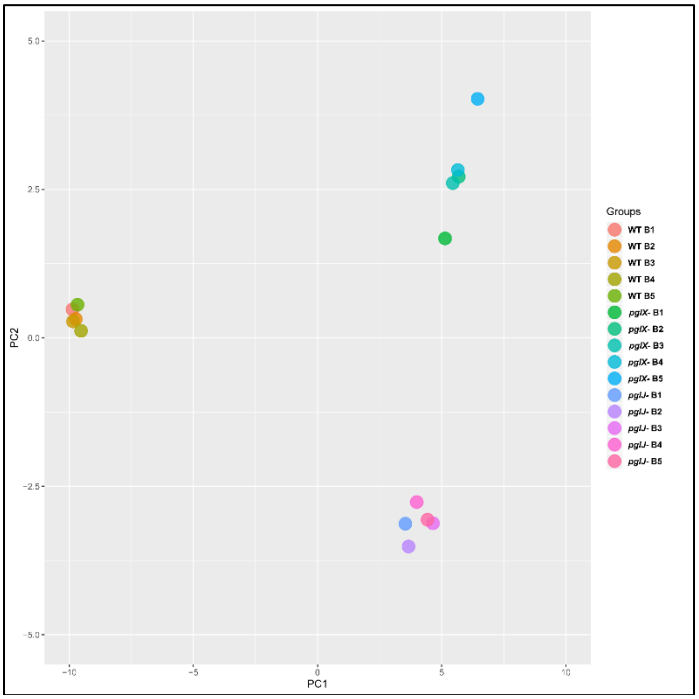

Figure 2.11. Principal component analysis (PCA) of LFQ proteome analysis of *C. fetus* subsp. *fetus* ATCC 27374 WT, *pglJ* and *pglX* mutants. PCA analysis reveals segregation of each sample group (5 replicates (B1-5) for WT, *pglX*- and *pglJ*-) as indicated by the colour scheme.

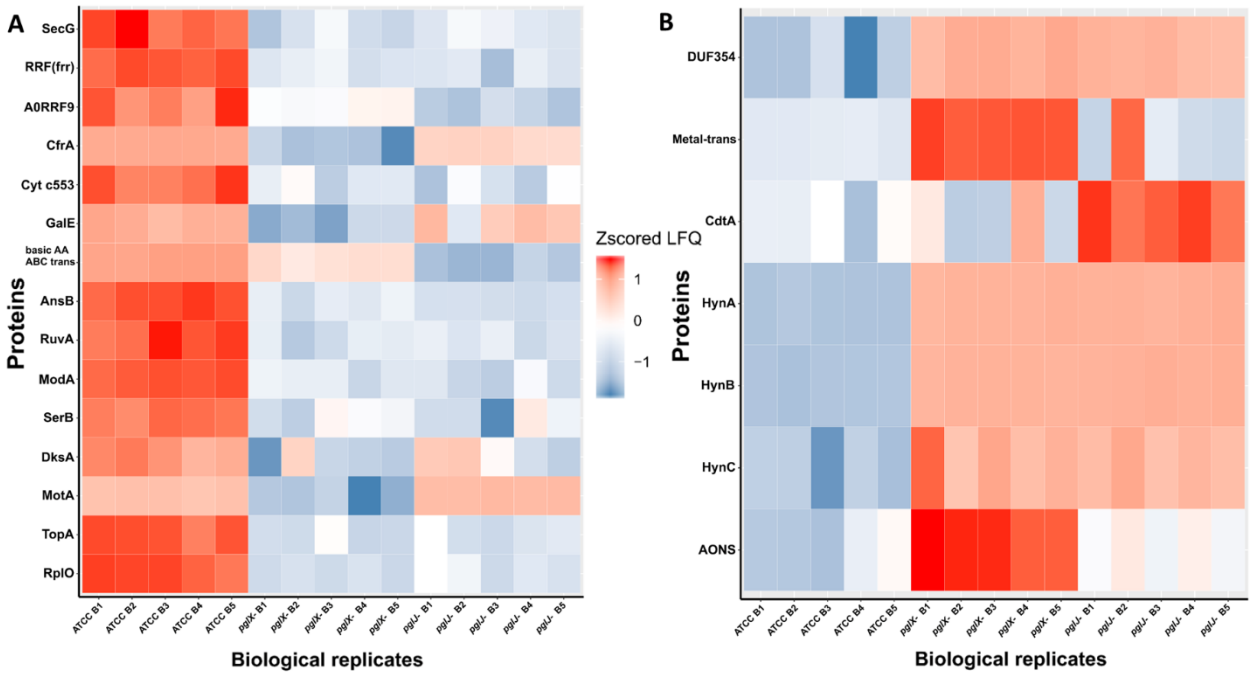

Figure 2.12. Label-free quantification of proteins in *Cff pglJ*- and *pglX*- strains compared to WT. (A-B) Heat maps of specific proteins with significant decreases (A) or increases (B) in *pglJ*- and *pglX*- mutants compared to WT (labeled ATCC). Values are gray where MS did not identify fragments. This data represents samples from five biological replicates (B1-B5).

Expression of the H_2-uptake hydrogenase complex HynABC is significantly induced in both *pglJ* and *pglX* N-glycosylation mutants

Among the proteins with increased abundance in both the *pglJ* and *pglX* mutants (compared to WT), were the three subunits (HynABC) of a putative nickel-iron [NiFe] H_2-uptake hydrogenase complex (Benoit et al. 2020). In both *pgl* mutants, the expression levels of all three hydrogenase subunits, HynA, HynB and HynC were significantly higher compared to the WT (means of 29.3-fold, 21.5-fold, and 7.8-fold, respectively) (Figure 2.13A). This complex, found in a number of bacterial pathogens, enables the microbes to use the electron donor H_2 as an energy source, thus providing an alternative respiratory pathway that is important for *in vivo* survival (Olson and Maier 2002; Benoit and Maier 2018). HynABC-associated proteins, such as hydrogenase accessory/maturation proteins (*e.g.* HypABCDEF) or the nickel specific

transcriptional regulator (NikR) also showed moderate increases in protein levels in both mutants compared to WT (Figure 2.13A).

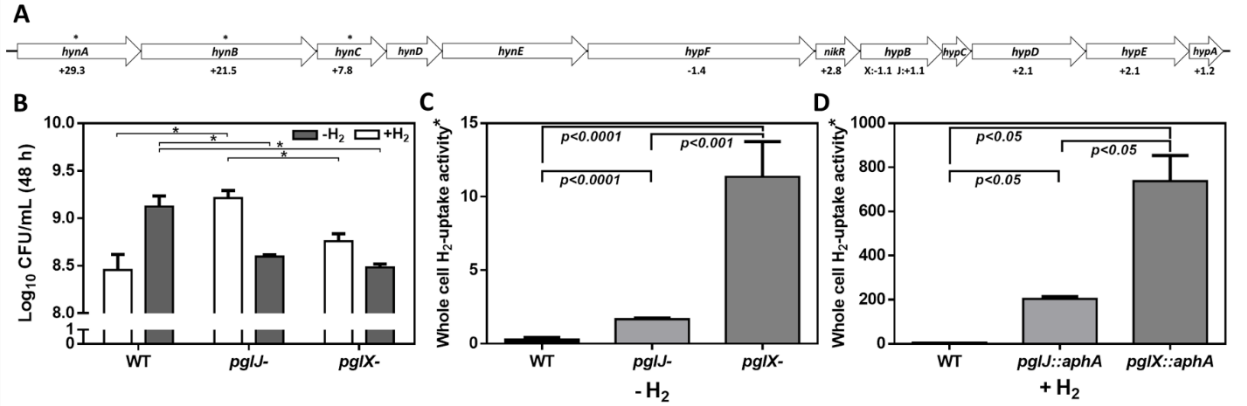

Figure 2.13. (A) Relative protein abundance, as determined by proteomics, of hydrogenase associated genes in *Cff pgl* mutants. Gene arrangements of *hyn* and *hyp* clusters in *Cff* ATCC 27374 with LFQ proteomic protein abundance vs WT are shown. Protein fold changes of *pglJ*- and *pglX*- with respect to WT is indicated above and below each gene respectively. Genes with no values associated had no coverage in our proteomics data. Genes with a * indicate significant protein level increases compared to WT. (B) Effect of H_2 on microaerobic growth of *Cff* WT, *pglJ*- and *pglX*- strains. The data set is derived from three biological replicates (with two technical replicates each) of cells grown under the indicated condition. Number of cells obtained after 48 h of growth is represented by Log_{10} colony forming units per mL (CFU/mL). The error bars represent the standard error within each group. ***p*-value ≤ 0.05 analyzed by a two-tailed *t* test are shown for each data set comparison (C-D) Whole cell H_2-uptake of *Cff* WT, *pglX*- and *pglJ*- strains. *Cff* was grown on BHI agar in microaerophilic conditions for 24 h at 37 °C in 10% H_2 ($+H_2$) or absence of hydrogen ($-H_2$). *Whole cell H_2-uptake activity is expressed as nanomoles of H_2 used per min per 10^9 cells. Results in (C) represent the mean ± SD of four independent assays; results in (D) represent the mean ± SD of two independent assays.

Since H_2 increases growth of various ε-proteobacteria species, including *Helicobacter pylori* and *Campylobacter concisus* (Kuhns et al. 2016; Benoit and Maier 2018), we determined whether higher hydrogenase expression in the *C. fetus* N-glycosylation mutants correlates with elevated H_2-supported microaerobic growth. To do so, the cell yield (CFU/mL) of the WT and the *pglJ* and *pglX* mutants was assessed after 48 h of growth under microaerobic conditions in the presence or absence of 20% H_2 (Figure 2.13B). We only determined the end point of growth due to the extended lag phase of *Cff* cultures grown under these conditions. With no added H_2, *Cff* WT had a significantly higher growth yield compared to both mutants. However, in H_2-

enriched conditions, WT cells showed growth levels comparable to both *pgl* mutants. Although the addition of H_2 was originally predicted to be beneficial for WT growth, we observed decreased growth in H_2 for other *Cf* strains, *Cft* 03-427 and *Cff* 82-40 (data not shown). In contrast, we observed a significant increase in *pglJ*- growth compared to the other strains in the presence of H_2. A slight increase in *pglX*- growth was also observed in the presence of H_2, but it was not significant compared to WT. These results indicate that the *pgl* mutants have increased growth yield in H_2 opposed to WT where H_2 is deleterious.

H_2-uptake in whole cells was examined to determine whether increased HynABC levels in the mutants correlate with increased H_2-uptake activity. Cells were grown in microaerobic conditions in the presence or absence of supplemental H_2 and hydrogenase activity was determined using a previously described amperometric method (Maier et al. 1996). The hydrogenase activity (expressed in nmoles of H_2 oxidized per min per 10^9 cells) was 0.3 ± 0.07, 1.7 ± 0.04, and 11.4 ± 1.2 for WT *pglJ*-, and *pglX*, respectively, when cells where grown under microaerobic conditions in the absence of supplemental H_2 (Figure 2.13C). This represented almost a 6-fold (for *pglJ*-) to 39-fold (for *pglX*-) increase in activity compared to WT. When cells were grown in the presence of 10% H_2, we observed a 122- and 65-fold increase in hydrogenase activity in *pglJ*- and *pglX*- respectively, and a 20-fold increase in WT (Figure 7D). The remarkable H_2-uptake levels measured for *pglJ*- (204 ± 7 nmoles H_2/min/10^9 cells) and *pglX*- (738 ± 82 nmoles H_2/min/10^9 cells) mutants grown with H_2, were the highest recorded values to date for a bacterial pathogen. Taken together, these results indicate an inverse correlation between N-glycosylation and H_2 usage (*i.e*. hydrogenase synthesis and activity) in *Cff.*

N-glycosylation influences transition metal profiles

Proteomics data indicate that multiple proteins associated with transition metals were significantly altered in both *pgl* mutants. These include ModA, involved in molybdenum transport, (-49.9-fold in *pglX*- and -71.8-fold in *pglJ*-,); the ZinT/AdcA family protein involved in zinc binding (-12.2-fold in *pglX*- and -6.5-fold in *pglJ*-); CfrA, a ferric receptor (-118.4-fold and -3.3-fold), and an iron ABC transporter (-5.1-fold and -7.6-fold) (not shown here). Also, a copper/cadmium-translocating P-type ATPase protein was found to be significantly increased (51.9-fold) in *pglX*-; however, the increase was not significant (1.4-fold) in *pglJ*-.

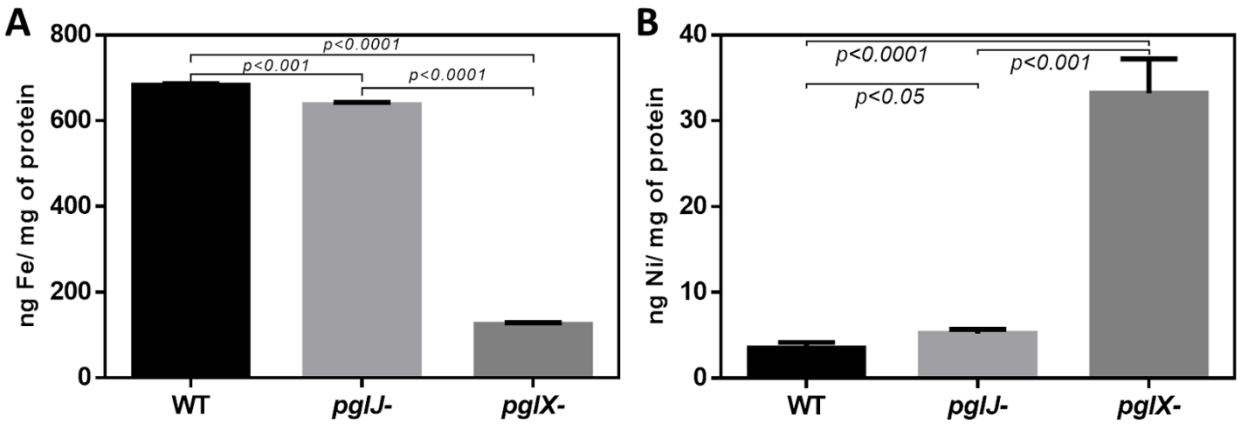

Figure 2.14. Cellular iron and nickel content of *Cff* WT, *pglX*- and *pglJ*- strains. Atomic absorption spectroscopy (AAS) was employed for the detection of (A) iron (Fe) and (B) nickel (Ni) in lysed cells of the indicated strain. Data are presented as the mean of at least three replicates, error bars depict the standard deviations. Statistically significant differences determined by a two-tailed *t* test are indicated.

The increased levels, especially of the HynABC (Ni-Fe) hydrogenase observed in both *pgl* mutants led us to further investigate nickel and iron levels in these strains. Using atomic absorption spectrometry (AAS) of lysed cells, we found that iron levels were dramatically decreased in *pglX*- (125.1 ng/mg protein), that is almost 6-fold lower when compared to WT (683.2 ng/mg protein) whereas iron levels in *pglJ*- were modestly, but statistically decreased (Figure 2.14A). In addition, the *pgl* mutants had significantly higher levels of cellular nickel

content compared to WT (Figure 2.14B); *pglX*- had a nickel content of 33.2 ng/mg protein that was almost 10-times higher than in the WT (3.5 ng/mg protein). Although still significantly higher when compared to the WT, *pglJ*- (5.2 ng/mg protein) had almost 6-fold less nickel than *pglX*-. These results indicate that N-glycosylation might be vital in regulation of nickel homeostasis, iron, or both.

Antibiotic sensitivity and increased membrane efflux

Antibiotic	***WT***	***pglJ-***	***pglX-***
Amoxicillin / Clavulanate	2	<= 1	<= 1
Ampicillin	4	<= 1	<= 1
Azithromycin	0.5	0.25	0.5
Cefoxitin (2nd gen.)	32	>32	32
Ceftiofur (3rd gen.)	>8	> 8	> 8
Chloramphenicol	8	4	4
Ciprofloxacin	0.5	0.5	0.5
Gentamicin	2	1	1
Sulfisoxazole	256	128	256
Tetracycline	<=4	<= 4	<= 4
Trimethoprim / Sulfamethoxazole	>4	4	>4

Table 2.1. Antibiotic resistance of *Cff* WT, *pglX*- and *pglJ*- strains. Sensititre™ was used to assess the minimum inhibitory concentration (MIC) of the indicated *Cff* strains. The data (in $\mu g/ml^{-1}$) represent one assay done at the Athens Veterinary Diagnostic Facility.

Our previous study showed that *C. jejuni* N-glycosylation was required for optimal activity of the CmeABC multidrug efflux pump necessary for antibiotic resistance (Dubb et al. 2019). In *Cff*, albeit not statistically significant, we found increased levels of CmeA, CmeB and CmeC in *pglX*- and *pglJ*-, (mean of both mutants: 2.0-fold CmeA, 1.9-fold CmeB, and 2.0-fold CmeC). Therefore, we examined the antibiotic sensitivity profiles of both *Cff* N-glycosylation mutants. As shown in Table 2.1, the *pglX*- and *pglJ*- strains showed 2-fold increase in sensitivities to chloramphenicol, gentamicin, azithromycin and sulfisoxazole, and a 4-fold increase in sensitivity to ampicillin suggesting a correlation between N-glycosylation and antibiotic resistance in *C. fetus*, similar to previously observed in *C. jejuni* (Abouelhadid et al.

2019; Dubb et al. 2019). To explore this further, we used ethidium bromide (EtBr), a DNA intercalating agent, to quantitatively assess efflux pump activity over time. Both *pglJ* and *pglX* mutant strains showed significantly higher levels of EtBr accumulation compared to WT (Figure 2.15), however, accumulation was less pronounced in the *pglX* mutant. Taken together, these results suggest that N-glycosylation in *C. fetus* may be important for efflux pump activity and antibiotic sensitivity.

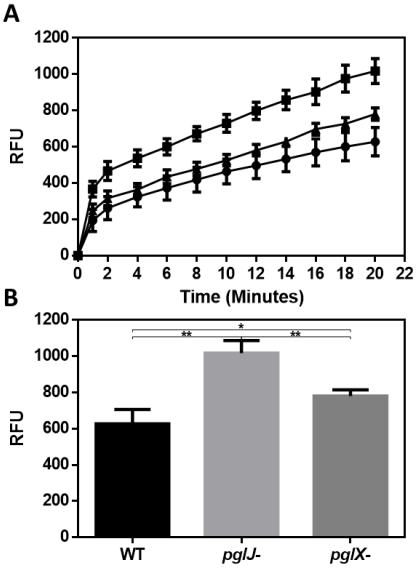

Figure 2.15. Mutations in N-linked protein glycosylation decreased efflux in *pglX*- and *pglJ*- strains. (A) Accumulation of ethidium bromide in cultures of *Cff* WT (diamond), *Cff pglJ*- (square), and *Cff pglX*- (triangle) over a time frame of 20 minutes, relative fluorescent units (RFU) are indicated on the y-axis (B) Bar graph depicting the relative fluorescence at t=20 minutes. The error bars represent the standard error for each data set consisting of four biological replicates with three technical replicates each. ****p*-value ≤0.001, **p*-value ≤ 0.05 as determined by a two-tailed *t* test.

Discussion

N-glycosylation is a conserved mechanism in all domains of life. The prototypical *pgl* N-glycosylation system, originally characterized in *C. jejuni* (*Cj*), has orthologues in many δ- and ε-Proteobacteria (Nakagawa et al. 2007; Jervis et al. 2010; Ielmini and Feldman 2011; Nothaft et al. 2012; Mills et al. 2016). Non-thermotolerant *Campylobacter* species, like *C. fetus* (*Cf*), including *C. fetus fetus (Cff)* and *C. fetus venerealis (Cfv)* have been found to produce more than

one N-glycan, unlike *Cj* which expresses one distinct heptasaccharide (Scott et al. 2011; Nothaft et al. 2012; Cain et al. 2019). In our study, we generated mutants in PglX and PglJ in *Cff* strain ATCC 27374. Glycopeptides from the *pglX*- mutant showed fragmentation patterns consistent with the conserved diNAcBac-GalNAc$_2$ (Nothaft et al. 2012) suggesting that PglX is responsible for the addition of the first GlcNAc residue to the *Cf* N-glycan structure (Figure 2.1). The loss of *Cf* N-glycan-specific serum reactivity and WGA lectin binding to lysates from the *pglX*- strain support this claim. Proteomics of the *pglJ*- strain resulted in a mixture of glycopeptides, primarily consisting of diNAcBac and a few fragments of diNAcBac-HexNAc, typically more characteristic of a *Cj* PglA mutant. To investigate this further, we used an *E. coli* expression system followed by MS-analyses and were able to show that the *Cff*-PglJ and *Cff*-PglA had similar transferase activities onto recombinantly expressed *Cj*-CmeA as the *Cj* homologues. However, we did not see reactivity with WGA or the *Cff*-N-glycan specific antiserum, except for a single band in the WGA blot. These results suggest possible WGA interaction with another glycan, such as LPS, however the reason behind the absence of specific binding in the *pglJ* mutant strain has yet to be explained. Nevertheless our results suggest that the formation of the diNAcBac-GalNAc$_2$ trisaccharide is conserved between *Cj* and *Cff* and that the observed differences in antigenicity (Jervis et al. 2010; Nothaft et al. 2012) stem from the non-reducing end.

Expression of *Cff*-PglX in *E. coli* showed a CmeA mass shift consistent with transfer of an additional sugar, consistent with our MS-analysis of glycopeptides from the native host (i.e. diNAcBac-GalNAc$_2$-GlcNAc). Since we were unable to generate a *Cff* mutant in PglY, we also used the *E. coli* system to investigate *Cff* PglY activity and detected a major glycoform with an additional sugar only when both PglX and PglY were co-expressed, suggesting that PglY's

activity is dependent on the initial modification by PglX. Based on our MS results, an N-linked glycan with a composition resembling the minor *Cff* N-glycan (i.e. GlcNAc-α1-6-[Glc-β1-3]-GlcNAc-α1-4-GalNAc-α1-4-GalNAc-α1-3-diNAcBac) was also observed in *E. coli* p*pgl-pglH*::*kan* expressing *pglX* in combination with *pglY*, although the addition of the Glc residue by *Cj*-PglI could not be ruled out since we observed less peptides containing the minor *Cff*-N-glycan in the p*pgl-pglHI* background, and also observed Glc addition in a p*pgl-pglHI*::*kan* mutant demonstrating that an *E. coli* enzyme could be contributing this residue. Thus, the GlcTF reaction requires further investigation either in *Cff* or *in vitro*. No N-glycan that resembles the major form of the *Cff* N-glycan could be detected with any *Cj-pgl* mutant/*Cff-pgl* gene combinations. Nevertheless, these data suggest that *pglX* and *pglY* can mediate the construction of a partial *C. fetus* N-linked glycan using the *C. jejuni* diNAcBac-$GalNAc_2$ trisaccharide as a substrate. *C. jejuni* PglB does not have strict substrate specificity and can transfer full-length and truncated N-glycans and diverse O-antigen structures in *E. coli* and to a lesser extent, in the native host (Feldman et al. 2005; Linton et al. 2005). Therefore, we did not expect preferential transfer of certain *Cj-Cff* hybrid N-glycans to CmeA. However, since we only generated one potential variant of the *Cff*-N-glycan, this suggests that the GTase involved in the formation of the second *Cff*-N-glycan structure is either not fully functional in *E. coli* or is not part of the *pgl* locus, similar to the lack of *pgl* gene clustering in *Helicobacter* species and *Desulfovibrio desulfuricans* (Jervis et al. 2010; Nothaft and Szymanski 2010).

To better understand the role of N-glycosylation in *Cff*, we utilized LFQ proteomics comparing *Cff* ATCC 27374 with two isogenic *pgl* mutants, *pglX*- and *pglJ*-. Through this approach, we were able to detect almost 77% of the (genome-inferred) total proteins. Analysis of proteins that were significantly up- or down -regulated indicated that more than 100 proteins

were altered in the *Cff pgl* mutants in comparison to WT. It is worth noting that differences between *pgl* mutants may be due to differences in glycan length (diNAcBac-GalNAc in *pglJ*- and diNAcBac-$GalNAc_2$ in *pglX*-) or differential feedback regulation in these two backgrounds. Although N-glycosylation was not completely eliminated, we observed a decrease in NapB (-6.7-fold in *pglX*- and -8.4-fold in *pglJ*-, Table S1), similar to that previously seen in a *Cj-pglB* mutant (Cain et al. 2019). In *C. jejuni*, the nitrate reductase NapAB has been shown to be a two-subunit enzyme, with both subunits being N-glycosylated (Scott et al. 2011; Mintmier et al. 2018; Abouelhadid et al. 2019; Cain et al. 2019). In contrast, in *Cff* ATCC 27374, NapA lacks an N-glycosylation sequon, while at the same time NapB has two potential sequons. This may explain why we only observed a decrease in NapB (see above), while the difference in NapA protein levels was not significant (1.1- fold in both *pgl* mutants).

No effect on growth or on the expression of downstream genes was observed, but the *pgl* mutants were impaired in motility. Similarly, loss of *pglB* (and therefore complete loss of N-glycosylation) in *C. jejuni* JHH1 and *C. jejuni* 11168 also resulted in decreased motility when compared to wildtype cells (Scott et al. 2012; Cain et al. 2019). In addition, Cain and colleagues demonstrated that levels of specific proteins required for motility were expressed at significantly lower levels in the *C. jejuni* 11168 *pglB* mutant; among them MotA, MotB and FlgP (Cain et al. 2019). We also observed lower levels of MotA and MotB (significantly lower in *pglX*- (94- and 8.6-fold, respectively), but not in *pglJ*- (Table S1); FliG (significantly lower in *pglX*- (5.7-fold) and *pglJ*- (4.7-fold) (data not shown), as well as the *Cj*-FlaA homologue flagellin protein (significantly lower in *pglX*- (9.7-fold) and *pglJ*- (7.1-fold) (Table S1). This could imply that motility may be correlated with N-glycosylation changes in some *Campylobacters*. However, *pglB, pglE, pglF* and *pglH* mutants in *C. jejuni* 81-178 were described to display wildtype levels

of motility (Szymanski et al. 1999; Hendrixson and DiRita 2004), therefore it seems that this regulatory network varies even among strains.

We did not observe a reduction in CmeABC in either the *Cff pglX* or *pglY* mutant. In contrast, we observed a slight, but not statistically-significant increase in these efflux proteins in both mutants. Despite that discrepancy, our *pgl* mutants still displayed decreased EtBr efflux activity compared to wildtype when cells were grown under the same conditions that were used to prepare whole cell lysates for proteomic analysis. This suggests that *Cf* N-glycosylation directly influences the activity of the efflux pump, an effect that has previously been described for *C. jejuni*. However, the increased sensitivity to various classes of antibiotics observed in both *Cff-pgl* mutants is most likely indirect since not all of those antibiotics are substrates for the efflux pump in other *Campylobacter* species; however, variations in CmeABC substrate specificities have been observed even between strains (Lin et al. 2002; Akiba et al. 2006; Guo et al. 2010). One might speculate that membrane permeability increases due to lower abundance of certain periplasmic and/or membrane proteins or that loss of periplasmic fOS could result in a higher influx of those antibiotics and therefore lead to the observed decrease in MICs. It is worth noting that the observed effects were less pronounced in *pglX*- compared to *pglJ*-. This could be due to the fact that glycoproteins contain a longer N-glycan chain in *pglX*- compared to *pglJ*. Together these results indicate that N-glycosylation in *Cf* plays a role in efflux, although the mechanism is currently unknown.

Our proteomics data indicate that all three components (HynABC) of the [NiFe]-containing H_2-uptake hydrogenase were significantly upregulated in both *pgl* mutants, suggesting that protein glycosylation plays a role in H_2 utilization. Based on homology with hydrogenase complexes found in related ε-proteobacteria, such as *H. pylori*, *C. jejuni* and *C.*

concisus(Olson and Maier 2002; Weerakoon et al. 2009; Benoit and Maier 2018), the *Cff* HynABC complex is likely to be involved in H_2 oxidation. Consistent with the proteomics data, higher H_2-mediated growth rates were observed in both *pgl* mutants compared to WT, with the highest growth rate seen in the *pglJ*- strain grown under H_2 rich conditions. Surprisingly, H_2-enriched conditions seemed to have a deleterious effect on WT growth. Nevertheless, we infer from these results that the improved growth observed in the mutants could be due to enhanced utilization of H_2 from the drastically increased expression levels of the HynABC complex. In correlation with higher HynABC protein levels, H_2-uptake activities were higher in both *pglJ*- and *pglX* mutants compared to WT in the absence and in the presence of H_2. The increased [NiFe] hydrogenase synthesis (and activity) observed in the mutants might be linked to changes in metal homeostasis, particularly that pertaining to Fe and Ni. Studies conducted in the related organism *H. pylori* can provide insight into the respective roles of Fe and Ni with respect to transcriptional regulation of hydrogenase genes, through Fur and NikR regulators, respectively. For instance, *H. pylori* apo-Fur has been shown to repress *hynABC* (Ernst et al. 2005). Furthermore, addition of Ni to the medium leads to decreased *hynABC* expression; however this repression was not observed in a *nikR* mutant background (Ernst et al. 2005) suggesting that either Ni-bound NikR represses or apo-NikR activates hydrogenase expression in *H. pylori*; in addition Ni-NikR has been shown to repress *fur* (Dosanjh et al. 2009). Taken together, these sets of results suggest the possible following mechanism in *Cff*: if Ni-bound NikR represses *fur* and (apo-) Fur represses *hynABC*, then elevated Ni levels (as observed in both *pgl* mutants) would be expected to de-repress Fur-controlled *hynABC.* The final outcome would be increased HynABC levels and increased hydrogenase activity, and indeed protein activities correlated well in cells and whole cell lysates grown under the same conditions. Obviously, the mechanism at play in *Cff*

has yet to be elucidated. Nevertheless, taken together, our results indicate a clear link between N-glycosylation (or the lack thereof) and [NiFe] HynABC hydrogenase expression and/or enzymatic activity.

It is worth noting that *Cff* contains two additional hydrogenase complexes: a [FeFe] hydrogenase (HydA), hypothesized to be a H_2-uptake type, and a [NiFe] H_2-evolving complex (HycBCDEFG) predicted to be part of a formate hydrogen lyase (FHL) complex that links formate oxidation to hydrogen production (Benoit et al. 2020). Based on our proteomic study, neither HydA nor HycBCDEFG hydrogenase subunits were found to be expressed at different levels between WT and the N-glycosylation mutants.

The increase in [NiFe] HynABC and decrease in certain metal-related proteins prompted us to quantify Ni and Fe levels. In both *pgl* mutants we saw a significant decrease in iron; however, the decrease in iron for *pglX*- was 5-fold lower than *pglJ*- and 6-fold lower than WT. This may be because *pglX*- has a 118.4-fold decrease, and only 3.3-fold decrease in *pglJ*-, in the CfrA ferric enterobactin receptor present in *Cj*, which is responsible for high-affinity iron acquisition (Miller et al. 2009).

Although nickel is essential for both nickel containing hydrogenases in *Cf*, it is also toxic in excessive amounts, potentially causing oxidative stress and perturbing enzyme activities (MacOmber and Hausinger 2011). One mechanism of modulating nickel levels that was previously identified in *E. coli* is the nickel defense system (RcnA), which utilizes a proton gradient to translocate nickel to the periplasm where it can either be bound by sequestering proteins or effluxed from the cell (MacOmber and Hausinger 2011). We observed a 50-fold increase in a metal P-type ATPase in *pglX*- (A0RQS6), annotated as copper/cadmium-translocating P-type ATPase with similarly predicted activities. These metal P-type ATPase

translocators are involved in detoxification of metals by transporting metals across the inner membrane (Ma et al. 2009). It is possible that this P-type metal translocator may be deficient at translocating; however, there is no clear link to N-glycosylation. These data are consistent with the cellular nickel levels of the *pglX*- strain, which were 6-times higher than the *pglJ*- strain. These increased nickel levels may be responsible for the higher hydrogenase activity levels measured in *pglX*- compared to the other two strains, while nickel toxicity could explain the decreased growth in H_2 growth assays. Our data indicate that N-glycosylation regulates [NiFe]-hydrogenases HynABC, correlating with cellular nickel levels. Taken together, this suggests a possible link between our findings; however, their specific interaction with N-glycosylation is still unknown.

Our research connects N-glycosylation to HynABC hydrogenase regulation and nickel/iron homeostasis, two cellular processes which have been associated with pathogenicity in other bacteria(Palyada et al. 2004; Maier and Benoit 2019; Benoit et al. 2020). The presented results deepen our understanding of the role of N-glycosylation in *C. fetus* cell physiology. In addition, the *Cf*-N-glycosylation system provides glycan diversity through PglX and PglY, which may further impact the biology of the microbe and warrants further investigation.

Materials and Methods

Bacterial strains, plasmids, oligonucleotides and growth conditions

Oligonucleotides used in this study are listed in Table S4. Bacterial strains and plasmids are listed in Table S5 *C. fetus* was grown using Brain-Heart Infusion (BHI) medium (BHI-Hardy Diagnostics) and Columbia agar (CBA-Hardy Diagnostics) with 5% defibrinated horse blood (Hemostat, Dixon, CA) under microaerobic conditions (10% CO_2, 5% O_2, 85% N_2) at 37 °C. *E. coli* was grown on 2xYT at 37 °C or as indicated. If required, antibiotics were added to the

following working concentrations: 100 µg/mL ampicillin, 25 µg/mL chloramphenicol, 50 µg/mL kanamycin and 100 µg/mL spectinomycin.

Preparation of whole cell lysates and western blotting

Whole cell lysates of bacterial cells were prepared as described previously (Liu et al. 2006). Protein concentrations were determined using either the NanoVue Plus Spectrophotometer (GE) at A_{280} or by the BioRad DC Bradford assay kit with bovine serum albumin as a protein standard. Samples were either analyzed immediately or were frozen at -20ºC until further use. Western blot analyzes was carried out as described (Nothaft et al. 2010) with anti-His (1:2000) (Rockland), anti-*Cff*-N-glycan (1:5000) (Nothaft et al. 2012) anti-*Cj*-N-glycan (R1, 1:7500) (Nothaft et al. 2012) or anti-CmeA (1:5000) (Wacker et al. 2002) as the primary, and anti-rabbit IgG (1:2000) (Santa Cruz Biotechnology) as the secondary antibody or with alkaline phosphatase labelled wheat germ agglutinin (WGA, 1:500) (EY Labs). Antibody and WGA-lectin reactive bands were visualized directly on the membrane with nitro-blue tetrazolium chloride (NBT) and 5-bromo-4-chloro-3'-indolyphosphate p-toluidine salt (BCIP) alkaline phosphatase substrate solution (Roche) according to the protocol of the manufacturer.

Free oligosaccharides (fOS) preparation and analysis

Free oligosaccharides were obtained by ethanol extraction as described previously (Dwivedi et al. 2013) from 1 g of wet cell pellets. fOS preparations were further purified using porous graphite carbon (PGC) columns as described (Liu et al. 2006). After elution and lyophilization fOS were dissolved in 100 µl of milliQ water and either stored at -20°C or directly analyzed by thin layer chromatography (TLC) as described (Dwivedi et al. 2013).

Generation of *Cff pgl* gene mutant constructs

First, a PCR product containing *Cff-pglKXYJ* (4868 nt) was generated with oligo CS469 and CS470 using chromosomal DNA from *Cff* as a template and inserted into the EcoRV site of plasmid pPCR-Script Amp SK(+). After transforming *E. coli* DH5α, plasmid-containing cells were isolated on plates supplemented with Amp and X-gal (40 μg/ml) and plasmids isolated from white colonies were analyzed by restriction digestion. One positive candidate (pPCR-Script-*Cffpgl*) that had the PCR product with the *Cff pgl* genes inserted in opposite direction to the *lacZ* gene was processed further. Next, plasmid pPCR-Script-*Cffpgl* was digested with either EcoRV (1 site within *pglX*), AccI (1 site within *pglY*) or SpeI (1 site within *pglJ*). The linearized plasmid backbones were isolated and in the case of the AccI and SpeI digests, T4 DNA polymerase was used to generate blunt ends before the DNA fragments were purified by agarose gel extraction. The kanamycin (*kan*) resistance cassette obtained and isolated after SmaI digestion of plasmid pMW2 was ligated with each vector backbone preparation. Amp and Kan resistant colonies obtained after ligation and transformation were screened and verified by restriction analyzes. One positive clone in which the *kan* cassette is transcribed in the same orientation as the corresponding reading frame (*pgl* gene) was used to generate the gene-specific insertions by double homologous recombination into the chromosome of *Cff*.

Transformation and insertion mutagenesis of *Cff*

Natural transformation (on a BHI agar surface) (Wang and Taylor 1990) and electroporation (Baillon et al. 1999) protocols were employed to introduce *Cff-pgl* gene::*kan* plasmid DNA for double homologous integration of the *kan* cassette into *Cff*. To do so, the corresponding suicide plasmids (pPCR-Script-*CffpglX::kan*, pPCR-Script-*CffpglY::kan* and pPCR-Script-*CffpglJ::kan*) were isolated from either *E. coli* DH5α or *E. coli* JM110. The latter

strain was used to generate non-methylated DNA to circumvent the *Campylobacter* restriction modification system. Transformants were selected on BHI plates for kanamycin resistance and individual colonies were isolated, streaked on fresh agar plates and used to isolate chromosomal DNA. Candidate colonies were analyzed and verified by PCR with oligonucleotides hybridizing outside of the recombination event (Figure S1) to confirm integration of the *kan* cassette at the correct position on the chromosome. One positive candidate (for *pglX*- and *pglJ*-) was used for further phenotypical analyzes, whereas (even after multiple attempts) no positive candidate could be obtained for the integration of the *kan* cassette into the *Cff-pglY* gene locus.

Growth curves and motility assays

Growth comparison was performed in BHI broth and growth curves were recorded as described (Dubb et al. 2019). Motility assays were carried out as outlined previously (Golden and Acheson 2002) with slight modifications. Briefly, *Cff*-wildtype and *pgl* mutant strains were grown for 18 h on BHI agar. Cells were harvested from the plates with 2 ml of BHI broth and cell suspensions were diluted to an OD_{600} of 0.05. Then, 1 µl of each cell suspension was spotted onto a BHI 0.3% agar plate and after 24 h of incubation, images were taken and the diameter of the motility zone was measured horizontally and vertically.

Reverse transcriptase (RT) PCR

RT-PCR was performed according to Muraoka and Zhang (Muraoka and Zhang 2011) with RNA extracted from cells grown on BHI agar for 18 h using the RNeasy Kit following the instructions of the manufacturer (Qiagen). PCR conditions after the RT-step were identical for each primer pair and were carried out as follows: 35 cycles with 30 sec, 95°C; 30 sec, 52°C and 20 sec, 72°C followed by a 72°C finalizing step for 3 min. Samples were stored at 4°C before 15 µl of each 50 µl reaction were analyzed by 0.8% agarose gel electrophoresis.

Pgl gene expressing plasmids

Gene-specific oligonucleotides were used to amplify *Cj-pglH, Cj-pglA, Cj-pglJ, Cff-pglA, Cff-pglJ*, *Cff-pglX* and *Cff-pglY* as well as *Cff-pglXY* for expression in *E. coli*. To do so, PCR products obtained with specific template DNA (plasmid p*pgl* for the *C. jejuni pgl* genes or chromosomal DNA from *Cff*) were purified, treated with restriction enzymes and inserted into plasmid pCE111/28 digested with the same enzymes. To generate the *Cff-pglXY* expression plasmid, a PCR product encompassing both open reading frames was generated; in addition, a second plasmid was generated by inserting the *Cff-pglY* PCR product into the pCE111/28 (*Cff-pglX*) product via PstI (introduced by PCR during the cloning of *pglX*) and XhoI simultaneously introducing an optimized RBS site upstream of the *Cff-pglY* start codon, as was done for all the other *pgl* genes. After ligation, transformation and screening on selective (Cm) plates, plasmids isolated from candidate colonies were analyzed by restriction analyzes and verified by DNA sequencing. One positive candidate for each construct was used for further analysis.

Pgl operon expression plasmids

To generate p*pgl* operon mutant plasmids that are compatible with the generated *Cj* and *Cff-pgl* gene expression plasmids (pCE111/28-derivatives, Cm^R), the *cat* cassette from all *pgl* operon plasmids with a *kan* cassette insertion in the various *pgl* genes (Linton et al. 2005) was deleted. To do so, plasmids p*pgl-pglH*::*kan*, p*pgl-pglI*::*kan*, p*pgl-pglJ*::*kan* and p*pgl-pglA*::*kan* were treated with BsaAI excising the *cat* gene but leaving the rest of the plasmid intact. The complete DNA digest reactions were purified and directly re-ligated. To generate the *pgl* operon plasmid lacking *pglH* and *pglI* (p*pgl-pglHI*::*kan*), two PCR products were generated: the first reaction was performed with plasmid p*pgl-pglH*::*kan* as a template and with oligonucleotides pglHI-kan-R and pglHI-pACYC-F amplifying the 5-prime half of the *kan* cassette in *pglH* and

the upstream part of the *Cj-pgl* operon. The second reaction was performed with plasmid p*pgl-pglI*::*kan* as template and with oligonucleotides pglHI-aph-FR and pglHI-pACYC-R amplifying the 3-prime half of the *kan* cassette in *pglI*, the *pglI* downstream region of the *pgl* operon, as well as the origin of replication. The obtained PCR products were purified and ligated without further treatment.

After transformation of DH5α candidate colonies for each ligation reaction were pre-screened on LB agar for Kan^R and Cm^S. The loss of the *cat* cassette and the correct gene organization on plasmids isolated form those colonies were further verified by restriction digest analyzes and DNA sequencing. One positive candidate for each construct (p*pgl*op *pgl*-gene*::kan*, cat- derivative) was used for further analyzes.

Expression of CmeA-His6 in glycosylation competent *E. coli* cells

Functional analysis of certain *Cff-pgl* proteins was performed in the heterologous *E. coli* glycosylation system. *E. coli* CLM24 was sequentially transformed with the individual *pgl* gene expression plasmids (pCE11/28 derivatives), the CmeA-His_6 expression plasmid (pIH18, pEXT21-derivative) and either the plasmid carrying the wildtype *Cj-pgl* operon on p*pg*l or the compatible *pgl* operon mutant plasmids (*cat*- derivatives) with a *kan* cassette inserted into *pglA, pglJ, pglH* and *pglHI* (double mutant). Cells stably maintaining the plasmid combinations were grown as 4 ml cultures over night before inoculating 100 ml of fresh medium to a starting OD_{600} of 0.1. Cells were further grown until an OD_{600} of 0.5-0.7 was reached and CmeA-His_6 expression (constitutively low expressed from the tetracycline promoter on pIH18) was further induced by the addition of IPTG to a final concentration of 0.5 mM. After growth for an additional 4 h, cells were cooled on ice for 10-15 min, pelleted by centrifugation (10 min, 12,000 rpm, 4 °C) and washed twice with ice-cold 1 x PBS buffer. Then, 1/10 of the pellet

(corresponding to 10 ml of culture volume) was used to produce whole cell lysates using Bacterial Protein Extraction Reagent B-PER (Thermo Scientific) according to the instructions of the manufacturer and the remainder of cells was used to generate whole cell lysates (as described, (Liu et al. 2006) for the purification of the corresponding CmeA-His_6 proteins by Ni-NTA affinity chromatography. To do so, whole cell extracts were filtered (0.22 µm), and loaded onto a 10 ml gravity-flow cartridge (Amersham Pharmacia Biosciences) pre-loaded with 0.5 ml Ni-NTA agarose and pre-equilibrated with 1 column volume 1 x PBS. The column was subsequently washed with at least 5 column volumes of 1 x PBS containing 20 mM imidazole and bound CmeA-His_6 protein was eluted with 0.5 – 1.5 ml of PBS containing 0.5 M imidazole. Purified proteins were stored at 4 °C until further use or immediately analyzed by 12.5% PAGE/mass spectrometry and/or western blotting.

Hydrogen growth conditions

Growth of *Cff* under hydrogen was performed according to the following protocol (Benoit and Maier 2018) with the following changes. *Cff* cells were grown for 48 h then streaked on BHI plates and further incubated for 12 h at 37°C under microaerobic conditions. Cells were resuspended in BHI broth and standardized to the same optical density at 600 nm (OD_{600}), 3.0 to 4.0. Sealed 165 mL bottles containing 10 mL BHI were flushed with N_2 gas for 10 min, then CO_2 (10% headspace partial pressure, h.p.p.) and O_2 (5% h.p.p.) were injected in every bottle. H_2 (20% h.p.p.) was added as indicated. Cells were inoculated (1:100) and grown at 37 °C while shaking at 200 rpm. Growth yields from 3 biological replicates (each performed in duplicate) were determined after 48 h by serially diluting in BHI and plating on CBA. Plates were incubated at 37 °C in microaerobic conditions for three days before being counted.

Whole-cell H_2-uptake hydrogenase assays

H_2-uptake was performed as previously described (Maier et al. 1996). *Cff* cells were grown at 37 °C for 24 h on BHI plates under microaerobic conditions either with 10% H_2 or without. Cells were harvested and resuspended in phosphate buffered saline (PBS) to an optical density (OD_{600}) of 1 which corresponds to ~2.3 x 10^9 cells/mL. A 2 mL chamber was filled with cells followed by an injection with PBS saturated with H_2. H_2-uptake was monitored as previously described (Maier et al. 1996). Values are reported as nanomoles of H_2 used per min per 10^9 cells and represent 4 independent measurements for cells grown in microaerobic conditions (and no H_2) and 2 measurements for cells grown in microaerobic conditions with the addition of 10% H_2.

Determination of iron and nickel content

Cff cells grown at 37 °C for 24 h on two BHI plates under microaerobic conditions and harvested with a loop in 1 mL metal-free double distilled water. Samples were centrifuged at 10,000 *g* for 5 min, washed once with water, resuspended and lysed by sonication A portion of lysed sample was used to determine the protein concentration using the bicinchoninic acid assay (BCA, Thermo Scientific Pierce) assay. Samples were centrifuged at 15, 000 x *g* for 5 min and the supernatant was analyzed for iron and nickel. The remaining sample portion was used for metal (Fe or Ni) content analysis. Briefly, Fe and Ni concentrations were measured by atomic absorption, using a Shimadzu AA-6701F spectrophotometer. All samples were diluted (in 1% HNO_3) to be in the range of the standard curve (0 to 0.4 μM of either Fe or Ni) generated using atomic absorption-grade standard Fe or Ni solutions (Sigma). Results shown are means and standard deviations for 3 to 5 measurements.

Ethidium bromide accumulation assay

Accumulation of ethidium bromide (EtBr) was performed using the following protocol (Lin et al. 2002) with the following changes. *Cff* strains were grown overnight on BHI agar at 37°C in microaerobic conditions and harvested with MEM (Gibco). Cultures were adjusted to OD_{600} of 0.2 and then incubated at 37 °C for 30 min in microaerobic conditions. EtBr was added to a final concentration of 2 µg/mL. Fluorescence was measured, with an excitation of 530 nm and emission of 600 nm, every 2 min over a 20 min time using a Bio Tek Synergy H1 plate reader. This was performed in three biological replicates, which included three technical replicates. Background fluorescence of MEM with EtBr was subtracted from these values.

Antibiotic MIC assay

Cff cells were grown for 24 h at 37 °C in microaerobic conditions on CBA plates. Antibiotic MIC was assessed using the Sensititre (Trek Diagnostic Systems) platform. Sensititre plate EQUIN1F was used, following manufacturer's instructions.

Preparation of bacterial whole cell proteome samples

Cff cells were grown for 24 h at 37 °C under microaerobic conditions on BHI agar. Cells were harvested with ice-cold PBS and inactivated with PBS, 10% sodium azide for 30 min at 4°C. Cell pellets obtained after centrifugation (4,000 x g for 15 min) were lyophilized and stored at -20°C until further use. Cell lysates for proteomic analyses were prepared as follows: cells were solubilized in 4% SDS, 100 mM Tris pH 8.0, and 20 mM DTT and boiled at 95˚C with shaking at 2000 rpm for 10 min. Insoluble material was removed by centrifugation at 17,000 x *g* for 10 min at room temperature and the supernatant was collected. Protein concentrations were determined using the bicinchoninic acid assay (Thermo Scientific Pierce) and 200 µg of protein from each sample was acetone-precipitated overnight at -20 ˚C by mixing 4 volumes of ice-cold

acetone with one volume of sample. Samples were then spun down at 16,000 X *g* for 10 min at 4˚C. The precipitated protein pellets were resuspended with 80% ice-cold acetone and precipitated for an additional 4 hours at -20 ˚C. Samples were spun down at 17,000 X *g* for 10 min at 4 ˚C to collect the precipitated protein.

Digestion of complex protein lysates

Dried protein pellets were resuspended in 6 M urea, 2 M thiourea, 40 mM NH_4HCO_3 and reduced / alkylated prior to digestion with Lys-C (1/200 w/w) and then trypsin (1/50 w/w) overnight as previously described (Scott et al. 2011). Digested samples were acidified to a final concentration of 0.5% formic acid and desalted with home-made high-capacity StageTips composed on 5mg Empore™ C18 material (3M, Maplewood, Minnesota) and 5 mg of OLIGO R3 reverse phase resin (Thermo Fisher Scientific) according to the protocol of Ishihama and Rappsilber (Ishihama et al. 2006; Rappsilber et al. 2007). Bound peptides were eluted with buffer B, dried and stored at -20 ˚C.

Reversed phase liquid chromatography- mass spectrometry (LC-MS)

Purified peptides were resuspended in Buffer A* and separated using a two-column chromatography set up comprising a PepMap100 C18 20 mm x 75 μm trap and a PepMap C18 500 mm x 75 μm analytical column (Thermo Scientific). Samples were concentrated onto the trap column at 5 μl/min for 5 min and infused into an Orbitrap Elite™ Mass Spectrometer (Thermo Scientific) at 300 nl/min via the analytical column using a Dionex Ultimate 3000 UPLC (Thermo Scientific). Then, 180 min gradients were run altering the buffer composition from 3% buffer B to 28% B over 150 min, then from 28% B to 40% B over 10 min, then from 40% B to 100% B over 2 min, followed by the composition held at 100% B for 3 min, and then dropped to 3% B over 5 min and held at 3% B for another 10 min. The Orbitrap Mass Spectrometer was

operated in a data-dependent mode automatically switching between the acquisition of a single Orbitrap MS scan (60,000 resolution) followed by one data-dependent HCD (resolution 15 k AGC target of 4×10^5 with a maximum injection time of 250 ms, NCE 40) and CID (ion trap, AGC target of 5×10^4 with a maximum injection time of 100 ms, NCE 35) event for each precursor (total of five precursors per cycle with 45 seconds dynamic exclusion enabled).

Proteome Data analysis

Proteome analysis to assess the expression of proteins within *Cff* strains was undertaken with MaxQuant (v1.5.3.30 (Cox and Mann 2008)). Database searching was carried out against the *Campylobacter fetus* subsp. *fetus* strain ATCC 27374 proteome (generated from a Maxquant generated six frame translation of the in-house sequenced strain). Searches were undertaken with the following search parameters: carbamidomethylation of cysteine as a fixed modification; oxidation of methionine, acetylation of protein N-terminal trypsin/P cleavage with a maximum of 2 missed cleavages. To enhance the identification of peptides between samples, the Match between Runs option was enabled with a precursor match window set to 2 min and an alignment window of 10 min. For label free quantitation, the MaxLFQ option within Maxquant was enabled in addition to the re-quantification module (Cox et al. 2014). The resulting outputs were processed within the Perseus (v1.5.0.9) analysis environment to remove reverse matches and common proteins contaminations prior to further analysis (Tyanova et al. 2016). Statistical analysis was undertaken in Perseus by grouping biological replicates, imputing missing values based on observed values (downshifted by 2.5 standard deviations with a width of 0.3 standard deviations) and then comparing groups using a student t-test. To define an appropriate *p*-value threshold, multiple hypothesis correction was undertaken using a Benjamini Hochberg correction with an FDR of 0.05. All statistical outputs are provided within Supplementary Table S1. All

mass spectrometry proteomics data have been deposited to the ProteomeXchange Consortium via the PRIDE partner repository (Vizcaíno et al. 2016) with the dataset identifier PXD014538 (LFQ experiments of *C. fetus fetus* mutants accessible using the **username:** reviewer71456@ebi.ac.uk, **Password:** B5YuYNx8) and PXD017832 (analysis of *C. fetus fetus pgl* enzymes in the heterologous *E. coli* glycosylation system (Supplementary MS data 2) accessible using the **username:** reviewer23740@ebi.ac.uk **Password:** PHKlhnSp).

Glycopeptide data analysis

Glycopeptides were identified by manually interrogating possible glycopeptide scans based on the presence of the diagnostic oxonium ion (204.09 m/z) of HexNAc. To facilitate glycopeptide assignments from HCD scans, the ions below the mass of the predicted deglycosylated peptides were extracted with Xcalibur v2.2 using the Spectrum list function. Ions with a deconvoluted mass above that of the deglycosylated peptide and ions corresponding to known carbohydrate oxoniums were removed in a similar approach to post-spectral processing of ETD data and then searched with Mascot (http://www.matrixscience.com/, v2.5). Searches were carried out using semi-trypsin specificity, carbamidomethylation of cysteine as a fixed modification and oxidation (M) as a variable modification. A precursor and product tolerance of 20 ppm was used, and the taxonomy restricted to "Other Proteobacteria". All spectra were searched with the decoy option enabled with all peptides passing a 1% FDR. Identified glycopeptide spectra were manually inspected and spectra annotated according to the nomenclature of Roepstorff and Fohlman (Roepstorff and Fohlman 1984) for peptides as well as Domon and Costello (Domon and Costello 1988) for glycans.

Data Availability

All mass spectrometry proteomics data have been deposited to the ProteomeXchange Consortium via the PRIDE partner repository with the dataset identifier PXD014538.

Acknowledgements

We thank the Melbourne Mass Spectrometry and Proteomics Facility of the Bio21 Molecular Science and Biotechnology Institute at The University of Melbourne for mass spectrometry analysis. We also thank Susan Sanchez and the Athens Veterinary Diagnostic Laboratory for help with the antibiotic sensitivity assay.

CHAPTER 3

CHARACTERIZATION OF A PUTATIVE BACTERIOPHAGE GLUCOSYLATION OPERON IN *CAMPYLOBACTER FETUS* TYPE A STRAINS[2]

[2]**Duma, J.**, Nothaft, H., Vinogradov, E., Hussack, G., Zhao, Y., Elsayed M., Kadouri, D., Curtis J., Maier, R., Szymanski, C.M. To be submitted to Glycobiology

Abstract

In *Campylobacter fetus,* S-layer (Sap)-type and serotype correlate and are subsequently linked to lipopolysaccharide (LPS) composition. These surface antigens are closely linked to the *C. fetus* subspecies niche and virulence; for instance, type A strains are more commonly isolated from human blood than type B. Here we identify a putative bacteriophage-associated glucosylation operon known as *gtrABC*, which we have found in all sequenced type A *C. fetus* strains. In other microbes, this three-component operon is normally involved in serotype conversion of LPS. Using UDP-Glo^{TM} assays of recombinant GtrB indicate that GtrB in *C. fetus* subsp. *fetus* 82-40 utilizes UDP-glucose and decaprenyl-phosphate, an analog of undecaprenyl-phosphate. In conjunction, we analyzed the lipid product of overexpressed GtrB, which is consistent with undecaprenyl-phosphate-glucose. Together, these results indicate that the operon in *C. fetus* subsp. *fetus* 82-40 functions like a canonical *gtr* operon. To further elucidate the function of the *gtr* operon we generated an insertional mutant in *gtrB* in *C. fetus* subsp. *fetus* 82-40. Using NMR, we were able to determine that the wild-type and *gtrB* LPS O-antigen primarily consists of →3)-*α*-D-Man*p*2Ac-(1→, previously seen, and a newly described a-GalNAcA-3-b-Glc- modification. Also, we show that the O-antigen is capped with a-GlcNAc-3-a-GlcNAc- but is absent in the *gtrB* mutant suggesting a possible Glc to GlcNAc mechanism. Interestingly, the *gtrB* mutant showed decreased S-layer protein (SLP) association in S-layer extractions. We saw a three-fold decrease in serum-resistance in the *gtrB* mutant which suggests *gtrB* mutant has impaired S-layer. Our research links bacteriophage acquired glycosyltransferases to LPS-SLP interactions. In addition, the presence of the *gtr* operon in a sequenced type A strains may indicate that the *gtr* operon may be essential for S-layer formation.

Introduction

Campylobacter fetus is an emerging pathogen consisting of three subspecies, *C. fetus* subsp. *fetus*, *C. fetus* subsp. *venerealis*, and *C. fetus* subsp. *testudinum*. These species are known to colonize the mucosal surfaces of animals and humans where they can cause reproductive failure, invasive infections, diarrhea, and mortality (Blaser 1988; Wagenaar et al. 2014). In cases of *Campylobacter*-mediated bacteremia, C. *fetus* is the most-often detected species ranging from 19-53% depending on the study (Guerrant et al. 1978; Pacanowski et al. 2008; Fernández-Cruz et al. 2010). However, *C. fetus* subsp. *venerealis* (*Cfv*) is primarily adapted to bovines, where it can colonize the genital tract causing bovine genital *Campylobacter*iosis, an infection resulting in infertility or abortion. Similarly, *C. fetus* subsp. *fetus* (*Cff*) can also cause reproductive failure and abortions in livestock but is generally found in the intestines of sheep. However, *Cff* is considered a generalist because it can colonize a wider variety of hosts compared to the other subspecies; this includes sheep, cattle, birds, reptiles, and humans. *C. fetus* subsp. *testudinum* (*Cft*), a newly sequenced reptile-associated isolate, has been associated with human infections (Fitzgerald et al. 2014; Wang et al. 2015). A more recent study found that 8% of humans had *C.* fetus in their fecal metagenomes, suggesting that it might be an unacknowledged pathobiont in the human (Iraola et al. 2017).

One of the main adaptive mechanisms of *C. fetus* is the paracrystalline proteinaceous array that forms a capsule-like structure known as the S-layer. There are two S-layer proteins (SLP), surface array protein (Sap) SapA and SapB; they make up sap-types A, B and the rare AB type (Kienesberger et al. 2014; Gilbert et al. 2016). These SLPs can vary their antigenicity by gene recombination, with up to 9 s*ap* gene homologs found in the genome (Perez-perez et al.

1986; Dworkin et al. 1997; Tu et al. 2001). S-layer in *C. fetus* can provide resistance to antibody-mediated and complement-dependent killing, through Sap-protein recombination and capsule-like coating, respectively (Blaser et al. 1988). This serum resistance attributed to the S-layer, causes increased dissemination in mice, sheep, and humans (Pei and Blaser 1990; Blaser and Pei 1993; Neuzil et al. 1994; Grogono-Thomas et al. 2000).

The sap-type correlates with the antigenic serotype, sero-/sap-type (type), which is subsequently linked to lipopolysaccharide (LPS) composition. As mentioned above, there are three serotypes reported A, B and occasionally AB. Interestingly, however serotype AB does not share similar LPS composition as A (Perez-Perez et al. 1986; Moran et al. 1994). Interestingly type A strains have been predominantly associated with human origins (Kienesberger et al. 2014; Iraola et al. 2017). Bovine associated *Cfv* is reported to be exclusively type A (Kienesberger et al. 2014). This is supported by a recent model suggesting that cattle-derived *C. fetus* may have originated from a human ancestor during livestock domestication (Iraola et al. 2017).

Type-specific interactions between SLP and LPS are believed to be mediated through SLP binding to the O-antigen, with the LPS binding domain located in the N-terminal (Yang et al. 1992). This SLP-LPS association was also found to mask LPS from lectin binding, suggesting another mechanism in immune evasion (Fogg et al. 1990). The O-antigens of type A and B share no structural homology, with type A consisting of →3)-*α*-D-Man*p*2Ac-(1→ with 80 - 90% o-acetylation at position 2, and type B *α*-D-Rha*p*3Me-(1→3)-*β*-D-Rhap-(1→2)-*α*-D-Rha*p*(1→$_{1,2}$ (S N Senchenkova et al. 1996; S N Senchenkova et al. 1997). However, the overall composition indicates that they may share similar attributes in the core structure (Moran et al. 1994).

In our analysis of the *Cff* 82-40 genome, we identified an insertional element associated with O-antigen serotype conversion. These genes are homologous to the bacteriophage

glucosylation operon, *gtr*, which is involved in the addition of glucose to the O-antigen. This is a three-component system consisting of three proteins: GtrA, a flippase for the UndP-Glc intermediate, GtrB, a Undecaprenyl (Und) glucosyltransferase, and GtrC/Gtr*, a serotype-specific glucosyltransferase (Mann and Whitfield 2016). Here, we annotate a putative glucosylation operon located in the protein glycosylation (*pgl*) cluster of *C. fetus* as a bacteriophage-associated glucosylation *gtr* operon. Although, this operon is inserted in the N-glycosylation cluster of all type A *C. fetus* strains, its absence in type B strains indicates that it plays no role on N-glycosylation (Nothaft et al. 2012, Duma et al. 2020). *In vitro* assays were performed, characterizing the GtrB homolog, indicating that this three-component system is consistent with previously annotated *gtr* systems like those found in *Shigella* and *Salmonella*. Using mutant of *gtrB* in *Cff* 82-40 we were able to see a decrease in LPS molecular weight and decreased SLP association. In addition, we were able to identify two new modifications on the LPS by NMR, α-GalNAcA-3-β-Glc- and a α -GlcNAc-3- α -GlcNAc- cap which was absent in the *gtrB* mutant. Although we were unable to see Glc present on the LPS by NMR, previous publications have reported seeing Glc of relative values of 6.5% composition in other type A strains (Moran et al. 1994; S N Senchenkova et al. 1997). In addition, we generated a *gtrB* insertional mutant, which had a significant decrease in serum resistance and lost its S-layer compared to the wild-type. These findings indicate that the *gtr* operon may be a conserved feature in all type A strains and is required for generating a stable SLP-LPS association.

Results

Annotation and presence of the *gtr* operon

Analysis of the *Cff* 82-40 genome indicate a three-component operon within the *pgl* cluster with CFF8240_1391 belonging to the GtrA family and two hypothetical proteins with

GT2 domains (Figure 3.1A). Conserved domain analysis of CFF8240_1390, indicates that it shares a glucosyl transferase GtrII (pfam14264) domain, with Gtr*/GtrC of *S. flexneri*. This suggests that CFF8240_1390, is likely involved in the transfer of Glc to the glycan backbone and not to the lipid-carrier. Point mutants and structural data of the *Synechocystis* sp. PCC6803 GtrB indicates that CFF8240_1389 is likely GtrB (Figure 3.2) (Ardiccioni et al. 2016). Amino acids found to be relevant in GtrB activity also aligned with the *Cff* GtrB (CFF8240_1389), except for A_{136}, which is S_{162}. CFF8240_1389, CFF8240_1390 and CFF8240_1391 will be referred to as *gtrB*, *gtrC*, and *gtrA* respectively from here on. The *gtr* operon has been previously annotated as having a decrease in GC content compared to flanking regions (Jakhetia et al. 2013). In comparison, our *gtr* operon has a GC content of ~23% compared to the flanking *pgl* locus, which has a GC content of ~34%; suggesting a bacteriophage genomic insertion (data not shown).

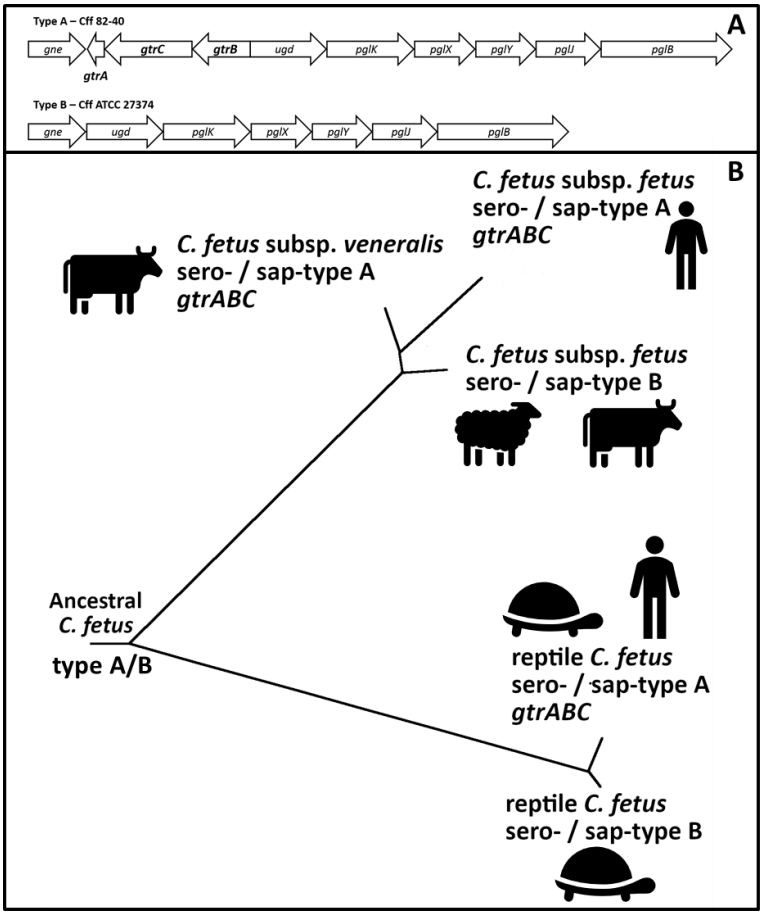

Figure 3.1. Bacteriophage-associated glucosyltransferase, *gtr* operon in *C. fetus*. (A) Cluster of protein glycosylation, *pgl*, genes in *C. fetus* subspecies *fetus* (*Cff*) 82-40, type A, with putative glucosyltranferase operon, *gtr*, insertion between *gne* and *ugd. GtrA* is predicted to be a putative flippase, *gtrB* a glycosyltransferase, and *gtrC* a glucosyltransferase with homology to *Shigella flexneri* Gtr (type) proteins. In *C. fetus* subsp. *fetus* ATCC 27374, (type B) this region lacks the operon and is not present in the genome (data not shown) (B) *C. fetus* subspecies phylogeny, host/source, sero-/ sap-type (type), and *gtr* operon, adapted from Dingle K.E. et al. 2010 (Dingle et al. 2010). All of type A *C. fetus* strains annotated in File S1, contain genes with high homology to the *gtr* operon, which has been reported to be involved in O-antigen serotype conversion (Mann E. and Whitfield C., 2016).

Identification of the *gtr* operon in all sequenced *Cf* strains indicated that it was present in all subspecies. In addition, the presence of the *gtr* operon was exclusively found in all *sap*-/sero-type A (type A) strain (Figure 3.1B) (Table 3.1) (Gilbert et al. 2016). The *gtr* operon was only located between the glucose-6-epimerase (gne) and UDP-glucose dehydratase (ugd) (Nothaft et al. 2012).

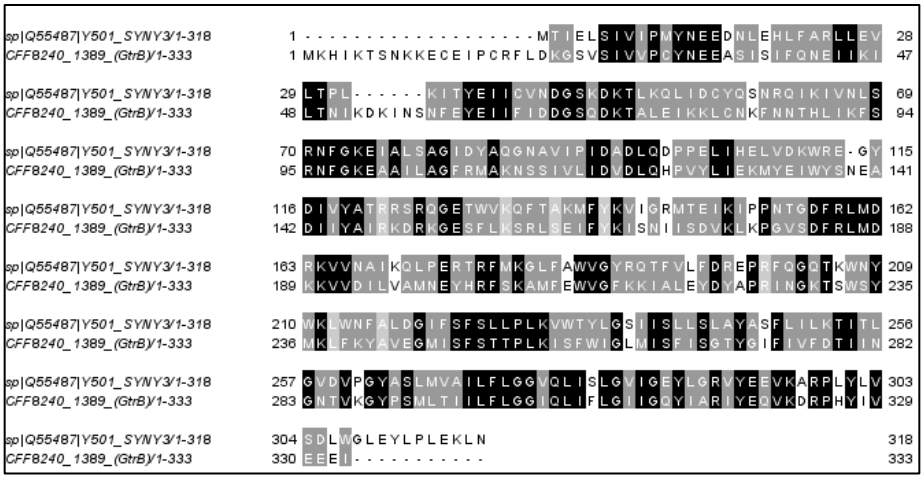

Figure 3.2. Sequence alignment of *C. fetus* subsp. *fetus* 82-40 GtrB (CFF8240_1389) with annotated *Synechocystis* sp. PCC6803 GtrB (Q55487). Light grey boxes indicate amino acids previously identified with the function of the *Synechocystis* sp. PCC6803 GtrB (Ardiccioni et al. 2016). Black boxes highlight amino acids that are conserved in both sequences, while dark grey indicates conserved amino acids of 6 or greater according to Jalview (Waterhouse et al. 2009).

Analysis of type A *C. fetus* LPS

To determine if the *gtr* enzymes are responsible for the addition of Glc to LPS we made a *gtrB* mutant in *Cff* 82-40 (Figure 3.3). A *gtrB* mutant (*gtrB*) would be unable to make the Und-P-Glc intermediate necessary for GtrC, and subsequently unable to transfer it to the LPS. Previous analysis of *Cff* type A LPS indicated the presence of Glc, however this was not structurally assigned to the LPS (Moran et al. 1994; S N Senchenkova et al. 1997). To confirm if the *gtr* operon was responsible for modifying LPS, we performed a silver stain of crude LPS isolate. The *gtrB* mutant showed a decrease in molecular weight which is consistent with the loss of a sugar residues (Figure 3.5C) (Kienesberger et al. 2014). These results indicated that the *gtr* operon was likely playing a role in LPS biosynthesis.

Table 3.1. *In silico* annotation of *gtr* operon in *C. fetus* and correlation to serotype, and sap-type. *Cft*, *C. fetus* subsp. *testudinum*; *Cff*, *C fetus* subsp. *fetus*; *Cfv*, *C. fetus* subsp. *veneralis*. ARG, Argentina; AUS, Australia; BEL, Belgium; CHN, China; FRA, France; NLD, Netherlands; ZAF, South Africa; GBR, United Kingdom; USA, United States; URY, Uruguay. [a] Predicted *sap* type adapted from Gilbert M. J. et al. 2016 with additions based on sequence (Gilbert et al. 2016). [b] Serotype based on sequence homology: serotype A, putative mannosyltransferase (WP_002848815.1); serotype B, *wcbK* (SQH29839.1). [C] Presence of gtr genes is based on sequence homology to *gtrABC* in our reference strain Cff 82-40. *Pseudogene

Species	Strain	Host	Source	Origin	*sap*[a]	Serotype[b]	*gtr* genes[C]		
							A	B	C
Cft	D4335	Human	Feces	USA	A	A	+	+	+
Cft	11S02557-2	Chelonian (*Mauremys annamensis*)	Feces	NLD	A	A	+	+	+
Cft	CF78.2	Lizard (*Tiliqua nigrolutea*)	Feces	GBR	A	A	+	+	+
Cft	SP3	Snake (*Heterodon nasicus*)	Feces	GBR	A	A	+	+	+
Cft	12S02263-3	Chelonian (*Aldabrachelys gigantea*)	Feces	NLD	A	A	+	+	+
Cft	12S02225-3	Lizard (*Tiliqua rugosa*)	Feces	NLD	A	A	+	+	+
Cft	D6856	Human	Bile	USA	A	A	+	+	+
Cft	D6690	Human	Blood	USA	A	A	+	+	+
Cft	D6683	Human	Hematoma	USA	A	A	+	+	+
Cft	D6659	Human	Pleural fluid	USA	A	A	+	+	+
Cft	pet-3	Lizard (*Hydrosaurus pustulatus*)	Feces	CHN	A	A	+	+	+
Cft	03-427	Human	Blood	USA	A	A	+	+	+
Cft	D6783	Human	Feces	USA	A	A	+	+	+
Cft	12S05168-1	Snake (*Python reticulatus*)	Feces	NLD	A	A	+	+	+
Cft	772	Human	Ascitic fluid	CHN	A	A	+	+	+
Cft	85-387	Chelonian (*Terrapene carolina*)	Feces	USA	AB	B	-	-	-
Cft	12S02855-1	Snake (*Orthriophis taeniurus*)	Feces	NLD	AB	B	-	-	-
Cft	12S02847-1	Snake (*Boa constrictor*)	Feces	NLD	AB	B	-	-	-
Cft	12S02842-30	Chelonian (*Aldabrachelys gigantea*)	Feces	NLD	B	B	-	-	-
Cft	13S00388-15	Chelonian (*Chelonoidis denticulata*)	Feces	NLD	A	A	+	+	+
Cft	12S04217-1	Chelonian (*Cuora mouhotii*)	Feces	NLD	B	B	-	-	-
Cft	12S00416-3	Chelonian (*Geochelone elegans*)	Feces	NLD	B	B	-	-	-
Cff	BT 10/98	Ovine	Unknown	GBR	A	A	+	+	+

Cff	**MMM01**	**Human**	**Blood**	**IND**	**A**	**A**	**+**	**+**	**+**
Cff	**NCTC10842**	**Ovine**	**Fetal brain**	**USA**	**B**	**B**	**-**	**-**	**-**
Cff	**ATCC 27374**	**Ovine**	**Fetal brain**	**USA**	**B**	**B**	**-**	**-**	**-**
Cff	**82-40**	**Human**	**Blood**	**USA**	**A**	**A**	**+**	**+**	**+**
Cff	**H1-UY**	**Human**	**Blood**	**URY**	**A**	**A**	**+**	**+**	**+**
Cff	**04/554**	**Bovine**	**Fetus**	**ARG**	**B**	**B**	**-**	**-**	**-**
Cff	**98/v445**	**Bovine**	**Prepuce**	**GBR**	**B**	**B**	**-**	**-**	**-**
Cfv	**cfvi9825**	**Bovine**	**Fetus fluid**	**ARG**	**A**	**A**	**+**	**+**	**+**
Cfv	**cfvi02/298**	**Bovine**	**Feces**	**ARG**	**A**	**A**	**+**	**+**	**+**
Cfv	**ADRI1362**	**Bovine**	**Unknown**	**AUS**	**A**	**A**	**+**	**+**	**+**
Cfv	**cfvi03/596**	**Bovine**	**Fetus**	**ARG**	**A**	**A**	**+**	**+**	**+**
Cfv	**99/541**	**Bovine**	**Prepuce**	**ARG**	**A**	**A**	**+**	**+**	**+**
Cfv	**66Y**	**Bovine**	**Genital**	**CAN**	**A**	**A**	**+**	**+**	**+**
Cfv	**TD**	**Bovine**	**Genital**	**CAN**	**A**	**A**	**+**	**+**	**+**
Cfv	**cfvB10**	**Bovine**	**Unknown**	**USA**	**A**	**A**	**+**	**+**	**+**
Cfv	**LMG 6570**	**Bovine**	**Unknown**	**BEL**	**A**	**A**	**+**	**+**	**+**
Cfv	**NCTC 10354**	**Bovine**	**Vagina**	**GBR**	**A**	**A**	**+**	**+**	**+**
Cfv	**CCUG 33900**	**Bovine**	**Abortion**	**FRA**	**A**	**A**	**+**	**+**	**+**
Cfv	**cfvi97/532**	**Bovine**	**Vagina**	**ARG**	**A**	**A**	**+**	**+**	**+**
Cfv	**01/165**	**Bovine**	**Mucus**	**ARG**	**A**	**A**	**+**	**+**	**+**
Cfv	**cfvi92/203**	**Bovine**	**Placenta**	**ARG**	**A**	**A**	**+**	**+**	**+***
Cfv	**WBT011/09**	**Unknown**	**Unknown**	**GBR**	**A**	**A**	**+**	**+**	**+**
Cfv	**zaf65**	**Bovine**	**Unknown**	**ZAF**	**A**	**A**	**+**	**+**	**+**
Cfv	**84-112**	**Bovine**	**Genital Secretion**	**USA**	**A**	**A**	**+**	**+**	**+**
Cfv	**97/608**	**Bovine**	**Placenta**	**ARG**	**A**	**A**	**+**	**+**	**+**
Cfv	**B6**	**Bovine**	**Vagina**	**GBR**	**A**	**A**	**+**	**+**	**+**
Cfv	**cfvi03/293**	**Bovine**	**Unknown**	**ARG**	**A**	**A**	**+**	**+**	**+**
Cfv	**zaf3**	**Bovine**	**Fetus**	**ZAF**	**A**	**A**	**+**	**+**	**+**
Cfv	**CCUG 33872**	**Unknown**	**Abortion**	**FRA**	**A**	**A**	**+**	**+**	**+**
Cfv	**ADRI513**	**Unknown**	**Unknown**	**AUS**	**A**	**A**	**+**	**+**	**+**
Cfv	**642-21**	**Bovine**	**Vagina**	**AUS**	**A**	**A**	**+**	**+**	**+**

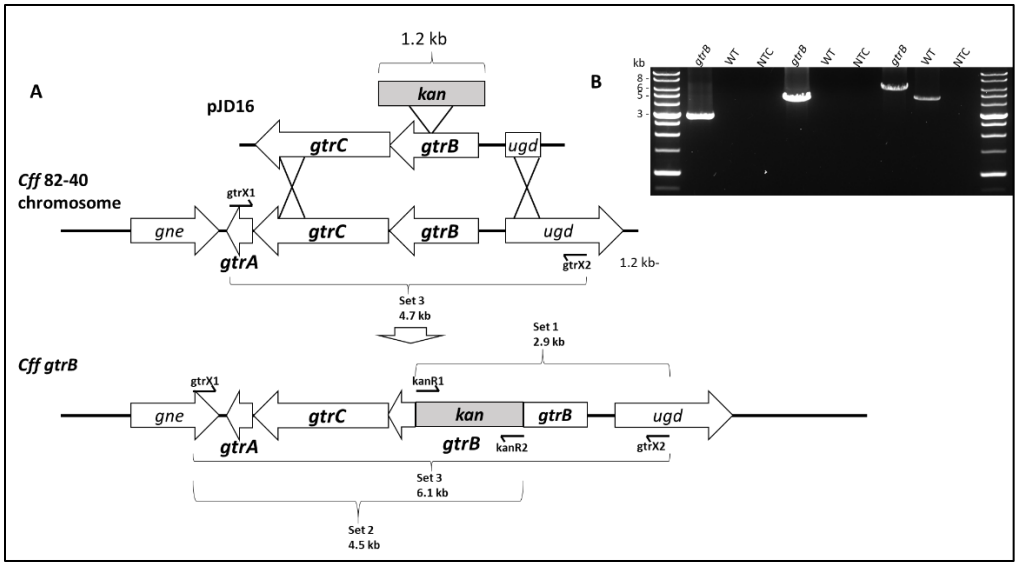

Figure 3.3. Gene disruption of *gtrB C. fetus* subspecies fetus 82-40. (**A**) The *gtrB* gene was disrupted by recombination with a suicide vector, pJD16, containing a copy of *gtrB* with a kanamycin resistance cassette (Km) inserted into the gene. Suicide plasmid pJD16 was introduced into strain 82-40 by electroporation; the double-crossover event resulted in the formation of strain Cff 82-40 *gtrB*. Primer sets 1, 2 and 3 contained specific combinations of gtrX1, gtrX2, kanR1, and kanR2, which were used to amplify from the *kan* insert or span the whole gene region. ***(B)*** Agarose gel with PCR products to verify the insertion of *kan* into the genome from *gtrB::kan*. *C. fetus* subsp. *fetus* 82-40 was used as a wild-type (WT) control, which should not have products with primer sets 1 and 2. A no-template control (NTC) was included which comprised the normal PCR reaction mixture minus the *gtrB* template DNA. The following PCRs are consistent with an insertion event into *gtrB* of *Cff* 82-40.

To determine if a Glc was indeed being added to LPS we extracted LPS from both WT and *gtrB* and hydrolyzed it with 2% AcOH to generate O-antigen polysaccharide (PS), which was used for NMR assignment. The ^{1}H-^{13}C HSQC spectrum showed that the PS consisted of -3-α-D-Man*p*2OAc- with a length of approximately 5-10 residues, which is consistent with prior findings of type A LPS (Figure 3.4) (Moran et al. 1994; S N Senchenkova et al. 1997). However, we saw no distinct signals of core LPS or indications of alterations in the PS.

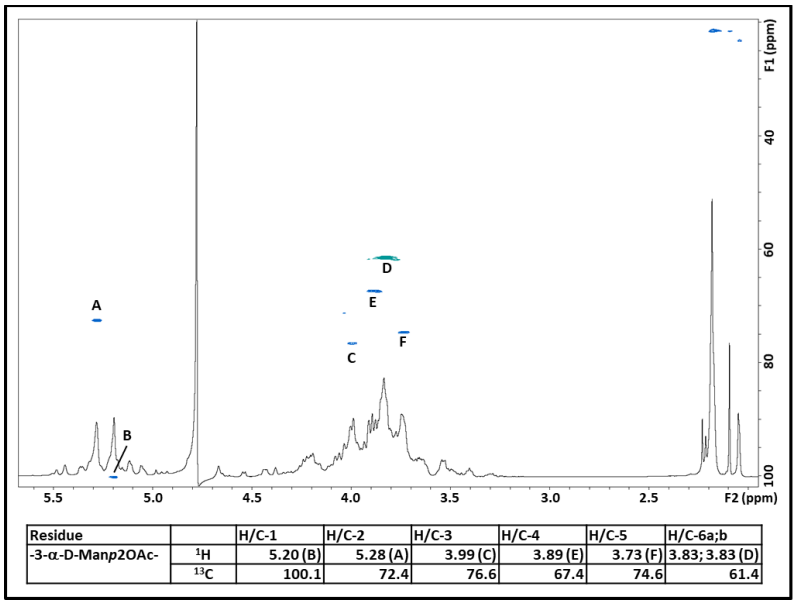

Residue		H/C-1	H/C-2	H/C-3	H/C-4	H/C-5	H/C-6a;b
-3-α-D-Man*p*2OAc-	^{1}H	5.20 (B)	5.28 (A)	3.99 (C)	3.89 (E)	3.73 (F)	3.83; 3.83 (D)
	^{13}C	100.1	72.4	76.6	67.4	74.6	61.4

Figure 3.4. NMR spectrum of LPS O-antigen purified from *Cff* 82-40. ^{1}H-^{13}C HSQC– low intensity. D_2O, 25°C, 600 MHz. OAc at 2.07/23.5 ppm. Repeat of approximately 5-10 residues determined as determined by NMR. Chemical shifts (δ_H/δ_C) for 3-a-D-Manp2OAc are found in the table below, letters represent assigned signals.

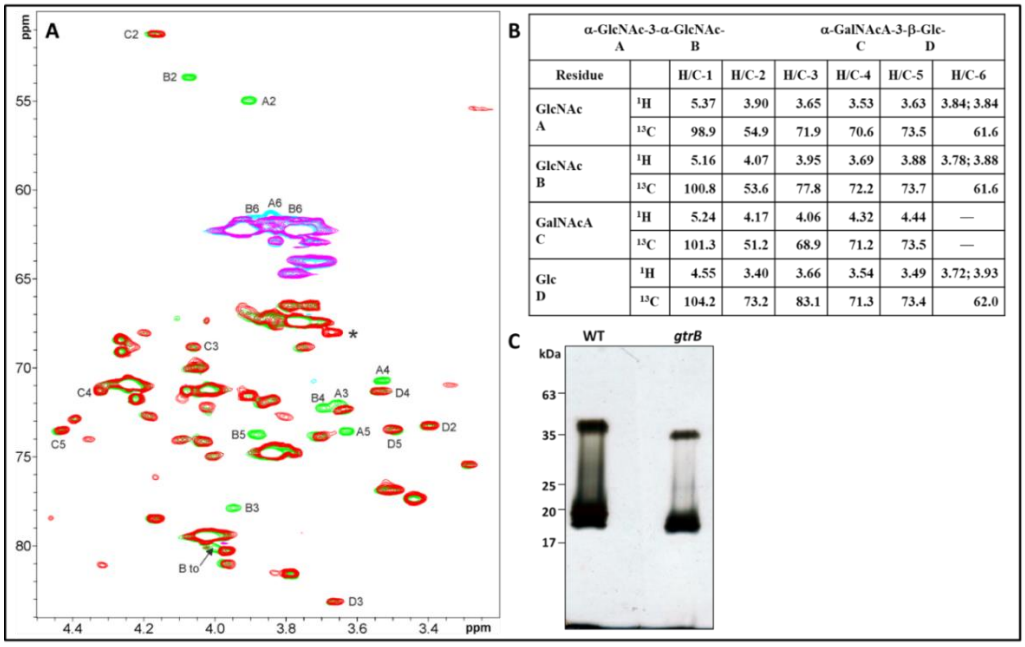

α-GlcNAc-3-α-GlcNAc- A B				α-GalNAcA-3-β-Glc- C D			
Residue		H/C-1	H/C-2	H/C-3	H/C-4	H/C-5	H/C-6
GlcNAc A	^{1}H	5.37	3.90	3.65	3.53	3.63	3.84; 3.84
	^{13}C	98.9	54.9	71.9	70.6	73.5	61.6
GlcNAc B	^{1}H	5.16	4.07	3.95	3.69	3.88	3.78; 3.88
	^{13}C	100.8	53.6	77.8	72.2	73.7	61.6
GalNAcA C	^{1}H	5.24	4.17	4.06	4.32	4.44	—
	^{13}C	101.3	51.2	68.9	71.2	73.5	—
Glc D	^{1}H	4.55	3.40	3.66	3.54	3.49	3.72; 3.93
	^{13}C	104.2	73.2	83.1	71.3	73.4	62.0

Figure 3.5. Analysis of *Cff* LPS modifications associated with *gtr* operon. (A-B) ^{1}H-^{13}C HMR data of overlap of the HSQC spectra of deacylated PS from WT (green-cyan) and *gtrB* mutant (red-pink) D_2O, 25 °C, 600 MHz. Letters correspond to chemicals shifts (δ_H/δ_C) found in the corresponding table (**B**). * Denotes an additional signal not present in the *gtrB* strain likely associated with H/C-4 of mannose or heptose. (**C**) Silver stain of *Cff* crude LPS prepped from WT and *gtrB* mutant.

To improve signal assignment, we deacetylated the PS, which improved interpretation of the spectrum. In both PS samples a disaccharide consisting of α-GalNAcA-3-β-Glc- was identified (Figure 3.4). Overlapping of HSQC spectra indicated the absence of signals assigned to α-GlcNAc-3-*α*-GlcNAc- in the *gtrB* mutant. These signals are believed to be located on the cap of the PS. An additional peak likely associated with H/C-3 of mannose or heptose was also absent in the *gtrB* strain but could not be assigned. These results indicate that a *gtrB* mutation results in the loss of a GlcNAc disaccharide cap.

***In vitro* characterization of GtrB and analysis of lipid-intermediate**

Given the unexpected findings from the NMR analysis, we wanted to know whether *Cff* GtrB performs the same function as other GtrB proteins. *In vitro* experiments were performed to confirm the expected activity of *Cff* GtrB as an Und glucosyltransferase. Both of the Gtr glycosyltransferases (GtrB and GtrC) were tested using a UDP-Glo^{TM} assay, which converts free UDP into ATP which is detected by luminescent derivative. Decaprenyl-phosphate (DecP), an UndP analog, was used as a substrate acceptor. Various UDP-sugars were assayed for activity to assess the functionality of the enzyme (Figure 3.6A). GtrB produced significant luminescence in the presence of both UDP-Glc and DecP, but not when UDP-GlcNAc, -Gal, or –GalNAc were used as the substrate donor or in the absence of the DecP acceptor. This is consistent with the role of other GtrB homologs (Guan and Verma 1997; Ardiccioni et al. 2016). GtrC produced no luminescence under any of these conditions.

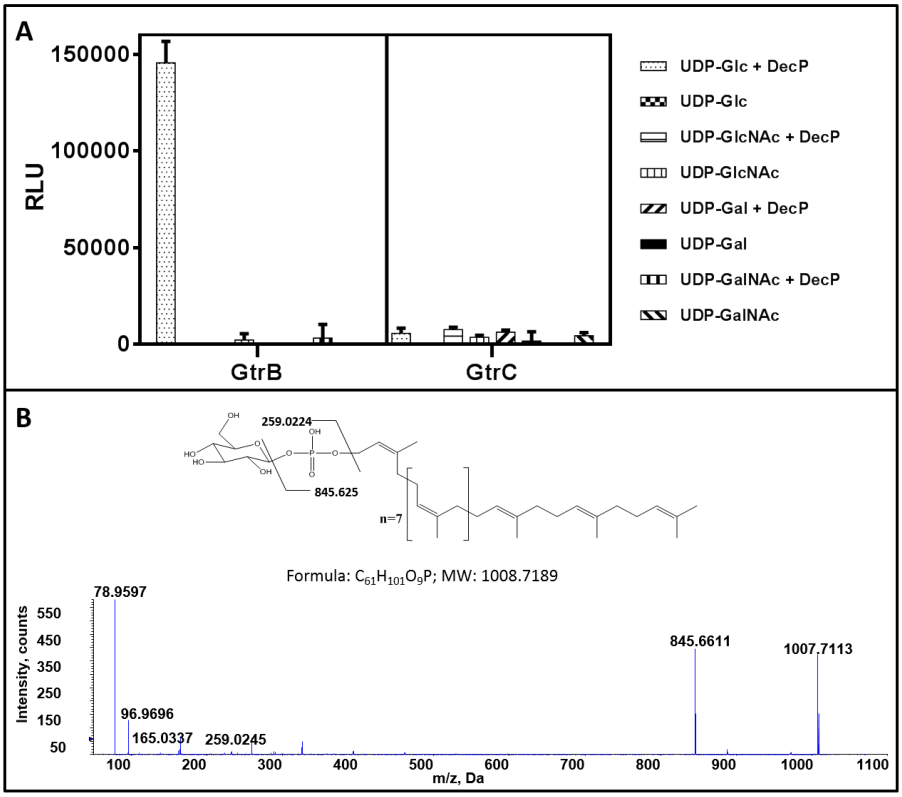

Figure 3.6. *In vitro* analysis of GtrB. (**A**) Purified GtrB-His$_6$ (CFF8240_1389) and GtrC-His$_6$ (CFF8240_1390) reactions with 50 µM UDP-sugar with 100 µM DecP for overnight at 37 °C, and the release of UDP was monitored by the UDP-Glo™ assay. The values represent the mean of three trials subtracted from the mean of the background, which is all components without enzyme; the error bars represent standard deviation. These tests were performed in technical triplicates. (**B**) LC-MS spectrum of lipid purified from the reaction of *E. coli* membranes overexpressing GtrB with UDP-Glc and UndP produces a species at *m/z* of 1007.7113, consistent with the [M-H]-ion of UndP-Glc. In a sample with just GtrB these species were not seen (Data not shown). Fragments generated by tandem mass spectrometry (MS/MS) identify species *m/z* 78.96, and 96.97, which correspond to phosphate and 259.02 characteristic of phosphate-Glc. The spectra were detected by ESI-MS in negative ion mode.

We next wanted to characterize the product of *Cff* GtrB. We set up *in vitro* reactions consisting of UDP-Glc, UndP, and membrane enrichments from cells that overexpress GtrB and then purified the resulting lipids for ESI-MS (Figure 3.6B). Species [*m/z* 1007.721] [M-H] consistent with UndP-Glc [1008.72] were present in reactions containing only UDP-Glc and UndP. Further fragmentation of the sample showed species consistent with fragmented phosphate [*m/z* 78.96 and 96.97] and phosphate-Glc [259.02], which are consistent with UndP-

Glc (Ardiccioni et al. 2016). However, samples containing membranes overexpressing GtrB lack detectable levels of these species (data not shown). Taken together these results suggest that *Cff* GtrB functions similarly to homologs founds in other species.

A *gtrB* mutant impacts serum resistance and S-layer

Due to the association of S-layer to LPS we wanted to investigate the effect of *gtrB* on S-layer composition. S-layer was extracted, run on a polyacrylamide gel and visualized with Coomassie. Only WT was the only sample that showed a band at around 98-100 kDa which is characteristic of the SapA S-layer protein found in type A strains (Figure 3.7A) (Blaser et al. 1988; Dworkin et al. 1995a). The other predominant band at ~65 kDa is consistent with flagellin. Whole cell lysate prepped from the same cells shows no accumulation of SapA internally. Mass spectrometry of in-gel trypsin digest at 98-100 kDa, indicated a 66% coverage to SapA6 (CFF8240_0484) with a score of $38e^{-34}$ (Figure 3.7B). To ensure that this loss of SapA6 is not due to polar-effects, or disruption of the promoter we performed RT-PCR of SapA6 and sequenced the promoter (Figure 3.7C, Figure 3.8). The results indicated that the *gtrB* mutant has decreased SapA6 compared to WT.

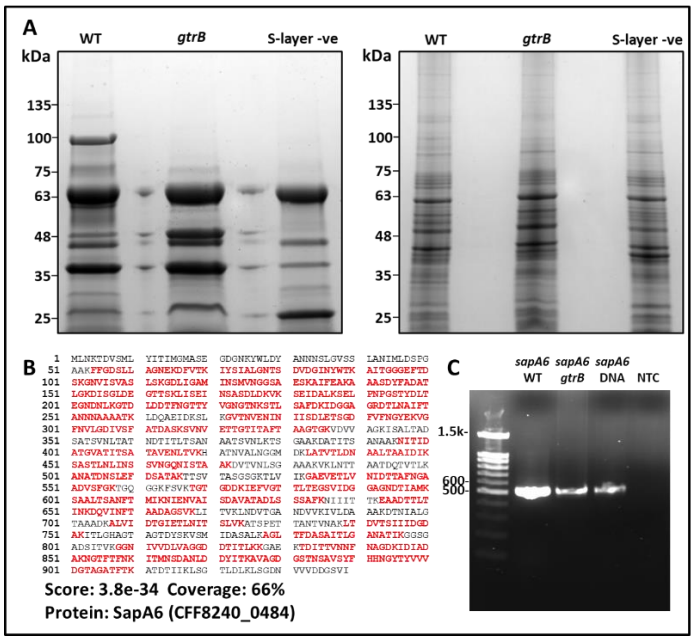

Figure 3.7. Analysis of *Cff* S-layer in *gtrB* mutant. (A) S-layer extracts and whole-cell lysate (WCL) of *C. fetus*. S-layer was extracted from the bacterium using 0.2 M glycine HCl, pH2.2 and the remaining pellet was lysed and run on a 4-20% polyacrylamide gel. Proteins were visualized with Coomassie stain. The band present at ~100 kDa in *Cff* 82-40 is consistent with SapA in previous S-layer, and 63 kDa is consistent with flagellin (Blaser et al. 1988; Dworkin et al. 1995a). *Cff* ATCC 27374 was used as a negative control as it lacks *sapCDEF* and cannot make S-layer. (B) The Mass spectral-based identification of an in-gel trypsin digested band at ~100kDa indicates a protein with 66% coverage to SapA6 (CFF8240_0484). Matched peptides are shown in red. (C) RT-PCR of *sapA6* WT and *gtrB* shows the presence of *sapA6* transcripts at ~550 bp. NTC is a no template control.

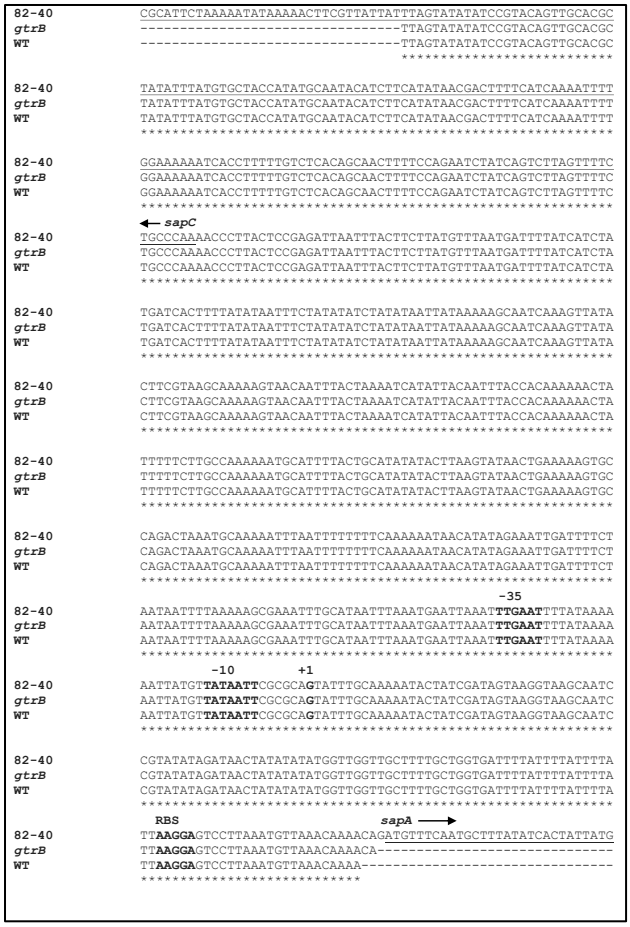

Figure 3.8. Sequence alignment of *gtrB* mutant sapA promoter. The promoter region was amplified and cloned into pCR 2.1 for sequencing. The 82-40 sequence denotes the reference sequence, *gtrB* is the *Cff* 82-40 *gtrB* mutant strain and WT is *Cff* 82-40 control sequence. Alignments were performed using Geneious consensus alignment (Kearse et al., 2012).

We next wanted to investigate the effects of serum resistance associated with type A *C. fetus* strains (Perez-Perez et al. 1986). *S*erum resistance in *C. fetus* has been shown to be dependent on the presence of an S-layer (Blaser et al. 1988; Pei and Blaser 1990; Gilbert et al. 2016). The *gtrB* mutant had a 35% decrease in serum-survival compared to the wild-type (Figure 3.9).

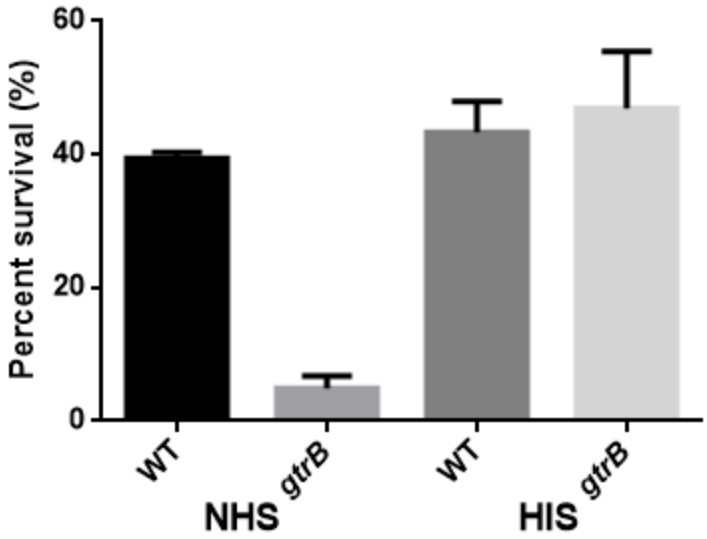

Figure 3.9. Importance of *gtr* operon in serum resistance. *Cff* serum resistance assays. Strains were incubated with normalized human serum (NHS), heat-inactivated serum (HIS colony forming units (CFU) were counted. Percent survival represents three biological triplicates performed in technical triplicates. Untreated cells were used to standardize pretreatment to 100%.

Discussion

Many of the bacterial serotypes can be attributed to bacteriophage-derived genes. *C. fetus* contains remarkably few serotypes/types (A, B and AB) when compared to other *gtr* containing organisms like *Shigella flexneri* and *Salmonella enterica*, which have 19 and 1,454 serotypes, respectively (Brenner et al. 2000; Muthuirulandi Sethuvel et al. 2017). The lack of serotype diversity in *C. fetus* could be due to the presence of its S-layer protein (SLP), for which it can recombine and express up to 9 gene copies (Perez-perez et al. 1986; Dworkin et al. 1997; Tu et al. 2001). In *C. fetus*, serotype and surface array protein type, or simply type, are conserved (Yang et al. 1992). This conservation is likely needed for the association of SLP to LPS, which is mediated through the N-terminus of the SLP (Dworkin et al. 1995a). Here we describe a bacteriophage-derived serotype conversion mechanism and its role on S-layer association in a gram-negative bacteria species.

We annotated the bacteriophage glucosylation *gtr* operon in *C. fetus* subsp. *fetus* 82-40. It has been suggested that this operon is carried and transferred by bacteriophages, and is potentially involved in phage superinfection (Gwen E. Allison and Verma 2000; Bogomolnaya et al. 2008; Broadbent et al. 2010; Kim and Ryu 2012). In a broad analysis of *C. fetus* genomes, we discovered that a seemingly ancestral horizontal acquisition of the *gtr* operon is present in all *C. fetus* type A strains regardless of subspecies and is absent in type B strains. This operon is consistently found in the *pgl* N-glycosylation cluster, but previous research would indicate that it plays no role in N-glycosylation (Nothaft et al. 2012, Duma et al. 2020). The pervasiveness of this genetic element is in agreeance with *C. fetus* genomic comparisons, which supports that horizontal gene elements maintain nearly 100% nucleotide identity between strains and subspecies (Kienesberger et al. 2014). This suggests that *C. fetus* evolution is likely driven primarily through acquisition of gene elements and not through mutations and genetic drift. Together, this suggests that the acquisition of the *gtr* operon may predate the divergence of the subspecies.

In other bacterial species, this operon is involved in serotype conversion through the addition of Glc to the O-antigen of LPS (Gwen E. Allison and Verma 2000; Bogomolnaya et al. 2008; Broadbent et al. 2010; Kim and Ryu 2012). We utilized a *gtrB* mutant, which could not generate the UndP-Glc intermediate required for the transfer of Glc to the O-antigen. Silver stain analysis indicated a molecular shift consistent with the loss of a glycan residue. However, our NMR analysis indicated that an LPS consisting primarily of →3)-*α*-D-Man*p*2OAc-(1→ with no loss of Glc but instead a loss of a disaccharide cap consisting of α-GlcNAc-3-*α*-GlcNAc- (Moran et al. 1994; S N Senchenkova et al. 1997). The loss of α-GlcNAc-3-*α*-GlcNAc- would suggest that the *gtr* operon is involved in the transfer of the reducing end GlcNAc. In addition, we were

able to identify α-GalNAcA-3-β-Glc- branch on the LPS, which has not been described in prior *Cf* LPS studies (Moran et al. 1994; Sof'ya N. Senchenkova et al. 1996; Sof'ya N. Senchenkova et al. 1997). These results suggest that the *Cff gtr* operon is involved in the transfer of the reducing end GlcNAc in the disaccharide GlcNAc cap.

Due to the unpredicted results of our NMR analysis we performed *in vitro* assays to confirm the role of the *gtr* enzymes. We were able to assay the *Cf* GtrB homolog, which was capable of transferring to DecP, and subsequently produce UndP-Glc. Our findings were consistent with prior GtrB lipid-analyses indicating that our GtrB has the attributes of a canonical GtrB (Ardiccioni et al. 2016). Due to the nature of the substrate and complexity of the reaction we were unable to assay GtrC. Previous research in *C. fetus* N-glycosylation indicate a similar unidentified mechanism in generating the major N-glycan which differ by the substitution of a Glc with a GlcNAc (Duma et al. 2020). It is possible that *C. fetus* may possess a non-specific mechanism of converting Glc into GlcNAc, however this remains to be seen. Currently there is no known enzyme that converts Glc into GlcNAc. There are however, examples of sugar conversion occuring outside the cytoplasm and on lipid carriers (Buchert and Viikari 1988; Crellin et al. 2011; Thomas 2017). Despite the *Cff gtr* operon utilizing Glc our *gtrB* mutant lacks the GlcNAc disaccharide cap, the reason for this is not understood.

The lack of a disaccharide GlcNAc cap on our *gtrB* strain LPS prompted us to investigate its effect on S-layer association. Our results indicate that the *gtrB* mutant has decreased SapA6 in S-layer extracts. This is consistent with our serum resistance assay which show a decreased survival in the *gtrB* mutant. This bacterium's ability to resist serum is linked to S-layer production and is generally associated with type A (Perez-Perez et al. 1986). This could be due to decreased SLP-LPS association N-terminal binding domain of SapA to the GlcNAc cap of

LPS (Figure 3.10) (Yang et al. 1992). Another possibility could be a destabilized axial interaction between SLP proteins. This interaction could be achieved through shortening of the LPS, which has been associated with the *gtr* operon (Yang et al. 1992; West et al. 2005; Hölzer et al. 2009). Modelling of type B *C. fetus* LPS, with a *C. jejuni* LOS core, found that the S-layer needed divalent bridging for S-layer stability (Roberts et al. 2013). This bridging could be possible through calcium association with two LPS molecules or with LPS-SLP; calcium has been shown to be important in *C. fetus* and other bacterium's S-layer association (Roberts et al. 2013; Sleytr et al. 2014; von Kügelgen et al. 2020).

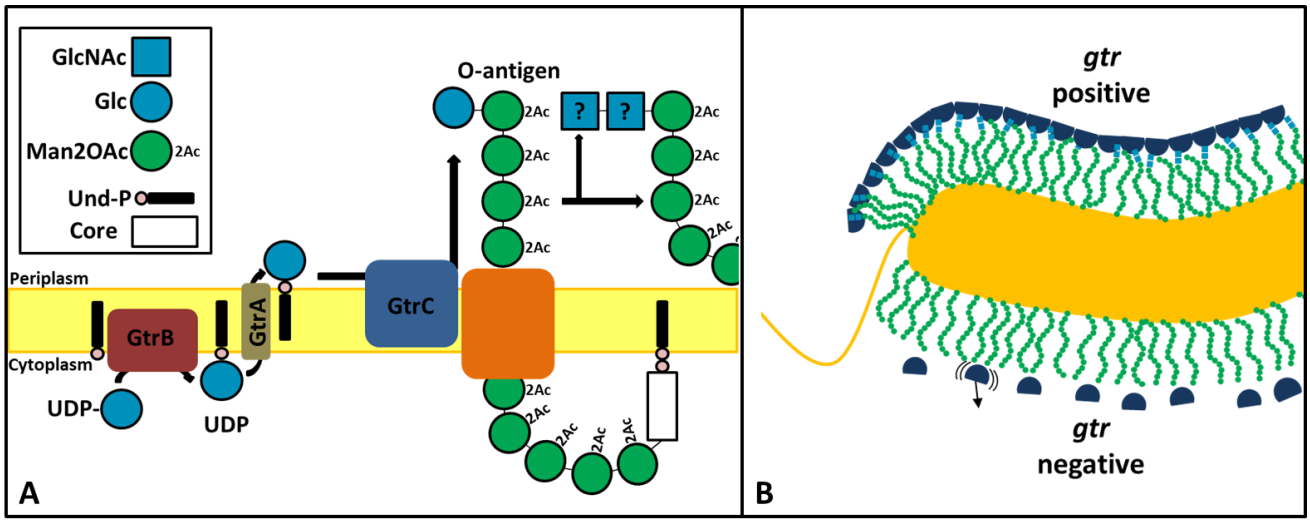

Figure 3.10. Proposed model of *gtr* biosynthesis and role in S-layer association. (A) LPS modification by *gtr* operon. GtrB transfers Glc from UDP-Glc to undecaprenyl-phosphate resulting in undecaprenyl-phosphate-glucose and free UDP. This intermediate is flipped into the periplasm via the flippase GtrA. GtrC then transfers it to the cap of the LPS as it enters the periplasm, a model consistent with ABC-dependent LPS biosynthesis (Tytgat and Lebeer 2014; Mann et al. 2015). There is no clear understanding of how the *gtr* operon influences the GlcNAc cap. (B) Proposed mechanism of *gtr* mediated effect on SLP-LPS association. The addition of Glc by the *gtr* operon may play a role in SapA binding or association resulting in downregulation or dissociation from the cell. The *gtr* operon has also previously been shown to generate shorter LPS chains through helices (West et al. 2005; Hölzer et al. 2009). Increased LPS length and decreased SLP-SLP interaction may lead to destabilized S-layer resulting in dissociation or changes in regulation.

Our research is the first that we know of to link bacteriophage-derived serotype conversion and S-layer association. Furthermore, we show that the *gtr* operon is an ancestral

genetic element consistent with all type A strains in *C. fetus*. Interestingly, mutation of *gtrB* indicated the transfer of GlcNAc to the cap of LPS, however our *in vitro* experiments of GtrB indicated that it facilitates the canonical glucosyltransferase mechanism. The reason for this inconsistency is unknown: in a previous study we were unable to identify the mechanism involved in Glc to GlcNAc conversion in *Cf* N-glycosylation (Duma et al. 2020) indicating that this bacterium may possess an unknown system of post-glycosylation conversion of Glc to GlcNAc.

Materials and Methods

Bacterial strains, plasmids, and growth conditions.

Bacterial strains, plasmids and oligonucleotides are listed in Table S2 and Table S3. *C. fetus* was grown using Brain Heart Infusion medium (BHI, Hardy Diagnostics) and Columbia agar with 5% horse blood (CBA, Hardy Diagnostics under microaerobic conditions (10% CO_2, 5% O_2, 85% N_2) at 37°C. *E. coli* was grown on 2xYT at 37°C or as indicated. If required, antibiotics were added in the following working concentrations: 100 µg/mL ampicillin, 25 µg/mL chloramphenicol, 50 µg/mL kanamycin, and 20 µg/mL trimethoprim.

Construction of *C. fetus gtrB* mutant

A 2.9 kb fragment was PCR amplified containing the Cff 82-40 gene and TA-cloned into pGEM® T-Easy to generate pJD15. A kanamycin resistance (*kan*) cassette containing SwaI termini, and pJD15 were both treat with SwaI restriction enzyme, the purified DNA was ligated, and transformed into *E. coli* selecting for Amp and Km resistance. Colonies were screened for directionality and inserts by colony PCR and confirmation of *kan* insertion into *gtrB* was confirmed by sequencing, yielding suicide vector pJD16. This vector was introduced to *C. fetus*

subsp. *fetus* 82-40 by electroporation using the following protocol Kanamycin-resistant a kanamycin colony appeared after 10 days and was confirmed using PCR (Figure S#).

GtrB and GtrC expression and purification.

Purified detergent soluble His-tagged GtrB and C were purified as described (Bruni and Kloss 2013), following the mid-scale expression and purification protocol with the following changes. In summary, recombinant His_6- tagged GtrB and GtrC were expressed from pJD6 and pJD3.1 in *E. coli* BL21(DE3)pLysS, and TOP10 respectively. Cells were grown at 37°C at 250 rpm in 1 L of 2xYT to a OD_{600} 1.0 and induced with 1 mM of isopropyl β-D-1-thiogalactopyranoside (IPTG) for 4 hours harvested and stored at -80°C. After thawing all steps were performed at 4°C. The pellets were resuspended in 25 mL of resuspension buffer: 50 mM HEPES, pH7.8; 300 mM NaCl; 20 mM imidazole, pH 7.8; 5% glycerol; 1mM $MgCl_2$; 0.5 mM TCEP (tris(2-carboxyethyl)phosphine); 1 mM phenylmethanesulfonylfluoride (PMSF); 4U/mL benzonase nuclease. The cells were lysed twice by a constant pressure of 25 kpsi using a disrupter (Constant Systems). The resulting lysates were clarified by adding 5 mL of resuspension buffer with 12% n-Dodecyl-B-D-Maltoside (DDM) and without benzonase, then placed on a end-over-end shaker for 1 hr or until lysate clears. The insoluble portion was removed by centrifuging (6,800 x g, 20 min) and the supernatant was transferred to a new tube 50-mL falcon tube containing 200 µL of 50% (v/v) Ni-NTA slurry. The tubes were rotated end-over-end for 1 hr followed by centrifugation (500 x g, 5 min) to pellet the Ni-NTA. The supernatant was discarded, and the pellet was washed in a capped 5-mL Pierce® Centrifuge Column, shaking for 30 min with 1 mL of 50 mM HEPES, pH 7.8; 300 mM NaCl; 40 mM imidazole, pH 7.8; 5% (v/v) glycerol; 5mM $MgCl_2$; 5 mM NaATP; 0.1 mM TCEP; 0.85 mM DDM. Two subsequent washes were done similarly using a wash buffer composed of 25 mM

HEPES, pH 7.8; 500 mM NaCl; 75 mM imidazole, pH 7.8; 5% (v/v) glycerol; 0.1 mM TCEP; 0.34 mM DDM. The protein was eluted from the column by two 30 min shaking incubations with 500 µL of 25 mM HEPES, pH 7.8; 200 mM NaCl; 500 mM imidazole, pH 7.8; 5% (v/v) glycerol; 0.1 mM TCEP; 0.34 mM DDM, followed by a centrifugation (500 x g, 2 min) elution to collect eluates.

GtrB reaction and UDP-Glo™ assay

After purification, 20 µg/mL of GtrB and GtrC were added to 100 µM Ultra Pure UDP-sugars (Promega Corporation) and 50 µM DecP; buffer contained 25 mM HEPES, pH 7.8; 200 mM NaCl; 5% (v/v) glycerol; 0.1 mM TCEP; 0.34 mM DDM. After samples were incorporated with two brief 4 sonication pulses at 40% intensity (Sonicator Ultrasonic Processor XL 2020), then reactions were incubated overnight at room temperature. Detection of free UDP after glycosyltransferase reactions was detected using the UDP-Glo™ Glycosyltransferase Assay Kit (Promega Corporation), which detects free UDP as light. A standard curve was performed according to manufactures protocol by utilizing 0-25 µM UDP. Using white, flat bottom 384-well plates 5 µL of reaction was added to 5 µL of UDP-Glo™ Detection Reagent followed by a 1 h incubation, then luminescence was detected using a Gen5™ Microplate Reader.

In vitro UndP membrane assay

Flasks containing 1 L of 2xYT of *E. coli* BL21 (DE3) pLysS cells overexpressing GtrB were induced at OD_{600} 1.0 with 0.2 mM IPTG. Cells were harvested after 4 h of growth and stored at -80°C. Membranes were prepped according to (Nothaft et al. 2009). In brief, cells were lysed as described above and centrifuged (135, 000 x g, 60 min at 4°C). The pellets containing membrane fractions was resuspended with 100 mM Tris-HCl, pH 7.2, to 1/100 the original volume and stored in the -80°C. Using 30 µg/mL of membrane with 100 µM UDP-Glc and 100

μM UndP in 100 mM Tris-HCl, pH 7.2, followed by two 4 s sonication pulses at 40% intensity (Sonicator Ultrasonic Processor XL 2020). The reaction was incubated for 3 h at room temperature followed by a lipid extraction using the two-phase Bligh-Dyer method (Bligh and Dyer 1959). Samples were dried using a nitrogen evaporator and weighed.

Lipid LC-MS

The samples were analyzed using an Agilent 1200 series HPLC system coupled to a high resolution QSTAR Elite mass spectrometer (Applied Biosystem/MDS Sciex, Concord, ON, Canada) using an electrospray ion source in negative ion mode. Analyst QS2.0 was used for data acquisition and analysis. The mass spectrometer was tuned by infusing taurocholic acid (m/z 514.2844) at a resolution of greater than 10,000 and calibrated using an electrospray ionization low concentration tuning mix (Agilent Technologies Canada Inc., Mississauga, ON, Canada). A Hypercarb PGC column (2.1mmx100mm, 3μm) (Thermo Scientific, San Jose, CA) was used for LC separation. The mobile phase consisted of A methanol/CHCl 3 (90/10) with 50mM ammonium acetate, and B methanol/CHCl 3 (10/90) with 50mM ammonium acetate. The gradient was as follows: 0-5 min, 100% A, increase to 70% B over 20 min, hold at 70% B for 20 min, then went back to 100% A at 40.1 min for column re-equilibrium for 5 mins prior to the next injection. The flow rate of mobile phase was 200μl/min and the injection volume was 2 μl. The mass spectra scan range for full scan was 50-2000 amu and 50-1100 amu for MS/MS scan at a collision energy of -65V.

LPS purification and NMR analysis

LPS was prepped from cells obtained from approximately fifty plates of BHI agar as described above. LPS was extracted using phenol-water, dialyzed, treated with acetic acid, dialyzed, and treated with heated 2% acetic acid (100°C, 2h) and separated on Biogel P6. High

molecular weight fraction was separated on a Hitrap^{TM} Q HP column and eluted using a salt gradient. Fractions containing LPS were desalted by a Sephadex G-15 chromatography. A 600 MHz NMR at 25°C was used; connections were confirmed by NOE and HMBC.

Lipopolysaccharide analysis

C. fetus LPS was prepped using a method adapted from Hitchcock and Brown (1983) (Hitchcock and Brown 1983). Cells were grown on CBA agar for 48 h; washed with chilled phosphate-buffered saline (PBS) pH 7.2 and pelleted by centrifugation (4255 x g, 15 min). Pellets were resuspended in lysis buffer consisting of: 1M Tris-HCl, pH 6.8; 2% SDS; 4% β-mercaptoethanol; 10% glycerol; 0.002% bromophenol blue, then heated at 100°C for 30 min. After cooling, proteinase K is added to a final concentration of 30 mg/mL proteinase K and is incubated at 55°C for 4 h. Insoluble material was removed by centrifugation; sample was loaded on a 15% polyacrylamide gel and separated electrophoretically.

S-layer extraction and whole cell lysate preparation

Extraction of SLPs and other surface proteins was performed as previously described, with the following modifications (Fujimoto et al. 1991). Cultures from CBA agar were harvested using a loop and resuspended in 0.2 M glycine-HCl buffer (pH 2.2) at a concentration of 30mg wet cell mass/mL buffer. After end-over-end shaking for 20 min at room temperature, cells were pelleted by centrifugation (12,000 x g, 30 min at 4°C). Whole cell lysates of the pellet were prepared as described (Nothaft et al. 2010). Briefly, the pellet was resuspended in 1 × Laemmli sample buffer at 40 mg/mL and boiled at 95°C for 10 min. The supernatant was neutralized using 10M NaOH and filtered through a 0.22µM filter. After, 0.1mM PMSF was added and the extracts were dialyzed overnight against distilled water. The extracts were concentrated by lyophilizing and resuspending in 1/18th the original buffer volume used. Lysate and S-layer

extract was analyzed by separation on a 4–20% Mini-PROTEAN® TGX™ gel and visualized by Coomassie blue.

S-layer purification

Extraction of SLP proteins was performed as previously described with the following modifications (Pei and Blaser 1990; Yang et al. 1992). *Cf* cultures grown on BHI agar for 24 hr in microaerobic conditions were harvested with 5 mL of distilled water per plate. Cells were pelleted at 9,000 x *g* for 15 min, supernatant was kept, and the pellet was resuspended in 1 mL of distilled water per plate. Resuspended cells were vortexed again at 9,000 x *g* for 15 min

Serum resistance assay

Resistance to human serum was performed as previously described (Blaser et al. 1985). In brief, *C. fetus* was grown for 24h on CBA prior to the assay and adjusted to $1x10^7$ bacterial/mL (OD 0.1) using DMEM medium. Actual cell counts were determined by plating serial dilutions. In a 96 well plate, 150 µL of resuspended cells was mixed with 50 µL of 40% heat-inactivated- (56°C for 30 min) or active human serum and incubated for 1 h at 37°C in 5% CO_2. Cells were plated on CBA plates and counted after 48 h growth. All tests were done in biological and technical triplicates.

Acknowledgements

The authors would like to thank Dr. Barbara Imperiali for providing undecaprenyl-phosphate for lipid *in vitro* assays, and Dr. Hicham Zegzouti from Promega™ for UDP-Glo™ Kits. We would also like to show our gratitude to Dr. Sabine Kienesberger and Dr. Ellen L. Zechner for their *C. fetus* mutagenesis protocol and expression vectors. Special thanks to Dr. Harald Nothaft, Dr. Stéphane Benoit, Dr. William Miller, and Dr. Nichollas Scott for their constructive discussion and guidance. This study was funded in part by The Glycoscience Training Program (T32) which is funded by the National Institutes of Health, National Institute of General Medical Sciences.

CHAPTER 4

CONCLUSIONS

N-glycosylation in *C. fetus* and relation to physiology

In our first publication, we annotated the *C. fetus* (*Cf*) *pgl* locus and its role in physiology. Using comparisons to the *C. jejuni* (*Cj*) *pgl* locus, we found that *Cf* has two unannotated *pgl* glycosyltransferases, which we have named *pglX* and *pglY* (Nothaft and Szymanski 2010; Nothaft et al. 2012). Based on experiments involving mutagenesis and functional transfer into *E. coli*, PglX appears to be responsible for the transfer of the first GlcNAc residue to the N-glycan backbone, which marks the predominant difference between *Cf* and thermotolerant *Campylobacter* N-glycans (Nothaft et al. 2012). In addition, this work suggests that PglX or PglY may be able to transfer more than one residue like PglH, but their specific activities are unclear. Our results indicate that we unaware of how the GlcNAc of the major N-glycan is made. Something we did not address is the possibility that the *C. jejuni* PglB used in the *E. coli/Cj* hybrid expression system is unable to transfer the *Cf* major N-glycan. Another possibility is that *Cf* has genes external to the *pgl* loci involved in generating the major N-glycan GlcNAc residue.

Our annotation and future analysis of unannotated *pgl* genes provide a foundation for studying N-glycan diversity in non-thermotolerant *Campylobacters* and general mechanisms of glycosylation. Understanding of the *Cf pgl* cluster and functional transfer into *E. coli* would allow us to generate cost-effective live-vector vaccines, or diagnostics (Iwashkiw et al. 2012; Nothaft and Szymanski 2013; Nothaft et al. 2016).

Proteomic analysis of *pglX* and *pglJ* mutants provided insight into the function of N-glycosylation in *Cf*. Remarkably, these mutants showed a significant increase in the HynABC H_2-uptake hydrogenase complex, which correlated with increased H_2-uptake and increased growth in H_2 rich growth conditions (Benoit et al. 2020). In addition, we observed increased nickel and decreased iron levels, which have been linked to HynABC regulation (Ernst et al. 2005; Dosanjh et al. 2009). Our current hypothesis is that the nickel regulator, NikR, is derepressing *hynABC* at high-nickel concentrations by repressing *fur*, which represses *hynABC* (Ernst et al. 2005; Dosanjh et al. 2009). Our *pglX* mutant had the highest nickel content which also correlated with a significant increased in a metal export protein, suggesting imbalances in metal levels. Together with decreased efflux and increased antibiotic sensitivity, suggest that N-glycosylation alters membrane flux. This work is the first to connect N-glycosylation to nickel and iron regulation, and the H_2-uptake hydrogenase HynABC. In addition this study corroborates prior findings, which linked N-glycosylation to motility, efflux, and antibiotic sensitivity (Cuccui et al. 2012; Scott et al. 2012; Abouelhadid et al. 2019; Cain et al. 2019; Dubb et al. 2019).

This study connects traits, previously associated with pathogenesis, with N-glycosylation, which may explain *Cf*'s ability to colonize and infect certain hosts (Palyada et al. 2004; Guerry 2007; Luangtongkum et al. 2009; Stahl et al. 2012; Vieira et al. 2017; Benoit et al. 2020). This research represents the first study on the effect of truncated N-glycans on physiology and the role of N-glycosylation outside of the *C. jejuni* model.

Lipopolysaccharide modifications and association with S-layer

During our studies of the *Cf pgl* loci, we were able to identify and characterize a bacteriophage-associated glucosylating operon known as *gtr*. Traditionally this operon is involved in the addition of Glc to the O-antigen of lipopolysaccharide (LPS) and is believed to

be important in preventing superinfection by phages (Guan and Verma 1997; Gwen E Allison and Verma 2000). In addition, *gtr* mediated O-antigen glucosylation has also been linked to improved immune invasion and evasion, and type III secretion (Gwen E. Allison and Verma 2000; West et al. 2005). *Cf* is known to contain up four potential type IV secretions system which are believed to be involved in *Cf*'s ability to cause septicemia (Kienesberger et al. 2014). Our analysis of all sequenced *C. fetus* strains indicated that all type A strains possess the *gtr* operon. Type A strains have been more commonly associated with pathogenesis and host colonization, which may be due to the presence of the *gtr* operon improving type IV secretion (West et al. 2005; Kienesberger et al. 2014). This correlation suggests that the acquisition of the *gtr* operon occurred before the division of subspecies.

In addition, we identified an atypical LPS modification associated with a *gtr* operon activity. Our annotation and *in vitro* analysis of the *Cf gtr* operon indicated that it likely transfers Glc. However, NMR analysis of the LPS identified a previously undescribed LPS modifications, a α-GalNAcA-3-β-Glc- branch and α-GlcNAc-3-α-GlcNAc- LPS cap, associated with the *gtr* operon. This work does not provide an explanation for the presence of GlcNAc where a Glc residue is expected but suggests that there may be a mechanism to convert Glc to GlcNAc post-glycosylation. This study demonstrates a new and unknown connection of the *gtr* glucosylation operon with a diGlcNAc LPS cap.

In addition, our *gtrB* mutant, which lacked the diGlcNAc LPS cap, had no detectable S-layer proteins in S-layer extracts. This is consistent with prior *Cf* findings that indicate that S-layer-LPS associates in a type-dependent manner through SapA N-terminus associating to LPS (Yang et al. 1992; Thompson 2005). Suggesting that the *gtr* operon may be the LPS modification needed for type A association to S-layer. Further binding studies are being performed to confirm

the diGlcNAc-SapA association. In *C. fetus,* S-layer, has been shown to be essential in *C. fetus* serum resistance (Thompson 2005).

This is the first time the bacteriophage-associated *gtr* operon has ever been described in context of bacterial S-layer. Together this study has provided insight into a novel correlation and association of the bacteriophage glucosylation operon, *gtr*, S-layer, and LPS modifications. All of these factors have been previously associated with immune evasion and invasion, host colonization, and pathogenesis (Thompson 2002; West et al. 2005; Bogomolnaya et al. 2008).

Future work

Overall, this work describes two novel glycosylation systems in *Campylobacter fetus*, resulting in surface diversity. Together, our research suggests that *C. fetus* may have a mechanism to alter the Glc residue of the N-glycan and LPS into GlcNAc post-glycosylation. To determine if this is not due to additional activity of the glycosyltranferases *in vitro* reactions of GtrC, PglX, and PglY are needed. This would help determine if these enzymes are able to add GlcNAc to their glycans.

However, our *in vitro* and *E. coli* hybrid data suggest that there are likely factors external to these systems, which may be involved in Glc altering to GlcNAc. To our knowledge there is no known mechanism or proteins that would be able to perform this function. However, in *Mycobacterium tuberculosis* post-glycosylation sugar conversion has been described (Crellin et al. 2011). It is possible that this conversion could occur through an unannotated glycosylation cluster in *C. fetus*. This cluster consists of N-acetylglucosamine associated proteins, chitin biosynthesis-like proteins, glycosyltransferases, methyltransferases, twin asparagine synthetase B (AsnB), and primarily hypothetical/unannotated proteins. Two adjacent AsnB proteins have been previously associated with S-layer glycosylation (Zarschler et al. 2015), and amidation of

peptidoglycan, which can lead to resistance of certain antibiotics (Ammam et al. 2020). To further support this, our proteomics indicated that a DUF 354 (CFF8240_1618) protein, in this cluster, was significantly increased ~30-fold in the *pgl* mutants. This domain distantly resembles 2-epimerase, glycosyltransferase 2-like, and chitin deacetylase. In addition, a UDP-galactopyranose mutase, *glf* (CFF8240_1602), has been correlated with type A *Cf*, the most pathogenic strain type (Kienesberger et al. 2014). Studying this cluster may explain why type A strains are more likely to cause disease and potentially explain the source of GlcNAc in both of our studied systems.

Identifying glycosylated proteins in *C. fetus* would help make direct correlations to the phenotypes and proteins levels observed in our *pgl* mutant. This could also provide insight into which glycosylation sites and proteins are modified with the major or minor N-glycan. This would also determine if the N-glycosylation sequon is consistent within all *Campylobacter* species, which has not been done. In addition, this may directly determine if S-layer is glycosylated by either the N-glycosylation or another system. S-layer glycosylation has been described in all gram-negative S-layer containing species except for *Cf* (Sleytr et al. 2014).

All traits described in these works represent mechanisms of bacterial pathogenesis and colonization. It is possible to use the antigens studied in these works as affordable vaccines in cattle and sheep. These antigens can also be used for diagnostics to determine if cattle or sheep have had exposure to *Cf* (Iwashkiw et al. 2012).

.

References

Abouelhadid S, North SJ, Hitchen P, Vohra P, Chintoan-Uta C, Stevens M, Dell A, Cuccui J, Wren BW. 2019. Quantitative Analyses Reveal Novel Roles for N-glycosylation in a Major Enteric Bacterial Pathogen. MBio. 10(2). doi:10.1128/mBio.00297-19.

Akiba M, Lin J, Barton YW, Zhang Q. 2006. Interaction of CmeABC and CmeDEF in conferring antimicrobial resistance and maintaining cell viability in *Campylobacter jejuni*. J Antimicrob Chemother. doi:10.1093/jac/dki419.

Alagesan K, Khilji SK, Kolarich D. 2017. It is all about the solvent: on the importance of the mobile phase for ZIC-HILIC glycopeptide enrichment. Anal Bioanal Chem. doi:10.1007/s00216-016-0051-6.

Alaimo C, Catrein I, Morf L, Marolda CL, Callewaert N, Valvano MA, Feldman MF, Aebi M. 2006. Two distinct but interchangeable mechanisms for flipping of lipid-linked oligosaccharides. EMBO J. doi:10.1038/sj.emboj.7601024.

Alemka A, Nothaft H, Zheng J, Szymanski CM. 2013. N-glycosylation of *Campylobacter jejuni* surface proteins promotes bacterial fitness. Infect Immun. doi:10.1128/IAI.01370-12.

Allison Gwen E., Verma NK. 2000. Serotype-converting bacteriophages and O-antigen modification in *Shigella flexneri*. Trends Microbiol. 8(1):17–23. doi:10.1016/S0966-842X(99)01646-7.

Allison Gwen E, Verma NK. 2000. Serotype-converting bacteriophages *Shigella flexneri*. (99):17–23.

Ardiccioni C, Clarke OB, Tomasek D, Issa H a, von Alpen DC, Pond HL, Banerjee S, Rajashankar KR, Liu Q, Guan Z, et al. 2016. Structure of the polyisoprenyl-phosphate glycosyltransferase GtrB and insights into the mechanism of catalysis. Nat Commun. 7:10175. doi:10.1038/ncomms10175.

Baillon MLA, Van Vliet AHM, Ketley JM, Constantinidou C, Penn CW. 1999. An iron-regulated alkyl hydroperoxide reductase (AhpC) confers aerotolerance and oxidative stress resistance to the microaerophilic pathogen *Campylobacter jejuni*. J Bacteriol.

Benoit SL, Maier RJ. 2018. Site-directed mutagenesis of *Campylobacter concisus* respiratory genes provides insight into the pathogen's growth requirements. Sci Rep. 8(1). doi:10.1038/s41598-018-32509-9.

Benoit SL, Maier RJ, Sawers RG, Greening C. 2020. Molecular Hydrogen Metabolism: a

Widespread Trait of Pathogenic Bacteria and Protists. Microbiol Mol Biol Rev. doi:10.1128/MMBR.00092-19.

Van Bergen Marcel A.P., Dingle KE, Maiden MCJ, Newell DG, Van Der Graaf-Van Bloois L, Van Putten JPM, Wagenaar JA. 2005. Clonal nature of *Campylobacter fetus* as defined by multilocus sequence typing. J Clin Microbiol. doi:10.1128/JCM.43.12.5888-5898.2005.

Van Bergen M. A.P., Linnane S, Van Putten JPM, Wagenaar JA. 2005. Global detection and identification of *Campylobacter fetus* subsp. venerealis. OIE Rev Sci Tech. doi:10.20506/rst.24.3.1629.

Blaser MJ. 1988. *Campylobacter fetus* : Emerging Infection and Model System for Bacterial Pathogenesis at Mucosal Surfaces. Clin Infect Dis. 27(2):256–258.

Blaser MJ, Pei Z. 1993. Pathogenesis of *Campylobacter fetus* Infections: Critical Role of High-Molecular- Weight S-Layer Proteins in Virulence. J Infect Dis. 167(2):372–377. doi:10.1093/infdis/167.2.372.

Blaser MJ, Smith PF, Kohler PF. 1985. Susceptibility of *Campylobacter* isolates to the bactericidal activity of human serum. J Infect Dis. 151(2):227–235. doi:10.1093/infdis/151.2.227.

Blaser MJ, Smith PF, Repine JE, Joiner KA. 1988. Pathogenesis of *Campylobacter fetus* infections. Failure of encapsulated *Campylobacter fetus* to bind C3b explains serum and phagocytosis resistance. J Clin Invest. 81(5):1434–1444. doi:10.1172/JCI113474.

Bligh EG, Dyer WJ. 1959. A rapid method of total lipid extraction. Can J Biochem Physiol. 37(8):911–917. doi:10.1145/3163918.

Bogomolnaya LM, Santiviago C a., Yang H-JJ, Baumler AJ, Andrews-Polymenis HL. 2008. "Form variation" of the O12 antigen is critical for persistence of *Salmonella* Typhimurium in the murine intestine. Mol Microbiol. 70(5):1105–19. doi:10.1111/j.1365-2958.2008.06461.x.

Brenner FW, Villar RG, Angulo FJ, Tauxe R, Swaminathan B. 2000. *Salmonella* nomenclature. J Clin Microbiol. doi:10.1128/jcm.38.7.2465-2467.2000.

Broadbent SE, Davies MR, Van Der Woude MW. 2010. Phase variation controls expression of *Salmonella* lipopolysaccharide modification genes by a DNA methylation-dependent mechanism. Mol Microbiol. 77(2):337–53. doi:10.1111/j.1365-2958.2010.07203.x.

Bruni R, Kloss B. 2013. High-throughput cloning and expression of integral membrane proteins in *Escherichia coli*.

Buchert J, Viikari L. 1988. Oxidative d-xylose metabolism of *Gluconobacter oxydans*. Appl Microbiol Biotechnol. doi:10.1007/BF00265822.

Burrows L, Iobst ST, Drickamer K. 1997. Selective binding of N-acetylglucosamine to the chicken hepatic lectin. Biochem J. doi:10.1042/bj3240673.

Cain JA, Dale AL, Niewold P, Klare WP, Man L, White MY, Scott NE, Cordwell SJ. 2019. Proteomics Reveals Multiple Phenotypes Associated with N-linked Glycosylation in *Campylobacter jejuni*. Mol Cell Proteomics. 18(4):715–734. doi:10.1074/mcp.ra118.001199.

CDC. *Campylobacter* sepsis associated with "nutritional therapy"--California. 1981. MMWR Morb Mortal Wkly Rep.

Casadémont I, Chevrier D, Guesdon JL. 1998. Cloning of a sapB homologue (sapB2) encoding a putative 112-kDa *Campylobacter fetus* S-layer protein and its use for identification and molecular genotyping. FEMS Immunol Med Microbiol. doi:10.1016/S0928-8244(98)00081-9.

Chen MM, Weerapana E, Ciepichal E, Stupak J, Reid CW, Swiezewska E, Imperiali B. 2007. Polyisoprenol specificity in the *Campylobacter jejuni* N-linked glycosylation pathway. Biochemistry. 46(50):14342–14348. doi:10.1021/bi701956x.

Cid E, Gomis RR, Geremia RA, Guinovart JJ, Ferrer JC. 2000. Identification of two essential glutamic acid residues in glycogen synthase. J Biol Chem. 275(43):33614–33621. doi:10.1074/jbc.M005358200.

Coutinho PM, Deleury E, Davies GJ, Henrissat B. 2003. An evolving hierarchical family classification for glycosyltransferases. J Mol Biol. 328(2):307–317. doi:10.1016/S0022-2836(03)00307-3.

Cox J, Hein MY, Luber CA, Paron I, Nagaraj N, Mann M. 2014. Accurate proteome-wide label-free quantification by delayed normalization and maximal peptide ratio extraction, termed MaxLFQ. Mol Cell Proteomics. 13(9):2513–2526. doi:10.1074/mcp.M113.031591.

Cox J, Mann M. 2008. MaxQuant enables high peptide identification rates, individualized p.p.b.-range mass accuracies and proteome-wide protein quantification. Nat Biotechnol. 26(12):1367–72. doi:10.1038/nbt.1511.

Crellin PK, Brammananth R, Coppel RL. 2011. Decaprenylphosphoryl-β-D-Ribose 2′-epimerase, the target of benzothiazinones and dinitrobenzamides, is an essential enzyme in *Mycobacterium smegmatis*. PLoS One. doi:10.1371/journal.pone.0016869.

Cuccui J, Milne TS, Harmer N, George AJ, Harding S V, Dean RE, Scott AE, Sarkar-Tyson M, Wren BW, Titball RW, et al. 2012. Characterization of the *Burkholderia pseudomallei* K96243 capsular polysaccharide I coding region. Infect Immun. 80(3):1209–21. doi:10.1128/IAI.05805-11.

Davis LM, Kakuda T, DiRita VJ. 2009. A *Campylobacter jejuni* znuA orthologue is essential for growth in low-zinc environments and chick colonization. J Bacteriol. doi:10.1128/JB.01394-08.

Dingle KE, Blaser MJ, Tu ZC, Pruckler J, Fitzgerald C, Van Bergen MAP, Lawson AJ, Owen RJ, Wagenaar JA. 2010. Genetic relationships among reptilian and mammalian *Campylobacter fetus* strains determined by multilocus sequence typing. J Clin Microbiol. 48(3):977–980. doi:10.1128/JCM.01439-09.

Domon B, Costello CE. 1988. A systematic nomenclature for carbohydrate fragmentations in FAB-MS/MS spectra of glycoconjugates. Glycoconj J. 5(4):397–409. doi:10.1007/BF01049915.

Dosanjh NS, West AL, Michel SLJ. 2009. *Helicobacter pylori* NikR's interaction with DNA: A two-tiered mode of recognition. Biochemistry. doi:10.1021/bi801481j.

Dubb RK, Nothaft H, Beadle B, Richards MR, Szymanski CM. 2019. N-glycosylation of the CmeABC multidrug efflux pump is needed for optimal function in *Campylobacter jejuni*. Glycobiology. doi:10.1093/glycob/cwz082.

Duma J, Nothaft H, Weaver D, Fodor C, Beadle B, Linton D, Benoit SL, Scott NE, Maier RJ, Szymanski CM. 2020. Influence of Protein Glycosylation on *Campylobacter fetus* Physiology. Front Microbiol. 11:1191. doi:10.3389/fmicb.2020.01191.

Duncan JS, Leatherbarrow AJH, French NP, Grove-White DH. 2014. Temporal and farm-management-Associated variation in faecal-pat prevalence of *Campylobacter fetus* in sheep and cattle. Epidemiol Infect. 142(6):1196–1204. doi:10.1017/S0950268813002379.

Dwivedi R, Nothaft H, Reiz B, Whittal RM, Szymanski CM. 2013. Generation of free oligosaccharides from bacterial protein N-linked glycosylation systems. Biopolymers. doi:10.1002/bip.22296.

Dworkin J, Blaser MJ. 1997. Molecular mechanisms of *Campylobacter fetus* surface layer protein expression . Mol Microbiol. doi:10.1046/j.1365-2958.1997.6151958.x.

Dworkin J, Shedd OL, Blaser MJ. 1997. Nested DNA inversion of *Campylobacter fetus* S-layer genes is *recA* dependent. J Bacteriol. 179(23):7523–7529. doi:10.1128/jb.179.23.7523-7529.1997.

Dworkin J, Tummuru MKR, Blaser MJ. 1995a. A lipopolysaccharide-binding domain of the *Campylobacter fetus* S-layer protein resides within the conserved N terminus of a family of silent and divergent homologs. J Bacteriol. 177(7):1734–1741. doi:10.1128/jb.177.7.1734-1741.1995.

Dworkin J, Tummuru MKR, Blaser MJ. 1995b. Segmental conservation of sapA sequences in type B *Campylobacter fetus* cells. J Biol Chem. doi:10.1074/jbc.270.25.15093.

Ernst FD, Kuipers EJ, Heijens A, Sarwari R, Stoof J, Penn CW, Kusters JG, Van Vliet AHM.

2005. The nickel-responsive regulator NikR controls activation and repression of gene transcription in *Helicobacter pylori*. Infect Immun. doi:10.1128/IAI.73.11.7252-7258.2005.

Faridmoayer A, Fentabil MA, Mills DC, Klassen JS, Feldman MF. 2007. Functional characterization of bacterial oligosaccharyltransferases involved in O-linked protein glycosylation. J Bacteriol. doi:10.1128/JB.01318-07.

Feldman MF, Wacker M, Hernandez M, Hitchen PG, Marolda CL, Kowarik M, Morris HR, Dell A, Valvano M a., Aebi M. 2005. Engineering N-linked protein glycosylation with diverse O antigen lipopolysaccharide structures in *Escherichia coli*. Proc Natl Acad Sci U S A. 102(8):3016–21. doi:10.1073/pnas.0500044102.

Fernández-Cruz A, Muñoz P, Mohedano R, Valerio M, Marín M, Alcalá L, Rodriguez-Créixems M, Cercenado E, Bouza E. 2010. *Campylobacter* bacteremia: Clinical characteristics, incidence, and outcome over 23 years. Medicine (Baltimore). 89(5):319–330. doi:10.1097/MD.0b013e3181f2638d.

Fitzgerald C, Tu ZC, Patrick M, Stiles T, Lawson AJ, Santovenia M, Gilbert MJ, Van Bergen M, Joyce K, Pruckler J, et al. 2014. *Campylobacter fetus* subsp. *testudinum* subsp. nov., Isolated from humans and reptiles. Int J Syst Evol Microbiol. 64:2944–2948. doi:10.1099/ijs.0.057778-0.

Flanagan RC, Neal-McKinney JM, Dhillon AS, Miller WG, Konkel ME. 2009. Examination of *Campylobacter jejuni* putative adhesins leads to the identification of a new protein, designated FlpA, required for chicken colonization. Infect Immun. doi:10.1128/IAI.01266-08.

Fogg GC, Yang L, Wang E, Blaser MJ. 1990. Surface array proteins of *Campylobacter fetus* block lectin-mediated binding to type A lipopolysaccharide. Infect Immun. 58(9):2738–2744. Franklin B, Ulmer DD. 1974. Human infection with vibrio fetus. West J Med.

Fry BN, Korolik V, Ten Brinke JA, Pennings MTT, Zalm R, Teunis BJJ, Coloe PJ, Van Der Zeijst BAM. 1998. The lipopolysaccharide biosynthesis locus of *Campylobacter jejuni* 81116. Microbiology. doi:10.1099/00221287-144-8-2049.

Fujihara N, Takakura S, Saito T, Iinuma Y, Ichiyama S. 2006. A case of perinatal sepsis by *Campylobacter fetus* subsp. fetus infection successfully treated with carbapenem - case report and literature review. J Infect. doi:10.1016/j.jinf.2006.01.009.

Fujimoto S, Takade A, Amako K, Blaser MJ. 1991. Correlation between molecular size of the surface array protein and morphology and antigenicity of the *Campylobacter fetus* S layer. Infect Immun. 59(6):2017–2022.

Gagneux P, Aebi M, Varki A. 2015. Evolution of Glycan Diversity. In: Essentials of Glycobiology.

Ganeshram KN, Ross A, Cowell RPW, Cefai C, Woodward MJ. 2000. Recurring febrile illness

in a slaughterhouse worker. Postgrad Med J. doi:10.1136/pmj.76.902.790.

Gazaigne L, Legrand P, Renaud B, Bourra B, Taillandier E, Brun-Buisson C, Lesprit P. 2008. *Campylobacter fetus* bloodstream infection: Risk factors and clinical features. Eur J Clin Microbiol Infect Dis. 27(3):185–189. doi:10.1007/s10096-007-0415-0.

Gilbert MJ, Miller WG, Yee E, Zomer AL, Van Der Graaf-Van Bloois L, Fitzgerald C, Forbes KJ, Méric G, Sheppard SK, Wagenaar JA, et al. 2016. Comparative genomics of *Campylobacter fetus* from reptiles and mammals reveals divergent evolution in host-associated lineages. Genome Biol Evol. 8(6):2006–2019. doi:10.1093/gbe/evw146.

Glover KJ, Weerapana E, Chen MM, Imperiali B. 2006. Direct biochemical evidence for the utilization of UDP-bacillosamine by PglC, an essential glycosyl-1-phosphate transferase in the *Campylobacter jejuni* N-linked glycosylation pathway. Biochemistry. 45(16):5343–5350. doi:10.1021/bi0602056.

Glover KJ, Weerapana E, Imperiali B. 2005. In vitro assembly of the undecaprenylpyrophosphate-linked heptasaccharide for prokaryotic N-linked glycosylation. Proc Natl Acad Sci U S A. 102(40):14255–9. doi:10.1073/pnas.0507311102.

Golden NJ, Acheson DWK. 2002. Identification of motility and autoagglutination *Campylobacter jejuni* mutants by random transposon mutagenesis. Infect Immun. doi:10.1128/IAI.70.4.1761-1771.2002.

Good DM, Wenger CD, Coon JJ. 2010. The effect of interfering ions on search algorithm performance for electron-transfer dissociation data. Proteomics. 10(1):164–167. doi:10.1002/pmic.200900570.

Gorkiewicz G, Kienesberger S, Schober C, Scheicher SR, Gülly C, Zechner R, Zechner EL. 2010. A genomic island defines subspecies-specific virulence features of the host-adapted pathogen *Campylobacter fetus* subsp. *venerealis*. J Bacteriol. doi:10.1128/JB.00803-09.

Van Der Graaf-Van Bloois L, Miller WG, Yee E, Gorkiewicz G, Forbes KJ, Zomer AL, Wagenaar JA, Duim B. 2016. *Campylobacter fetus* subspecies contain conserved type IV secretion systems on multiple genomic islands and plasmids. PLoS One. doi:10.1371/journal.pone.0152832.

Grogono-Thomas R, Dworkin J, Blaser MJ, Newell DG. 2000. Roles of the surface layer proteins of *Campylobacter fetus* subsp. *fetus* in ovine abortion. Infect Immun. 68(3):1687–1691. doi:10.1128/IAI.68.3.1687-1691.2000.

Gross J, Grass S, Davis AE, Gilmore-Erdmann P, Townsend RR, St. Geme JW. 2008. The Haemophilus influenzae HMW1 adhesin is a glycoprotein with an unusual N-linked carbohydrate modification. J Biol Chem. doi:10.1074/jbc.M801819200.

Guan S, Verma NK. 1997. Functional analysis of the O antigen glucosylation gene cluster of *Shigella flexneri*. (1 999).

Guerrant RL, Lahita RG, Winn WC, Roberts RB. 1978. *Campylobacter*iosis in man: Pathogenic mechanisms and review of 91 bloodstream infections. Am J Med. 65(4):584–592. doi:10.1016/0002-9343(78)90845-8.

Guerry P. 2007. *Campylobacter* flagella: not just for motility. Trends Microbiol. doi:10.1016/j.tim.2007.09.006.

Guo B, Lin J, Reynolds DL, Zhang Q. 2010. Contribution of the multidrug efflux transporter CmeABC to antibiotic resistance in different *Campylobacter* species. Foodborne Pathog Dis. doi:10.1089/fpd.2009.0354.

Harding CM, Nasr MA, Kinsella RL, Scott NE, Foster LJ, Weber BS, Fiester SE, Actis LA, Tracy EN, Munson RS, et al. 2015. Acinetobacter strains carry two functional oligosaccharyltransferases, one devoted exclusively to type IV pilin, and the other one dedicated to O-glycosylation of multiple proteins. Mol Microbiol. doi:10.1111/mmi.12986.

Hendrixson DR, DiRita VJ. 2004. Identification of *Campylobacter jejuni* genes involved in commensal colonization of the chick gastrointestinal tract. Mol Microbiol. doi:10.1111/j.1365-2958.2004.03988.x.

Herget S, Toukach P V., Ranzinger R, Hull WE, Knirel YA, Von Der Lieth CW. 2008. Statistical analysis of the bacterial carbohydrate structure data base (BCSDB): Characteristics and diversity of bacterial carbohydrates in comparison with mammalian glycans. BMC Struct Biol. doi:10.1186/1472-6807-8-35.

Hitchcock PJ, Brown TM. 1983. Morphological heterogeneity among *Salmonella* lipopolysaccharide chemotypes in silver-stained polyacrylamide gels. J Bacteriol. 154(1):269–277.

Holst E, Wathne B, Hovelius B, Mårdh PA. 1987. Bacterial vaginosis: Microbiological and clinical findings. Eur J Clin Microbiol. 6(5):536–541. doi:10.1007/BF02014242.

Hölzer SU, Schlumberger MC, Jäckel D, Hensel M. 2009. Effect of the O-antigen length of lipopolysaccharide on the functions of type III secretion systems in *Salmonella enterica*. Infect Immun. 77(12):5458–5470. doi:10.1128/IAI.00871-09.

Houliston RS, Vinogradov E, Dzieciatkowska M, Li J, St Michael F, Karwaski MF, Brochu D, Jarrell HC, Parker CT, Yuki N, et al. 2011. Lipooligosaccharide of *Campylobacter jejuni*: Similarity with multiple types of mammalian glycans beyond gangliosides. J Biol Chem. 286(14):12361–12370. doi:10.1074/jbc.M110.181750.

Humphrey S, Chaloner G, Kemmett K, Davidson N, Williams N, Kipar A, Humphrey T, Wigley

P. 2014. *Campylobacter jejuni* is not merely a commensal in commercial broiler chickens and affects bird welfare. MBio. doi:10.1128/mBio.01364-14.

Ielmini M V., Feldman MF. 2011. *Desulfovibrio desulfuricans* PglB homolog possesses oligosaccharyltransferase activity with relaxed glycan specificity and distinct protein acceptor sequence requirements. Glycobiology. 21(6):734–742. doi:10.1093/glycob/cwq192.

Iraola G, Forster SC, Kumar N, Lehours P, Bekal S, García-Peña FJ, Paolicchi F, Morsella C, Hotzel H, Hsueh PR, et al. 2017. Distinct *Campylobacter fetus* lineages adapted as livestock pathogens and human pathobionts in the intestinal microbiota. Nat Commun. 8(1). doi:10.1038/s41467-017-01449-9.

Ishihama Y, Rappsilber J, Mann M. 2006. Modular stop and go extraction tips with stacked disks for parallel and multidimensional peptide fractionation in proteomics. J Proteome Res. 5(4):988–994. doi:10.1021/pr050385q.

Iwashkiw J a., Fentabil M a., Faridmoayer A, Mills DC, Peppler M, Czibener C, Ciocchini AE, Comerci DJ, Ugalde JE, Feldman MF. 2012. Exploiting the *Campylobacter jejuni* protein glycosylation system for glycoengineering vaccines and diagnostic tools directed against brucellosis. Microb Cell Fact. 11(1):13. doi:10.1186/1475-2859-11-13.

Jakhetia R, Talukder KA, Verma NK. 2013. Isolation, characterization and comparative genomics of bacteriophage SfIV: A novel serotype converting phage from *Shigella flexneri*. BMC Genomics. 14(1). doi:10.1186/1471-2164-14-677.

Jégouzo SAF, Nelson C, Hardwick T, Angel Wong ST, Kiat Lau NK, Emily Neoh GK, Castellanos-Rueda R, Huang Z, Mignot B, Hirdaramani A, et al. 2020. Mammalian lectin arrays for screening host-microbe interactions. J Biol Chem. doi:10.1074/jbc.RA120.012783.

Jervis AJ, Butler JA, Lawson AJ, Langdon R, Wren BW, Linton D. 2012. Characterization of the structurally diverse N-linked glycans of *Campylobacter* species. J Bacteriol. 194(9):2355–2362. doi:10.1128/JB.00042-12.

Jervis AJ, Langdon R, Hitchen P, Lawson AJ, Wood A, Fothergill JL, Morris HR, Dell A, Wren B, Linton D. 2010. Characterization of N-linked protein glycosylation in *Helicobacter pullorum*. J Bacteriol. 192(19):5228–5236. doi:10.1128/JB.00211-10.

Kakuda T, DiRita VJ. 2006. Cj1496c encodes a *Campylobacter jejuni* glycoprotein that influences invasion of human epithelial cells and colonization of the chick gastrointestinal tract. Infect Immun. doi:10.1128/IAI.00033-06.

Kakuda T, Koide Y, Sakamoto A, Takai S. 2012. Characterization of two putative mechanosensitive channel proteins of *Campylobacter jejuni* involved in protection against osmotic downshock. Vet Microbiol. doi:10.1016/j.vetmic.2012.04.044.

Kelly J, Jarrell H, Millar L, Tessier L, Fiori LM, Lau PC, Allan B, Szymanski CM. 2006. Biosynthesis of the N-linked glycan in *Campylobacter jejuni* and addition onto protein through block transfer. J Bacteriol. 188(7):2427–2434. doi:10.1128/JB.188.7.2427-2434.2006.

Ketley J, Konkel M. 2005. *Campylobacter*: Molecular and Cellular Biology.
Kienesberger S, Gorkiewicz G, Joainig MM, Scheicher SR, Leitner E, Zechner EL. 2007. Development of experimental genetic tools for *Campylobacter fetus*. Appl Environ Microbiol. 73(14):4619–30. doi:10.1128/AEM.02407-06.

Kienesberger S, Sprenger H, Wolfgruber S, Halwachs B, Thallinger GG, Perez-Perez GI, Blaser MJ, Zechner EL, Gorkiewicz G. 2014. Comparative genome analysis of *Campylobacter fetus* subspecies revealed horizontally acquired genetic elements important for virulence and niche specificity. PLoS One. 9(1). doi:10.1371/journal.pone.0085491.

Kim M, Ryu S. 2012. Spontaneous and transient defence against bacteriophage by phase-variable glucosylation of O-antigen in *Salmonella* enterica serovar Typhimurium. Mol Microbiol. 86(2):411–25. doi:10.1111/j.1365-2958.2012.08202.x.

Kitagawa H, Shimakawa H, Sugahara K. 1999. The tumor suppressor EXT-like gene EXTL2 encodes an α1, 4-N- acetylhexosaminyltransferase that transfers N-acetylgalactosamine and N-acetylglucosamine to the common glycosaminoglycan-protein linkage region: The key enzyme for the chain initiation of hepa. J Biol Chem. doi:10.1074/jbc.274.20.13933.

Klein BS, Vergeront JM, Blaser MJ, Edmonds P, Brenner DJ, Janssen D, Davis JP. 1986. *Campylobacter* infection associated with raw milk. An outbreak of gastroenteritis due to *Campylobacter jejuni* and thermotolerant *Campylobacter fetus* subsp *fetus*. JAMA J Am Med Assoc. 255(3):361–364. doi:10.1001/jama.1986.03370030081032.

Korolik V, Fry BN, Alderton MR, Van der Zeijst BAM, Coloe PJ. 1997. Expression of *Campylobacter hyoilei* lipo-oligosaccharide (LOS) antigens in *Escherichia coli*. Microbiology. doi:10.1099/00221287-143-11-3481.

Kowarik M, Young NM, Numao S, Schulz BL, Hug I, Callewaert N, Mills DC, Watson DC, Hernandez M, Kelly JF, et al. 2006. Definition of the bacterial N-glycosylation site consensus sequence. EMBO J. 25(9):1957–1966. doi:10.1038/sj.emboj.7601087.

von Kügelgen A, Tang H, Hardy GG, Kureisaite-Ciziene D, Brun Y V., Stansfeld PJ, Robinson C V., Bharat TAM. 2020. In Situ Structure of an Intact Lipopolysaccharide-Bound Bacterial Surface Layer. Cell. doi:10.1016/j.cell.2019.12.006.

Kuhns LG, Benoit SL, Bayyareddy K, Johnson D, Orlando R, Evans AL, Waldrop GL, Maier RJ. 2016. Carbon fixation driven by molecular hydrogen results in chemolithoautotrophically enhanced growth of *Helicobacter pylori*. J Bacteriol. 198(9):1423–1428. doi:10.1128/JB.00041-16.

Kukowska-Latallo JF, Larsen RD, Nair RP, Lowe JB. 1990. A cloned human cDNA determines

expression of a mouse stage-specific embryonic antigen and the Lewis blood group α(1,3/1,4)fucosyltransferase. Genes Dev. doi:10.1101/gad.4.8.1288.

Larsen JC, Szymanski C, Guerry P. 2004. N-linked protein glycosylation is required for full competence in *Campylobacter jejuni* 81-176. J Bacteriol. doi:10.1128/JB.186.19.6508-6514.2004.

Lin J, Overbye Michel L, Zhang Q. 2002. CmeABC functions as a multidrug efflux system in *Campylobacter jejuni*. Antimicrob Agents Chemother. 46(7):2124–2131. doi:10.1128/AAC.46.7.2124-2131.2002.

Linton D, Dorrell N, Hitchen PG, Amber S, Karlyshev A V., Morris HR, Dell A, Valvano MA, Aebi M, Wren BW. 2005. Functional analysis of the *Campylobacter jejuni* N-linked protein glycosylation pathway. Mol Microbiol. 55(6):1695–1703. doi:10.1111/j.1365-2958.2005.04519.x.

Liu J, Mushegian A. 2003. Three monophyletic superfamilies account for the majority of the known glycosyltransferases. Protein Sci. doi:10.1110/ps.0302103.

Liu X, McNally DJ, Nothaft H, Szymanski CM, Brisson JR, Li J. 2006. Mass spectrometry-based glycomics strategy for exploring N-linked glycosylation in eukaryotes and bacteria. Anal Chem. doi:10.1021/ac060516m.

Lizak C, Gerber S, Numao S, Aebi M, Locher KP. 2011. X-ray structure of a bacterial oligosaccharyltransferase. Nature. 474(7351):350–5. doi:10.1038/nature10151.

Luangtongkum T, Jeon B, Han J, Plummer P, Logue CM, Zhang Q. 2009. Antibiotic resistance in *Campylobacter*: Emergence, transmission and persistence. Future Microbiol. doi:10.2217/17460913.4.2.189.

Luis F. Leloir and the Biosynthesis of Saccharides. 2005. Luis F Leloir Biosynth Saccharides.
Ma Z, Jacobsen FE, Giedroc DP. 2009. Coordination chemistry of bacterial metal transport and sensing. Chem Rev. doi:10.1021/cr900077w.

MacOmber L, Hausinger RP. 2011. Mechanisms of nickel toxicity in microorganisms. Metallomics. doi:10.1039/c1mt00063b.

Maertzdorf WJ, Mouton RP. 1974. *Vibrio foetus* infections in an infant ward. Ned Tijdschr Geneeskd.

Maier RJ, Benoit SL. 2019. Role of nickel in microbial pathogenesis. Inorganics. doi:10.3390/INORGANICS7070080.

Maier RJ, Fu C, Gilbert J, Moshiri F, Olson J, Plaut AG. 1996. Hydrogen uptake hydrogenase in Helicobacter pylori. FEMS Microbiol Lett. 141(1):71–76. doi:10.1016/0378-1097(96)00211-X.

Maita N, Nyirenda J, Igura M, Kamishikiryo J, Kohda D. 2010. Comparative structural biology of eubacterial and archaeal oligosaccharyltransferases. J Biol Chem. doi:10.1074/jbc.M109.081752.

Man SM. 2011. The clinical importance of emerging *Campylobacter* species. Nat Rev Gastroenterol Hepatol. doi:10.1038/nrgastro.2011.191.

Mann E, Ovchinnikova OG, King JD, Whitfield C. 2015. Bacteriophage-mediated glucosylation can modify lipopolysaccharide O-antigens synthesized by an ATP-binding Cassette (ABC) Transporter-dependent assembly mechanism. J Biol Chem. doi:10.1074/jbc.M115.660803.

Mann E, Whitfield C. 2016. A widespread three-component mechanism for the periplasmic modification of bacterial glycoconjugates. Can J Chem. 94(11):883–893. doi:10.1139/cjc-2015-0594.

Marchand-Senécal X, Bekal S, Pilon PA, Sylvestre JL, Gaudreau C. 2017. *Campylobacter fetus* Cluster among Men Who Have Sex with Men, Montreal, Quebec, Canada, 2014-2016. Clin Infect Dis. 65(10):1751–1753. doi:10.1093/cid/cix610.

McCoy EC, Doyle D, Burda K, Corbeil LB, Winter AJ. 1975. Superficial antigens of *Campylobacter* (*vibrio*) *fetus*: characterization of an antiphagocytic component. Infect Immun. doi:10.1128/iai.11.3.517-525.1975.

Miller CE, Williams PH, Ketley JM. 2009. Pumping iron: Mechanisms for iron uptake by *Campylobacter*. Microbiology. doi:10.1099/mic.0.032425-0.

Mills DC, Jervis AJ, Abouelhadid S, Yates LE, Cuccui J, Linton D, Wren BW. 2016. Functional analysis of N-linking oligosaccharyl transferase enzymes encoded by deep-sea vent proteobacteria. Glycobiology. 26(4):398–409. doi:10.1093/glycob/cwv111.

Mintmier B, McGarry JM, Sparacino-Watkins CE, Sallmen J, Fischer-Schrader K, Magalon A, McCormick JR, Stolz JF, Schwarz G, Bain DJ, et al. 2018. Molecular cloning, expression and biochemical characterization of periplasmic nitrate reductase from *Campylobacter jejuni*. FEMS Microbiol Lett. doi:10.1093/femsle/fny151.

Moran a. P, O'Malley DT, Kosunen TU, Helander IM. 1994. Biochemical characterization of *Campylobacter fetus* lipopolysaccharides. Infect Immun. 62(9):3922–9.

Morooka T, Takeo H, Yasumoto S, Mimatsu T, Yukitake K, Oda T. 1992. Nosocomial meningitis due to *Campylobacter fetus* subspecies *fetus* in a neonatal intensive care unit. Pediatr Int. doi:10.1111/j.1442-200X.1992.tb01001.x.

Mshelia GD, Amin JD, Woldehiwet Z, Murray RD, Egwu GO. 2010. Epidemiology of bovine venereal *Campylobacter*iosis: Geographic distribution and recent advances in molecular diagnostic techniques. Reprod Domest Anim. doi:10.1111/j.1439-0531.2009.01546.x.

Muraoka WT, Zhang Q. 2011. Phenotypic and genotypic evidence for L-fucose utilization by *Campylobacter jejuni*. J Bacteriol. doi:10.1128/JB.01252-10.

Muthuirulandi Sethuvel DP, Devanga Ragupathi NK, Anandan S, Veeraraghavan B. 2017. Update on: *Shigella* new serogroups/serotypes and their antimicrobial resistance. Lett Appl Microbiol. doi:10.1111/lam.12690.

Naegeli A, Neupert C, Fan YY, Lin CW, Poljak K, Papini AM, Schwarz F, Aebi M. 2014. Molecular analysis of an alternative N-glycosylation machinery by functional transfer from actinobacillus pleuropneumoniae to *Escherichia coli*. J Biol Chem. doi:10.1074/jbc.M113.524462.

Nakagawa S, Takaki Y, Shimamura S, Reysenbach AL, Takai K, Horikoshi K. 2007. Deep-sea vent ε-proteobacterial genomes provide insights into emergence of pathogens. Proc Natl Acad Sci U S A. 104(29):12146–12150. doi:10.1073/pnas.0700687104.

Neuzil KM, Wang E, Haas DW, Blaser MJ. 1994. Persistence of *Campylobacter fetus* bacteremia associated with absence of opsonizing antibodies. J Clin Microbiol. 32(7):1718–1720. doi:10.1128/jcm.32.7.1718-1720.1994.

Nita-Lazar M, Wacker M, Schegg B, Amber S, Aebi M. 2005. The N-X-S/T consensus sequence is required but not sufficient for bacterial N-linked protein glycosylation. Glycobiology. doi:10.1093/glycob/cwi019.

Nothaft H, Davis B, Lock YY, Perez-Munoz ME, Vinogradov E, Walter J, Coros C, Szymanski CM. 2016. Engineering the *Campylobacter jejuni* N-glycan to create an effective chicken vaccine. Sci Rep. doi:10.1038/srep26511.

Nothaft H, Liu X, McNally DJ, Li J, Szymanski CM. 2009. Study of free oligosaccharides derived from the bacterial N-glycosylation pathway. Proc Natl Acad Sci. 106(35):15019–15024. doi:10.1073/pnas.0903078106.

Nothaft H, Liu X, McNally DJ, Szymanski CM. 2010. N-linked protein glycosylation in a bacterial system. In: Methods in molecular biology (Clifton, N.J.). p. 227–243.

Nothaft H, Perez-Muñoz ME, Gouveia GJ, Duar RM, Wanford JJ, Lango-Scholey L, Panagos CG, Srithayakumar V, Plastow GS, Coros C, et al. 2017. Coadministration of the *Campylobacter jejuni* N-glycan-based vaccine with probiotics improves vaccine performance in broiler chickens. Appl Environ Microbiol. doi:10.1128/AEM.01523-17.

Nothaft H, Scott NE, Vinogradov E, Liu X, Hu R, Beadle B, Fodor C, Miller WG, Li J, Cordwell SJ, et al. 2012. Diversity in the protein N-glycosylation pathways within the *Campylobacter* genus. Mol Cell Proteomics. 11(11):1203–1219. doi:10.1074/mcp.M112.021519.

Nothaft H, Szymanski CM. 2010. Protein glycosylation in bacteria: sweeter than ever. Nat Rev

Microbiol. 8(11):765–78. doi:10.1038/nrmicro2383.

Nothaft H, Szymanski CM. 2013. Bacterial protein N-glycosylation: new perspectives and applications. J Biol Chem. 288(10):6912–20. doi:10.1074/jbc.R112.417857.

Olson JW, Maier RJ. 2002. Molecular hydrogen as an energy source for *Helicobacter pylori*. Science (80-). 298(5599):1788–1790. doi:10.1126/science.1077123.

Oriol R, Martinez-Duncker I, Chantret I, Mollicone R, Codogno P. 2002. Common origin and evolution of glycosyltransferases using dol-P-monosaccharides as donor substrate. Mol Biol Evol. doi:10.1093/oxfordjournals.molbev.a004208.

Pacanowski J, Lalande V, Lacombe K, Boudraa C, Lesprit P, Legrand P, Trystram D, Kassis N, Arlet G, Mainardi J, et al. 2008. *Campylobacter* Bacteremia: Clinical Features and Factors Associated with Fatal Outcome. Clin Infect Dis. 47(6):790–796. doi:10.1086/591530.

Palyada K, Threadgill D, Stintzi A. 2004. Iron acquisition and regulation in *Campylobacter jejuni*. J Bacteriol. doi:10.1128/JB.186.14.4714-4729.2004.

Patrick ME, Gilbert MJ, Blaser MJ, Tauxe R V, Wagenaar J a., Fitzgerald C. 2013. Human infections with new subspecies of *Campylobacter fetus*. Emerg Infect Dis. 19(10):1678–1680. doi:10.3201/eid1910.130883.

Pei Z, Blaser MJ. 1990. Pathogenesis of *Campylobacter fetus* infections. Role of surface array proteins in virulence in a mouse model. J Clin Invest. 85(4):1036–1043. doi:10.1172/JCI114533.

Perez-Perez GI, Blaser MJ, Bryner JH. 1986. Lipopolysaccharide structures of *Campylobacter fetus* are related to heat-stable serogroups. Infect Immun. 51(1):209–212.

Perez C, Köhler M, Janser D, Pardon E, Steyaert J, Zenobi R, Locher KP. 2017. Structural basis of inhibition of lipid-linked oligosaccharide flippase PglK by a conformational nanobody. Sci Rep. 7. doi:10.1038/srep46641.

Perez C, Mehdipour AR, Hummer G, Locher KP. 2019. Structure of Outward-Facing PglK and Molecular Dynamics of Lipid-Linked Oligosaccharide Recognition and Translocation. Structure. doi:10.1016/j.str.2019.01.013.

Pittman MS, Elvers KT, Lee L, Jones MA, Poole RK, Park SF, Kelly DJ. 2007. Growth of *Campylobacter jejuni* on nitrate and nitrite: Electron transport to NapA and NrfA via NrfH and distinct roles for NrfA and the globin Cgb in protection against nitrosative stress. Mol Microbiol. doi:10.1111/j.1365-2958.2006.05532.x.

Ramírez AS, Boilevin J, Mehdipour AR, Hummer G, Darbre T, Reymond J-L, Locher KP. 2018. Structural basis of the molecular ruler mechanism of a bacterial glycosyltransferase. Nat

Commun. 9(1):445. doi:10.1038/s41467-018-02880-2.

Rangarajan ES, Bhatia S, Watson DC, Munger C, Cygler M, Matte A, Young NM. 2007. Structural context for protein N-glycosylation in bacteria: The structure of PEB3, an adhesin from *Campylobacter jejuni* . Protein Sci. doi:10.1110/ps.062737507.

Rappsilber J, Mann M, Ishihama Y. 2007. Protocol for micro-purification, enrichment, pre-fractionation and storage of peptides for proteomics using StageTips. Nat Protoc. 2(8):1896–1906. doi:10.1038/nprot.2007.261.

Rini JM, Esko JD. 2015. Glycosyltransferases and Glycan-Processing Enzymes.
Roberts JMD, Graham LL, Quinn B, Pink DA. 2013. Modeling the surface of *Campylobacter fetus*: Protein surface layer stability and resistance to cationic antimicrobial peptides. Biochim Biophys Acta - Biomembr. 1828(3):1143–1152. doi:10.1016/j.bbamem.2012.10.025.

Roepstorff P, Fohlman J. 1984. Letter to the editors - Proposal for a common nomenclature for sequence ions in mass spectra of peptides. Biomed Mass Spectrom. 11(11):601. doi:10.1002/bms.1200111109.

Rosén ML, Edman M, Sjöström M, Wieslander Å. 2004. Recognition of fold and sugar linkage for glycosyltransferases by multivariate sequence analysis. J Biol Chem. doi:10.1074/jbc.M402925200.

Santos-Silva T, Dias JM, Dolla A, Durand MC, Gonçalves LL, Lampreia J, Moura I, Romão MJ. 2007. Crystal Structure of the 16 Heme Cytochrome from Desulfovibrio gigas: A Glycosylated Protein in a Sulphate-reducing Bacterium. J Mol Biol. doi:10.1016/j.jmb.2007.04.055.

Schäffer C, Messner P. 2017. Emerging facets of prokaryotic glycosylation. FEMS Microbiol Rev. 41(1):49–91. doi:10.1093/femsre/fuw036.

Schmid J, Heider D, Wendel NJ, Sperl N, Sieber V. 2016. Bacterial glycosyltransferases: Challenges and Opportunities of a Highly Diverse Enzyme Class Toward Tailoring Natural Products. Front Microbiol. doi:10.3389/fmicb.2016.00182.

Schulz BL, Jen FEC, Power PM, Jones CE, Fox KL, Ku SC, Blanchfield JT, Jennings MP. 2013. Identification of Bacterial Protein O-Oligosaccharyltransferases and Their Glycoprotein Substrates. PLoS One. doi:10.1371/journal.pone.0062768.

Scott NE, Bogema DR, Connolly AM, Falconer L, Djordjevic SP, Cordwell SJ. 2009. Mass spectrometric characterization of the surface-associated 42 kDa lipoprotein JlpA as a glycosylated antigen in strains of *Campylobacter jejuni*. J Proteome Res. doi:10.1021/pr900544x.

Scott NE, Marzook NB, Cain JA, Solis N, Thaysen-Andersen M, Djordjevic SP, Packer NH,

Larsen MR, Cordwell SJ. 2014. Comparative proteomics and glycoproteomics reveal increased n-linked glycosylation and relaxed sequon specificity in *Campylobacter jejuni* nctc11168 o. J Proteome Res. doi:10.1021/pr5005554.

Scott NE, Nothaft H, Edwards AVG, Labbate M, Djordjevic SP, Larsen MR, Szymanski CM, Cordwell SJ. 2012. Modification of the *Campylobacter jejuni* N-linked glycan by EptC protein-mediated addition of phosphoethanolamine. J Biol Chem. doi:10.1074/jbc.M112.380212.

Scott NE, Parker BL, Connolly AM, Paulech J, Edwards AVG, Crossett B, Falconer L, Kolarich D, Djordjevic SP, Højrup P, et al. 2011. Simultaneous glycan-peptide characterization using hydrophilic interaction chromatography and parallel fragmentation by CID, higher energy collisional dissociation, and electron transfer dissociation MS applied to the N-linked glycoproteome of *Campylobacter jejuni*. Mol Cell Proteomics. 10(2):M000031-MCP201. doi:10.1074/mcp.M000031-MCP201.

Senay C, Lind T, Muguruma K, Tone Y, Kitagawa H, Sugahara K, Lidholt K, Lindahl U, Kusche-Gullberg M. 2000. The EXT1/EXT2 tumor suppressors: Catalytic activities and role in heparan sulfate biosynthesis. EMBO Rep. doi:10.1093/embo-reports/kvd045.

Senchenkova S N, Shashkov a. S, Knirel Y a., McGovern JJ, Moran a. P. 1997. The O-specific polysaccharide chain of *Campylobacter fetus* serotype A lipopolysaccharide is a partially O-acetylated 1,3-linked alpha-D-mannan. Eur J Biochem. 245(3):637–641. doi:DOI 10.1111/j.1432-1033.1997.00637.x.

Senchenkova Sof'ya N., Shashkov AS, Knirel YA, Mcgovern JJ, Moran AP. 1997. The O-specific polysaccharide chain of *Campylobacter fetus* serotype A lipopolysaccharide is a partially O-acetylated 1,3-linked α-D-mannan. Eur J Biochem. 245(3):637–641. doi:10.1111/j.1432-1033.1997.00637.x.

Senchenkova S N, Shashkov AS, Knirel YA, McGovern JJ, Moran AP. 1996. The O-specific polysaccharide chain of *Campylobacter fetus* serotype B lipopolysaccharide is a D-rhamnan terminated with 3-O-methyl-D-rhamnose (D-acofriose). Eur J Biochem. 239(2):434–438. doi:DOI 10.1111/j.1432-1033.1996.0434u.x.

Senchenkova Sof'ya N., Shashkov AS, Knirel YA, McGovern JJ, Moran AP. 1996. The O-specific polysaccharide chain of *Campylobacter fetus* serotype B lipopolysaccharide is a D-rhamnan terminated with 3-O-methyl-D-rhamnose (D-acofriose). Eur J Biochem. 239(2):434–438. doi:10.1111/j.1432-1033.1996.0434u.x.

Skirrow MB, Jones DM, Sutcliffe E, Benjamin J. 1993. *Campylobacter* bacteraemia in England and Wales, 1981-91. Epidemiol Infect. doi:10.1017/S0950268800050986.

Sleytr UB, Schuster B, Egelseer EM, Pum D. 2014. S-layers: Principles and applications. FEMS Microbiol Rev. doi:10.1111/1574-6976.12063.

van Sorge NM, Bleumink NMC, van Vliet SJ, Saeland E, van der Pol WL, van Kooyk Y, Van

Putten JPM. 2009. N-glycosylated proteins and distinct lipooligosaccharide glycoforms of *Campylobacter jejuni* target the human C-type lectin receptor MGL. Cell Microbiol. doi:10.1111/j.1462-5822.2009.01370.x.

Spink WW. 1957. Human vibriosis caused by *Vibrio fetus*. J Am Med Assoc. doi:10.1001/jama.1957.82970380001007.

Stahl M, Butcher J, Stintzi A. 2012. Nutrient acquisition and metabolism by *Campylobacter jejuni*. Front Cell Infect Microbiol. 2:5. doi:10.3389/fcimb.2012.00005.

Szymanski CM, Burr DH, Guerry P. 2002. *Campylobacter* protein glycosylation affects host cell interactions. Infect Immun. 70(4):2242–2244.

Szymanski CM, St. Michael F, Jarrell HC, Li J, Gilbert M, Larocque S, Vinogradov E, Brisson JR. 2003. Detection of Conserved N-Linked Glycans and Phase-variable Lipooligosaccharides and Capsules from *Campylobacter* Cells by Mass Spectrometry and High Resolution Magic Angle Spinning NMR Spectroscopy. J Biol Chem. doi:10.1074/jbc.M301273200.

Szymanski CM, Wren BW. 2005. Protein glycosylation in bacterial mucosal pathogens. Nat Rev Microbiol. doi:10.1038/nrmicro1100.

Szymanski CM, Yao R, Ewing CP, Trust TJ, Guerry P. 1999. Evidence for a system of general protein glycosylation in *Campylobacter jejuni*. Mol Microbiol. 32(5):1022–1030. doi:10.1046/j.1365-2958.1999.01415.x.

Taujale R, Venkat A, Huang LC, Zhou Z, Yeung W, Rasheed KM, Li S, Edison AS, Moremen KW, Kannan N. 2020. Deep evolutionary analysis reveals the design principles of fold A glycosyltransferases. Elife. doi:10.7554/eLife.54532.

Thomas GH. 2017. On the pull: periplasmic trapping of sugars before transport. Mol Microbiol. doi:10.1111/mmi.13691.

Thompson SA. 2005. *Campylobacter* Surface-Layers (S-Layers) and Immune Evasion . Ann Periodontol. 7(1):43–53. doi:10.1902/annals.2002.7.1.43.

Tremblay C, Gaudreau C, Lorange M. 2003. Epidemiology and antimicrobial susceptibilities of 111 *Campylobacter fetus* subsp. *fetus* strains isolated in Québec, Canada, from 1983 to 2000. J Clin Microbiol. doi:10.1128/JCM.41.1.463-466.2003.

Troutman JM, Imperiali B. 2009. *Campylobacter jejuni* PglH is a single active site processive polymerase that utilizes product inhibition to limit sequential glycosyl transfer reactions. Biochemistry. 48(12):2807–2816. doi:10.1021/bi802284d.

Tu Z, Gaudreau C, Blaser MJ. 2005. Mechanisms Underlying *Campylobacter fetus* Pathogenesis in Humans: Surface-Layer Protein Variation in Relapsing Infections . J Infect Dis. 191(12):2082–2089. doi:10.1086/430349.

Tu ZC, Ray KC, Thompson SA, Blaser MJ. 2001. *Campylobacter fetus* uses multiple loci for DNA inversion within the 5′ conserved regions of sap homologs. J Bacteriol. 183(22):6654–6661. doi:10.1128/JB.183.22.6654-6661.2001.
Tu ZC, Zeitlin G, Gagner JP, Keo T, Hanna BA, Blaser MJ. 2004. *Campylobacter fetus* of reptile origin as a human pathogen. J Clin Microbiol. 42(9):4405–4407. doi:10.1128/JCM.42.9.4405-4407.2004.

Tummuru MKR, Blaser MJ. 1993. Rearrangement of sapA homologs with conserved and variable regions in *Campylobacter fetus*. Proc Natl Acad Sci U S A. doi:10.1073/pnas.90.15.7265.

Tyanova S, Temu T, Sinitcyn P, Carlson A, Hein MY, Geiger T, Mann M, Cox J. 2016. The Perseus computational platform for comprehensive analysis of (prote)omics data. Nat Methods. 13(9):731–740. doi:10.1038/nmeth.3901.

Tytgat HLP, Lebeer S. 2014. The Sweet Tooth of Bacteria: Common Themes in Bacterial Glycoconjugates. Microbiol Mol Biol Rev. doi:10.1128/mmbr.00007-14.

Valderrama-Rincon JD, Fisher AC, Merritt JH, Fan Y-Y, Reading C a., Chhiba K, Heiss C, Azadi P, Aebi M, DeLisa MP. 2012. An engineered eukaryotic protein glycosylation pathway in *Escherichia coli*. Nat Chem Biol. 8(5):434–6. doi:10.1038/nchembio.921.

Vieira A, Ramesh A, Seddon AM, Karlyshev A V. 2017. CmeABC multidrug efflux pump contributes to antibiotic resistance and promotes *Campylobacter jejuni* survival and multiplication in *Acanthamoeba polyphaga*. Appl Environ Microbiol. doi:10.1128/AEM.01600-17.

Vizcaíno JA, Csordas A, Del-Toro N, Dianes JA, Griss J, Lavidas I, Mayer G, Perez-Riverol Y, Reisinger F, Ternent T, et al. 2016. 2016 update of the PRIDE database and its related tools. Nucleic Acids Res. 44(D1):D447–D456. doi:10.1093/nar/gkv1145.

Wacker M, Feldman MF, Callewaert N, Kowarik M, Clarke BR, Pohl NL, Hernandez M, Vines ED, Valvano M a., Whitfield C, et al. 2006. Substrate specificity of bacterial oligosaccharyltransferase suggests a common transfer mechanism for the bacterial and eukaryotic systems. Proc Natl Acad Sci U S A. 103(18):7088–93. doi:10.1073/pnas.0509207103.

Wacker M, Linton D, Hitchen PG, Nita-Lazar M, Haslam SM, North SJ, Panico M, Morris HR, Dell A, Wren BW, et al. 2002. N-linked glycosylation in *Campylobacter jejuni* and its functional transfer into E. coli. Science. 298(5599):1790–1793. doi:10.1126/science.298.5599.1790.

Wagenaar JA, Van Bergen MAP, Blaser MJ, Tauxe R V., Newell DG, Van Putten JPM. 2014. *Campylobacter fetus* infections in humans: Exposure and disease. Clin Infect Dis. 58(11):1579–1586. doi:10.1093/cid/ciu085.

Wang C-M, Wu Z-Y, Shia W-Y, Jhou Y-J, Tung K-C, Shyu C-L. 2015. Complete Genome

Sequence of *Campylobacter fetus* subsp. *testudinum* Strain Pet-3, Isolated from a Lizard (*Hydrosaurus pustulatus*). Genome Announc. 3(1):e01420-14. doi:10.1128/genomeA.01420-14.

Wang Y, Taylor DE. 1990. Natural transformation in *Campylobacter* species. J Bacteriol. doi:10.1128/jb.172.2.949-955.1990.

Waterhouse AM, Procter JB, Martin DMA, Clamp M, Barton GJ. 2009. Jalview Version 2-A multiple sequence alignment editor and analysis workbench. Bioinformatics. 25(9):1189–1191. doi:10.1093/bioinformatics/btp033.

Weerakoon DR, Borden NJ, Goodson CM, Grimes J, Olson JW. 2009. The role of respiratory donor enzymes in *Campylobacter jejuni* host colonization and physiology. Microb Pathog. doi:10.1016/j.micpath.2009.04.009.

West NP, Sansonetti P, Mounier JJ, Exley RM, Parsot C, Guadagnini SS, Prévost M-CC, Prochnicka-Chalufour A, Delepierre M, Tanguy M, et al. 2005. Optimization of virulence functions through glucosylation of Shigella LPS. Science. 307(5713):1313–7. doi:10.1126/science.1108472.

Wetter M, Kowarik M, Steffen M, Carranza P, Corradin G, Wacker M. 2012. Engineering, conjugation, and immunogenicity assessment of *Escherichia coli* O121 O-antigen for its potential use as a typhoid vaccine component. Glycoconj J.(i). doi:10.1007/s10719-012-9451-9.

Wuhrer M. 2013. Glycomics using mass spectrometry. Glycoconj J. doi:10.1007/s10719-012-9376-3.

Yang L, Pei Z, Fujimoto S, Blaser MJ. 1992. Reattachment of surface array proteins to *Campylobacter fetus* cells. J Bacteriol. 174(4):1258–1267. doi:10.1128/jb.174.4.1258-1267.1992.

Yates LE, Mills DC, DeLisa MP. 2018. Bacterial Glycoengineering as a Biosynthetic Route to Customized Glycomolecules.

Young NM, Brisson JR, Kelly J, Watson DC, Tessier L, Lanthier PH, Jarrell HC, Cadotte N, St. Michael F, Aberg E, et al. 2002. Structure of the N-linked glycan present on multiple glycoproteins in the gram-negative bacterium, *Campylobacter jejuni*. J Biol Chem. doi:10.1074/jbc.M206114200.

Yu H, Chen X. 2007. Carbohydrate post-glycosylational modifications. Org Biomol Chem. doi:10.1039/b700034k.